Dissertation Thesis

Czech Technical University in Prague

F3

Faculty of Electrical Engineering
Department of Measurement

New Methods for Automatic Illuminance and Indoor Sound Distribution Measurement

Ing. Tomáš Drábek

Supervisor: prof. Ing. Jan Holub, Ph.D.
Ph.D. programme: Electrical Engineering and Information Technology (P2612)
Field of study: Measurement and Instrumentation (2601V006)
February 2022

Acknowledgements

There are many persons who have helped me in my research and writing this work. I would like to thank everyone for their help and support. In particular, I would like to thank my supervisor prof. Ing. Jan Holub, Ph.D. for supervising my work. I would also like to thank Ing. Vladimír Petrík, Ph.D. and Ing. Jan Plachý, Ph.D., who helped me a lot, as without them I would not have been able to finish the work to such an extent. I would also like to thank my colleagues from the Department of Measurement and Department of Electroenergetics for their valuable advices.

I mainly want to thank a lot my family for supporting me throughout my studies. First of all, I want to thank my fiancée Vendulka, my mother, my brother and my three-month-old son Oldřich, for letting me sleep in the last few months. *(smile)*

Declaration

I declare that this dissertation was created as a result of my independent work on a given topic in cooperation with my thesis supervisor Prof. Ing. Jan Holub, Ph.D. and in collaboration with Ing. Vladimir Petrík, Ph.D. The expert advisor regarding illumination measurement was Ing. Marek Balsky, Ph.D.

In Prague, 22. February 2022

Abstract

People spend most of day indoors, in their homes, workplaces, schools, production halls, or other buildings. For this reason, emphasis is put on providing a comfortable and healthy environment, which is verified by audits. Audits to verify that the living or working conditions meet the applicable standards are carried out for newly constructed buildings or after renovations of the buildings. Audits are performed, for example, to evaluate illuminance or acoustic noise in the building interior.

Audits of these quantities in the interior are currently done by human operators. The entire measurement process is divided into several parts, where each part requires human operators. The most time-consuming part is the demarcation of control points around a room, followed by the actual measurement using a measurement device and recording the measured data.

The aim of this work is to develop novel methods for an automatic measurement of the illuminance and acoustic noise in the interior of buildings so that the calculation of the control points, subsequent measurements and recording of values is done automatically without the need for the trained operator. Therefore, robotic units are equipped with measurement devices and have implemented the novel proposed measurement methods to carry out the measurements. Because automation using robotic units allows parallel measurements in multiple rooms at the same time, overall time and human resources requirements are reduced.

The main focus of this thesis is the proposed solution for the automatic measurement of illuminance and acoustic noise in the interior of the buildings. The proposed solution for the illuminance measurement is not based on the established procedure but on an automatically created virtual model of a measured luminaire and simulations of the light emitted from it, which is shown to be in line with the defined standards. The validity of the proposed automated illuminance measurement is verified by a series of experiments, which are divided into simulations and real experiments.

The next part of this thesis focuses on design of a novel method for the automatic measurement of acoustic noise using established procedures based on standards. The method is divided into two parts, each part focusing on a different type of acoustic noise source. The proposed solution includes an implementation of both parts and subsequent experiments aimed at its verification. The experiments are again divided into simulations and real experiments, which use a robotic unit equipped with a measurement device.

The result of the thesis is a functional verified solution for automatic measurement of illuminance and acoustic noise in the indoor environment. At the same time, the differences between the established measurement procedure and the proposed solution are described. The thesis contains a proposal for further research and future extension of the proposed solution.

Keywords: selection of control points, illuminance measurements, acoustic noise measurements, robotic unit, indoor

Supervisor: prof. Ing. Jan Holub, Ph.D.

Abstrakt

Lidé tráví velkou část dne uvnitř budov, ať už se jedná o jejich domovy, pracoviště, školy, výrobní haly, nebo jiné budovy. Z tohoto důvodu je kladen důraz na zajištění komfortního a zdravého prostředí, které je ověřováno za pomoci auditů. Audity, které ověřují, zda jsou podmínky splněny dle platných norem se provádí pro novostavby nebo po rekonstrukcích. Audity se provádějí například pro vyhodnocení osvětlenosti či akustického hluku v interiéru.

Audity těchto veličin jsou v interiéru v současnosti založeny na využití lidské obsluhy. Celý proces měření je rozdělen do několika částí a každá část vyžaduje lidskou obsluhu. Časově nejnáročnější je vytyčení kontrolních bodů po místnosti a dále samotné měření pomocí měřicího zařízení a zaznamenávání naměřených údajů.

Cílem této práce je navrhnout nové metody automatického měření osvětlenosti a akustického hluku v interiéru tak, aby výpočet kontrolních bodů i následného měření a záznam hodnot probíhal automaticky bez nutnosti zapojení výškolené osoby. Pro měření se proto použijí robotické jednotky, které obsahují měřicí zařízení a mají implementované nově navržené metody měření. Jelikož automatizace pomocí robotických jednotek umožňuje paralelní měření ve více místnostech zároveň, dochází k snížení celkové časové náročnosti a snížení nároků na lidské zdroje.

Těžištěm práce je navržené řešení pro automatické měření osvětlenosti a akustického hluku v interiéru. Navrhované řešení pro měření osvětlenosti nevychází ze zavedeného postupu, ale z automaticky vytvořeného virtuálního modelu měřeného svítidla a simulací vyzařování světla z něj, jenž je v souladu s normou. Automatizované měření osvětlenosti je ověřeno sérii experimentů, které jsou rozděleny na simulační a reálné.

Další část této práce je zaměřena na návrh nové metody pro automatické měření akustického hluku, která využívá zavedené postupy vycházející z norem. Metoda je rozdělena na dvě části, kdy každá část se zaměřuje na jiný typ zdroje akustického hluku. Součástí navrhovaného řešení je i implementace obou částí a následné experimenty zaměřené na jeho ověření funkcionality. Experimenty jsou opět rozděleny na simulované a reálné, které používají robotickou jednotku vybavenou měřicím zařízením.

Výsledkem práce je funkční ověřené řešení automatického měření osvětlenosti a akustického hluku v interiéru. Zároveň jsou posouzeny rozdíly mezi zavedeným postupem měření a navrhovaným řešením. Součástí práce je návrh dalšího výzkumu a budoucího rozšíření navrhovaného řešení.

Klíčová slova: výběr kontrolních bodů, měření osvětlenosti, měření akustického hluku, robotická jednotka, interiér

Glossary

CP control point

SLAM simultaneous localization and mapping

CCL concurrent communicating lists

MPVHD Methodical instructions for the calculation of sound pressure level from transport

NRI Noise Reduction Index

GP Gaussian process

1st alg. algorithm for long-term stationary noise

2nd alg. algorithm for short-term recurring noise

Contents

Figures

Tables

Chapter 1

Introduction

Today, process automation is seen almost everywhere, covering all branches of human activities, such as exploitation of robotics in the manufacturing processes. One of the areas where process automation can save money and time of the human operator, and achieve even better performance than the human operator is the field of measurement. Therefore, this dissertation thesis focuses on the design, development, implementation and testing of new methods for automatic measurement of illuminance and acoustic noise in the interior of buildings.

Indoor illuminance and indoor acoustic noise in a buildings are internal quantities due to measurements taking place inside buildings. The measurements of such internal quantities are used for several reasons. One of the reasons is the design of new lighting systems, or soundproofing of the space, as it is necessary to determine the soundproofing of the premises before starting construction work. Another reason for the exploitation of internal quantity measurement is the verification of deployed system parameters to check whether they are in line with the defined standards, both national [1, 2, 3, 4] and international [5, 6, 7].

In general, the measurement of internal quantities is a complex process consisting of multiple tasks. The first task lies in preparation of the measurement area and the measurement device. This is followed by the determination and delineation of control points (CPs) in the measurement area where the measurement via the measurement device takes place. The second task is the measurement itself, which is performed in each of the previously determined CP. The measured value is recorded in the measurement protocol, which also records the exact position of the CPs where the value was measured. The final task of the entire measurement process is processing of the measured values and their evaluation. The evaluation is done by determining whether the room meets the requirements of the standard.

In this dissertation thesis, new methods of determining and delineation of CPs for indoor illuminance and indoor acoustic noise measurement are proposed and evaluated. The novel methods are evaluated via simulations and real-world experiments to validate their functionality and to show their benefits. The real-world experiments are performed via autonomous robots, where one of the robots has been developed within the scope of the thesis

and has been presented in [8, 9, 10, 11].

In the scope of this thesis, I have supervised multiple bachelor projects that are a part of this dissertation thesis. In the thesis [12], localization of the robotic unit and determination of the measured area is implemented via a simultaneous localization and mapping (SLAM) technique. The thesis [13] consisted of adapting the robot's software to novel scenarios, while performance was evaluated via simulations and real-world experiments. The last but not least, work [14] consisted of creating a digital image of a room (floor plan) and testing a robotic unit to measure acoustic noise in the interior.

1.1 Thesis Outline

This thesis is divided into seven chapters. In Chapter 2, the formulation of the problem is described, and the measurement requirements are defined based on the standards for measurement of illuminance and acoustic noise. This Chapter also presents a unified description of the measurement space. Chapter 3 presents the latest research in the field of illuminance and acoustic noise measurements. The research done is divided based on the measured quantity. The new method of determining CPs for measuring illuminance is based on a virtual model of the measured luminaire and the measured values (Chapter 5).

The automated procedure for determining CPs for acoustic noise measurement in Chapter 6 is based on established procedures in practice. The CPs are therefore determined based on the dimensions of the room. In Chapters 5 and 6 describe complex testing of the proposed solution and the process of measurement both quantities. Testing includes simulations and robotic measurements in rooms using robotic units.

Chapter 2

Formulation of the Problem

In this chapter, we formulate the requirements for internal quantities and the problem of measuring indoor illuminance and indoor noise. Furthermore, the chapter contains a description of the measurement area for both measured internal quantities and a general description of the measurement uncertainties. The last section of this chapter is devoted to the goals of this dissertation. Parts of the text in this chapter have been published as [15, 16].

2.1 Illuminance

In the area of lighting, the significant quantity is the illuminance. Therefore, illuminance is defined as:

$$E = \frac{d\Phi_{\text{impact}}}{dA}\,. \tag{2.1}$$

where $d\Phi_{\text{impact}}$ is luminous flux relative to illuminated surface dA and indicates with which intensity the surface is being illuminated. The unit of the illuminance is 1 lux (lx) [17].

In illumination design is used to calculate the maintained illuminance $\bar{E}_m$, minimum illuminance E_{min} and uniformity of illumination U_0. The maintained illuminance is the average value of the illuminance in the measurement area at the end of the maintenance cycle. The minimum illuminance value is the lowest measured illuminance value in the measurement area of the room. The uniformity of illuminance is the ratio between them:

$$U_0 = \frac{E_{\text{min}}}{\bar{E}_m}\,. \tag{2.2}$$

These three values are the most important for the audit of the lighting system in a given room.

2.1.1 General Requirements for Measurement Procedure of Illuminance

Measurement of illuminance, also referred to as an audit of the lighting system, of the interior based on [1] is used for:

- Verification, whether the lighting conditions and illuminance values of the lighting system are met during the project realisation according to the documentation and whether they are consistent with the requirements of the valid standards.

- Detection of illuminance conditions, e.g., measuring the average illuminance value and determining uniformity, and visual comfort while using the lighting system and verification, whether they are consistent with the requirements of the valid standards. Visual comfort is a condition where people in a measured environment have a feeling of well-being [5].

- Comparison of different interior illuminance solutions in terms of achieving visual comfort conditions and regarding the economy and energy savings.

Measurement of the illuminance of the interior, based on [1] is divided in to:

- Precise, designated for assessment of the demanding interior or used for research purposes. Estimation of expanded measurement uncertainty is $U \leq 8$ (%).

- Operating, designated for verifications of the correctness of designed and implemented lighting conditions and visual comfort. Estimation of expanded measurement uncertainty is $8 < U \leq 14$ (%).

- Tentative, designated for verifications of the basic conditions of visual comfort. Estimation of expanded measurement uncertainty is $14 < U \leq 20$ (%).

It is further distinguished whether illuminance is measured without personnel (in the new interior before their commissioning or during their use, where the presence of personnel does not significantly affect the lighting conditions and visual comfort) or with personnel in their usual position when the shadow affects the illuminance [1].

2.1.2 Requirements of Measurement

The measurement procedure is specified by the standard [5] and is implemented in national legislation, e.g., [1]. It is used by the national supervisory authorities or by private companies that provide audit or a final inspection before issuing a conformity certificate. The standard verification procedure is based on discrete illuminance measurements performed on a network of the CPs. The CPs are located in a rectangular network, determined by a human operator and based on the room's dimensions, as shown in Fig. 2.1. The walls are shown in black, and the black crosses represent the CPs, the symbols x and y represent the spacings between the CPs. The distance between adjacent the CPs varies between 0.5 m and 6 m and depends on the room properties. The position and size of the network are chosen according to the formula (2.3)

from the standard [5]:

$$p = 0.2 \cdot 5^{\log_{10} d}, \tag{2.3}$$

where $p \leq 10$, d is the longer wall dimension (m), but if the ratio of the longer side to the shorter side is equal to or greater than 2, d is the shorter wall dimension and p is the maximum dimension of the network cell (m). An example, respecting the distance between the wall and the first the CP in a row/column is no less than 1 m, shown in Fig. 2.1. This figure shows a room with a marked network of CPs. The locations of these the CPs are determined manually by the operator, according to the dimensions of the room.

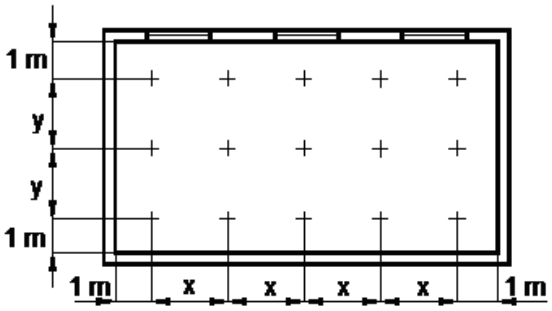

Figure 2.1: Arrangement of the CPs inside of area [1].

Illuminance measurements are performed at these points (the CPs) at a fixed height corresponding to the height of the standard working area in an office environment. Different height may be used for a non-office environment, for example, the height for pre-school facilities is set to 0.45 m [1].

The photometer devices, that are used for illuminance measurements must comply with the requirements specified in the standards [18, 19]. The historical development of illuminance measurement devices is presented in [20]. These measurement devices are subject to a calibration procedure [21] in which the current uncertainty of the device is determined. Subsequently, it is possible to calibrate the instrument and reduce the measurement uncertainty [15].

2.1.3 Preparation for the Measurement

Before the measurement can be done, the state of the measurement device is checked. Especially, the cleanness of all its parts is essential for accurate measurement. The verification that external light sources do not affect the measurement is verified too. Furthermore, the lighting system is brought to the state of its regular operation before the measurement. To measure the illuminance, the time of preliminary ageing of light sources should be kept at a minimum, but at the same time, before the start of the measurement, light bulbs should be continuously lighten minimally for 10 hours and discharge sources, e.g., fluorescent lamps, for 100 hours at least.

Before starting the measurement, the illuminance (lighting system) shall be switched on in advance so that the luminous flux stabilizes. The luminous flux is considered to be stabilized when the measured value of illumination does not show systematic changes three times in succession when measured at intervals of several minutes; the manufacturer's data are also taken into account when determining the stabilization time. For discharge sources, the minimum stabilization time for luminous flux is considered to be 20 minutes, with closed luminaires this time may be even longer. [1].

2.2 Acoustic Noise

The noise can be described as ambient sound, signal, etc. that is not wanted but always present. Noise is most often measured in decibels (dB) or A-weighted decibels (dB (A)), which correspond to the weighting curve A. Weight curve A is defined in [22] or [23]. Decibels are related to sound pressure, where 0 dB corresponds to 0.00002 Pa.

The acoustic noise level is measured in human-occupied buildings to ensure comfortable living conditions. As described in [24], temperature, humidity, and CO2 concentration are usually the monitored indoor quantities. Measurement of the acoustic noise level, together with the monitored indoor quantities, can be used to improve the quality of indoor living. The acoustic noise measurement process is described in international standards that specify, for example, restrictions for placing the CPs [7], the duration of the individual measurements [7], or measurement device specifications [23]. National supervisory authorities or private companies use these standards to measure acoustic noise levels both indoors and outdoors and provide recommendations on reducing the acoustic noise levels. The text in this section has been published in [16, 25].

2.2.1 Requirements of Measurement

The current measurement procedure is done by manually measurement of acoustic noise levels in a network of the CPs. The CPs are distributed within the measured room to comply with the standard [7], and their density and positions are determined by a trained and qualified operator. The distance of adjacent the CPs must be no less than 0.7 m, and at least one the CP must be located in the corner of the measured room. In addition, all points must be located at least 0.5 m away from the wall and at least 1 m away from any significantly sound-transmitting elements such as windows or entrances of openings for air supply. Windows and doors must be closed during measurement to avoid introducing any sound from outside of the measured room. The location of the measurement points defined in this way is determined manually by the operator according to the dimensions of the room. Acoustic noise measurements are done at the defined the CPs at a height between 1.2 m and 1.5 m from the ground. The measurement instrument is directed towards the source of the incoming acoustic noise or

vertically upwards if the direction of the acoustic noise source is not defined. A certified sound level meter is used as the measurement instrument [25].

2.3 Uncertainties of Measurements

The measurement uncertainty characterises the range of values around the result of the measurement where the actual measured value lies, e.g., in the case of 10% uncertainty and the measured value of 100, the actual value is in the range of 90 to 110. The uncertainty of the measurement is in general determined by the standard deviation of the measurements. The value of the standard uncertainty – u and represents the range of values around the measured value. Standard uncertainty is divided into the standard uncertainty of type A and type B.

2.3.1 Standard Uncertainty Type A – u_A

The uncertainty u_A is defined as a dispersion of a set of data from its mean value:

$$u_a = \sqrt{\frac{1}{n\,(n-1)} \sum_{i=1}^{n} (x_i - \bar{x})^2}, \tag{2.4}$$

where x_i is the measured value, $\bar{x}$ is the mean value of the samples, n is the number of repeated measurements (number of samples). This uncertainty is obtained by repeating measurement under the same conditions and calculated according to the presented formula. Note that in order to obtain this type of uncertainty, at least 10 samples must be collected [26].

2.3.2 Standard Uncertainty Type B – u_B

The measurements performed in this thesis include many aspects indicated by the standard deviations. Every possible source of the measurement errors corresponds to a certain partial standard uncertainty that forms the uncertainty of type B:

$$u_B = \sqrt{u_{B1}^2 + u_{B2}^2 + u_{B3}^2 + \cdots + u_{Bn}^2}, \tag{2.5}$$

where $u_{B1}^2 + \cdots + u_{Bn}^2$ are partial standard uncertainties of individual parameters influencing the accuracy of measurements in the same units as the overall uncertainty. For the measured values the uncertainties are indicated in percentage.

Partial uncertainty u_B is determined based on a detailed analysis of the sources of error, a professional estimation of the maximum possible deviation, and the probability of its occurrence. Partial relative standard uncertainty

$u_B x$ corresponds to a particular source of error while measurement the quantity x, and is calculated as follows:

$$u_{Bx} = \frac{Z_{X\max}}{\chi}, \tag{2.6}$$

where $Z_{X\max}$ is the estimation of the maximal possible deviation, χ is a coefficient given by the statistical distribution of error from the measured quantity X and is defined in the interval $\langle -Z_{\max}, +Z_{\max} \rangle$. It is necessary to consider several primary sources of error to measure internal quantities.

Illuminance measurement, as any other measurement, contains several possible sources of errors and corresponding partial standard uncertainties, as summarized in Tab. 2.1. The sources of errors in the measurement of the illuminance follow the information about illuminance measurement from article [27]. Similar to illuminance measurement, the acoustic noise measurement contains multiple possible sources of errors, and their corresponding partial standard uncertainties are summarized in Tab. 2.2. In Tab. 2.1 and Tab. 2.2, the partial standard uncertainties are referred to as type B uncertainties.

Table 2.1: The primary sources of possible errors and their assignment to the corresponding partial uncertainties for the measurement of the illuminance.

Error number	Source of error	Label
1	Location of the CPs in the interior	u_{Bl}
2	The uncertainty of the measurement device	u_{Be}
3	Instability of used devices	u_{Bs}
4	Influence of the final dimensions of the radiating surface of the luminaire (source) and the receiving surface of the sensor	u_{Bk}
4	Position the sensor in the correct position	u_{Bv}

Table 2.2: The primary sources of possible errors and their assignment to the corresponding partial uncertainties for the measurement of the acoustic noise.

Error number	Source of error	Label
1	Location of the CPs in the interior	u_{Bl}
2	The uncertainty of the measurement device	u_{Be}

2.3.3 Combined Standard Uncertainty u_C

The sum of uncertainties of type A and type B is uncertainty u_C. It specifies the interval at which the actual value of the measurement is presented. It is obtained from the following formula:

$$u_C = \sqrt{u_A^2 + u_B^2}. \tag{2.7}$$

2.3.4 Expanded uncertainty U

To increase the probability of correct value presence within the interval given by uncertainty $\langle -u_C, +u_C \rangle$, the extended standard uncertainty is introduced:

$$U = k_u \cdot u_C. \tag{2.8}$$

For the probability of 95%, the expansion coefficient $k_u = 2$ is used. It was determined based on a normal distribution [28, 26].

2.4 Task Formulation

The measurement of illuminance or acoustic noise is done in an empty room with a flat floor. In general, the real-world measurements of illuminance and acoustic noise are done by the trained operators. These operators must perform several actions before the actual measurement of illuminance and acoustic noise takes place. The entire measurement process can be seen in Fig. 2.2, where the first step is to prepare the room for measurement, next step is determining dimensions of the measured room.

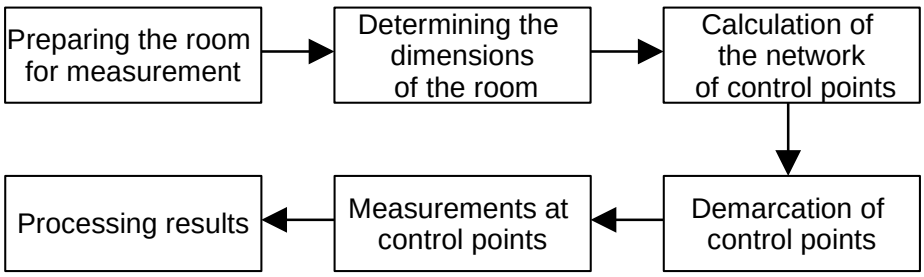

Figure 2.2: The entire measurement process.

Based on the room's dimensions, the operator determines a network of the CPs and then locates the individual points of the CPs on the room floor. The measurements of the required quantity are then done at the CPs. As described, the illuminance measurement task requires many subtasks and the involvement of the human operator to carry them out. This is, however, not practical, as this process can be automated to save operators time.

2.5 Measurement Area

The measurements take place in a measurement area (room) and are done by a sensor of the measured quantity. The position of the sensor in a room is defined as $\boldsymbol{x} \in \mathbb{R}^2$. The observation of the measured quantities, illuminance and acoustic acoustic noise, at position $\boldsymbol{x}_i$ are denoted by $f(\boldsymbol{x}_i)$ and $g(\boldsymbol{x}_i)$, respectively. Measurements of quantities are performed in an empty room

with a known floor plan. The floor plan is specified by a polygon $\mathcal{P}$, where $\partial\mathcal{P}$ defines the boundary of the polygon $\mathcal{P}$. The current measurement standards [1, 7] specify that measurements are performed at points within $\mathcal{P}$ at a distance no less than 1 m from boundary $\partial\mathcal{P}$. We denote this inner room area by symbol $\mathcal{I}$, and we define it as:

$$\mathcal{I} = \{\boldsymbol{x} \,|\, \boldsymbol{x} \in \mathcal{P} \wedge d(\boldsymbol{x}, \partial\mathcal{P}) \geq 1\}\,, \tag{2.9}$$

where $d(\cdot,\cdot)$ denotes the smallest distance between the point and the polygon boundary. The boundary of the inner area I is denoted by symbol $\partial\mathcal{I}$. The illustration of the room with boundaries is shown in Fig. 2.3 , where the walls of the room represented $\partial\mathcal{P}$, and $\mathcal{P}$ represents the area of the room. The inner room area $\mathcal{I}$ with boundary $\partial\mathcal{I}$, is placed 1 m from $\partial\mathcal{P}$, i.e., 1 m from the wall of the room.

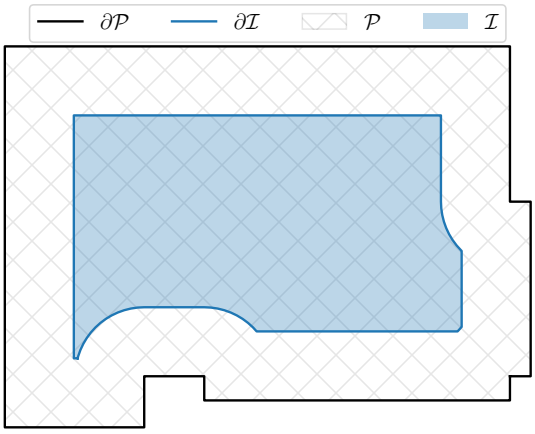

Figure 2.3: Illustration of the measured room with defined measurement area [15].

2.5.1 Measurement Area for Illuminance

In practice, the measurement area of a room $\mathcal{I}$ is defined by two national standards [1, 5], where the first standard [1] used in this thesis sets the boundary of the measurement area $\partial\mathcal{I}$ at 1 m from the wall. The second standard [5] sets this boundary $\partial\mathcal{I}$ at only 0.5 m from the wall. The second standard [5] is used more in practice. However, it will be proved that this different distance does not affect this thesis.

The goal of illuminance verification is to verify that the illuminance value is greater than the fixed threshold τ at all positions inside the inner room area:

$$f(\boldsymbol{x}) > \tau\,,\ \ \forall x \in \mathcal{I}\,. \tag{2.10}$$

If Eq. (2.10) is violated, the verification procedure should report the position at which the illuminance is lower than τ. Since area $\mathcal{I}$ is continuous, verification of Eq. (2.10) requires an infinite number of measurements, that is not only

impractical but also impossible. The measurement process implemented in practice is performed on a discrete rectangular network of the CPs in a given room based on the standard where the average illuminance value is used for the verification process instead of Eq. (2.10). We initially use objective Eq. (2.10) and based on the measurement introduced in practice, the average value of illuminance is then considered.

2.5.2 Measurement Area for Acoustic Noise

This section lists the requirements for the measurement area where the acoustic noise values are recorded. The standard [7] specifies the minimum requirement for the mutual Euclidean distance of the CPs, as 0.7 m, i.e.,:

$$d(\boldsymbol{x}_i, \boldsymbol{x}_j) \geq 0.7\,, \quad \forall i, j \in \{1, ..., n\}; i \neq j\,, \tag{2.11}$$

where $\boldsymbol{x}_i$ a $\boldsymbol{x}_j$ are the CPs. According to the standard [7] there should be at least one the CP in the corner of the room. The placement of the CPs is shown in Fig 2.4, where the walls of the room represent the boundary ($\partial\mathcal{P}$) of the area of the room $\mathcal{P}$. Within the room defined by $\mathcal{P}$, we have measurement area $\mathcal{I}$ with boundary $\partial\mathcal{I}$ at a distance of 1 m from $\partial\mathcal{P}$, i.e., the measurement area $\mathcal{I}$ is the same as for measurement illuminance.

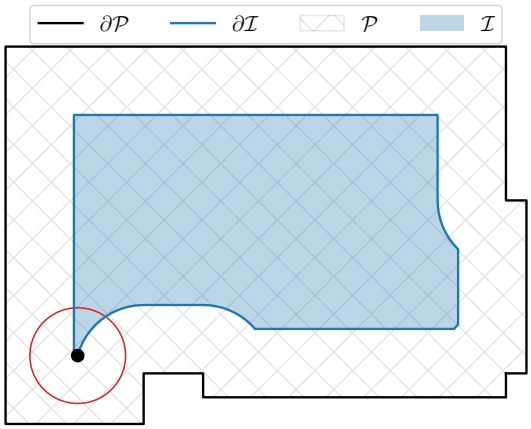

Figure 2.4: Illustration of the measured area for acoustic noise measurement.

Chapter 3

State of the Art

This chapter describes the current state of research in areas of illumination and acoustic noise measurement, emphasizing measurements inside buildings. The text in this chapter is based on the articles [15, 25].

3.1 The Field of Illuminance Measurement

Measurements of the illuminance at the CPs can be performed either simultaneously [29] or sequentially [30]. An example of the system for simultaneous measurements is shown in [29] and consists of 160 illuminance sensors. The sensors are statically distributed around the room to compare the illuminance distribution of intelligent and conventional light sources. The sequential measurements are preferred in practical applications, because simultaneous measurements require a very high number of sensors. These sensors must be calibrated and are more expensive [31], in comparison to equipment purchased from regular stores, due to their high accuracy requirements. For example, in [30] the authors designed an algorithm for the CP selection based on the illuminance distribution obtained from the Dialux simulation program [32]. The CPs are selected offline before the measurements are done. Subsequently, the operators then carry out measurements at the selected the CPs.

Automation of the sequential measurement process has been researched in multiple studies. In one of the studies, a mobile platform equipped with a photometer to perform sequential illuminance measurements has been exploited. This study has been described in a series of papers [33, 34, 35]. In the paper [33], the authors focused on the localization of the robot within a room. The follow-up paper [34] improved the self-localization capability with the use of a steady-state genetic algorithm. The next paper [35] provides a comprehensive test of joint mapping and localization capabilities together with the illumination measurements. All three papers focused on the localization of a mobile platform in a room for the purposes of illumination measurements.

The authors [36] described the robotic based for the lighting quality measurement process. The authors emphasized modelling the robot's behaviour and used concurrent communicating lists (CCL) to design the behaviour model. The authors claim that the use of CCL allows the platform to simu-

late the measurement process, and it is possible to verify the proposed process formally because the formal background of the CCL script allows the model to be transformed into a Labelled Transition System (LTS) [37] that can be validated.

The analysis of robotics-based building electric energy audits has been shown in [38]. In [38] various robotic platforms are used to simultaneously measure several quantities in different experiments. The paper describes several advantages of using a robot rather than a human operator, including repeatability, time-saving and cost-saving.

The use of robots for lighting verification is not limited to interior audits. This is shown for example in [39], where the authors proposed the use of three robotic manipulators in order to measure the spatial distributions of the illuminance from a single light source. In their scenario, the robotic system acted as a goniophotometer [40]. One arm was used to hold the light source, and the other robotic arms were used for positioning the photometers.

A more recent article [41] studied the measurement of illuminance using a robotic unit, with the location of individual the CPs being entered manually to the unit before the measurement. An innovation was the navigation strategy, which considered the objects when passing the room through the robotic unit. The robotic unit either avoided the obstacle, or if there was the CP behind the obstacle that it could not reach, it skipped the CP.

Another work [42] uses a humanoid robot to compare measurements with information obtained through a questionnaire filled in by persons using the the measured spaces. The properties of the room (temperature, illuminance, etc.) were measured in a network consisting of 20 points. The final report and suggestions for improvements were communicated to the occupant of the room.

The related works presented here either compute the location of the CPs in advance of the measurement process, or do not specify the approach used for the computation and focus on other aspects of the measurement, e.g., [30, 36, 41, 42].

3.2 The Field of Acoustic Noise Measurement

The acoustic noise level in the interior is one of the quantities specified by a standard and is subject to audits to ensure a comfortable living environment. Several published articles deal with acoustic noise (noise) measurement and its reduction. The article [43] dealt with the possibility of measuring aircraft noise using linear microphone arrays. Using this method, an undistorted record of aircraft noise was achieved. The article [44] also deals with determining aircraft noise and selecting this noise from background noise. Compared to previous research [43], the authors exploit neural networks to recognize the aircraft noise from all of the noise with accuracy up to 99.84 %.

The authors [45] measure noise in landing aircraft that use thrust reversers to slow down aircraft after landing at Madrid-Barajas Airport. The paper

presented possible improvements for detecting noise from the reverse thrust and the direction of incoming noise.

The article [46] analyzed the impact of noise on the surroundings of 248 European airports. An analysis has been performed considering a five monitored parameters, e.g., number of runways and distance from the airport to the city, and noise abatements measures. The analysed results show that if the monitored parameters are upper, the measures to reduce noise also increase.

Another industry where the noise is often monitored is for road traffic in cities. The article [47] investigates traffic noise pollution in Amman in monitored time intervals (from 7 am to 8 am and from 7 pm to 8 pm). Noise values were recorded at 28 locations twice a day (morning and evening rush hours). These measurements aimed to record high noise levels. The results showed that most measurements exceeded the specified limit of 62 dB(A), mentioned in the article.

A similar article [48] dealt with traffic noise on the campus of the University of Dublin. The level of noise exposure in the monitored area during daytime and nighttime was recorded. Night measurements show that the noise values are higher than the recommended WHO level, which is set at 45 dB(A) for nighttime exposure [49]. If the specified noise levels are exceeded, hearing loss may occur due to excessive noise. The output of the study is a proposal for road traffic management in the measured area with an emphasis on noise reduction at night.

The article [50] aimed to monitor the noise load of the population, using both the measurement of noise in the residential part of the city (Sao Paulo) and a questionnaire focused on the perception of noise by residents themselves. The questionnaire was filled in by 225 participants living in the measured area. The questionnaire results showed that 48.4 % of respondents are bothered by a loud noise from road traffic. The measurement took place at 75 locations of the measured area for 20 hours. Noise level values above the critical limit of 55 dB(A), which was determined in the article, were measured.

The noise measurements and its impact on people is not studied only from road traffic but also railway transport. One of the studies considering railway transportation is shown in article [51], which dealt with comparing two measuring methods used to measure noise in the vicinity of the railway. The first method Schall 03 places the measuring device at a vertical distance of 25 m from the axis of the railway line at the height of 4 m above the ground and is used in Slovakia. The second method Methodical instructions for the calculation of sound pressure level from transport (MPVHD) places the measuring device at a distance of 7.5 m from the axis of the railway line and is used in the Czech Republic. The study aimed to find out which of these methods is more suitable for measuring the noise arising from the running of modern trains. The results showed that the Schall 03 method is more suitable than the MPVHD method. The measurement results were more identical to the calculated values, and also, the method showed more minor deviations from the predicted model.

Another study focused on the reduction of noise from railways has been presented in [52]. Noise measurements took place in three urban areas (two hospitals and university campus), where noise meters were installed on the facades of buildings. The Schall 03 method was used. Based on the processed results, the study proposes three different solutions for noise reduction. The first solution is to avoid using a train siren, the second is to build noise barriers, and the third is to remove the railway tracks from the urban perimeter. Based on simulations of these solutions, a noise reduction of 2-12 dB(A) was achieved.

The next sector where noise is measured is the automotive industry. The article [53] presents and verifies the application of statistical energy analysis. The application is used for 3D modelling of noise reduction in the interior of a car from the drivetrain. The application then provides data that can be exploited to propose suitable measures to reduce the noise.

Research of noise impact on humanity and measurement of noise coming from traffic, whether from the air, rail, or road, is a well-researched area. Another area that deserves attention is the noise generated by wind turbines. The standards specify, noise measurement methods, requirements for measuring instruments and evaluation. Standard [54] provides overall wind turbine noise measurement standards. Conversely, standard [55] focuses more on the aeroacoustics noise of wind turbines, while [56] deals with noise measurement in the interior of buildings close to wind farms.

Another approach to noise measurement requires involving citizens and using their smart devices to monitor noise in their immediate vicinity. Such a measurement was dealt with in a study [57] which, using this method, created spatial and temporal maps of noise.

Noise measurements are also often performed indoors. In [58], the interior noise reduction index Noise Reduction Index (NRI) was determined. The [58] deals with the definition of the index for NRIs with open windows for the summer months. A theoretical model was created and compared with experimentally obtained data.

Today, several software programs simulate acoustic conditions in buildings. Based on the created model of rooms with specified noise sources, technicians can create a noise map. In [59], the authors simulated a noise map and used it to identify critical areas using reference measurements and room acoustics prediction and occupational noise exposure software.

Article [60] deals with the measurement of noise at the place of residence of 44 schoolchildren. The measurements were performed in the children's rooms and in the room where the schoolchildren spent most of their time. Outdoor noise was also recorded during the measurement.

The sound pressure level affects the workplace and, for example, medical facilities where patients are treated. Article [61] deals with the measurement of noise around and inside the hospital. A total of 24 measurements were performed on the outer facade of the hospital and 21 measurements inside. The measured data provided an insight into the noise situation in and around the hospital and showed that the noise levels were exceeded.

The difference between outdoor and indoor noise is also described in the

article [62]. The study performed noise measurements inside and outside the building at 102 inhabitants, with open, closed or semi-open windows playing a significant role. The result of the study was the creation of a statistical model that can be used to estimate the sound exposure inside the building.

Noise measurement using a robotic unit is becoming more common these days. In paper [42], the humanoid robotic unit was equipped with both a photometer and a sound level meter. The humanoid measured values of both quantities at 20 points in the room. Robot evaluated the comfort for the room based on an interaction with a human operator and from the measured values.

The article [63] on noise maps outside buildings also used an autonomous mobile robotic platform equipped with a sound level meter to measure noise. The measured values by the robot were compared with a model of known sources and with manual measurement. In conclusion, it was stated that noise maps should be based on the application and the environment.

Chapter 4

The Goals of the Dissertation

Many studies (Chapter 3) focus on processing the results of the illuminance and acoustic noise measurements. This thesis focuses on determining the CPs in the interior, where internal quantities are measured. This thesis aims to design, implement and test new methods for determining the CPs in the interior for measurement of illuminance and acoustic noise.

In state-of-the-art works or practice, the room dimensions are either measured by an operator or known from the floor plan. These dimensions are required to determine the coordinates of the calculated the CPs in the measured room. The proposed approach uses robotic units to autonomously move the measurement device to the location predicted by the new method. The entire time-consuming measurement process is therefore performed by a robot autonomously, without an operator.

The goals of the dissertation are:

- Design, implement and test a new method for determining the CPs for measurement of illuminance.
- Automate and test the process of determining the CPs for measurement of acoustic noise.
- Verify the measurement process of both quantities using an autonomous robot.

Chapter 5

Illuminance Measurement

In this chapter a novel solution for measurement of illuminance in the interior to perform audits of lighting systems is proposed. The core of this solution is to determine the the CPs where the illumination measurement should take place. The measurement itself is done via the robotic unit equipped with an illuminance measurement device. The robotic unit works in iterations by determining the CP, moving to the CP, performing the measurement and then repeating the process over again. This process is based on the proposed novel method of illuminance measurement that exploits the robotic unit that autonomously measures the illuminance, thus eliminating the need for a human operator. The proposed method adaptively determines the density of the CPs based on the collected illuminance measurements. The calculation of the new CP is based on a virtual model of the measured luminaire and a simulated propagation of light emitted from this luminaire.

This chapter contains the experimental evaluation of the proposed solution. The evaluation is done by both simulations and real measurements using a robotic unit. Furthermore, the uncertainties of illuminance measurements are calculated in the last section. This research has been published and the text in this chapter is based on [15].

5.1 Proposed Approach

The illuminance measurement proposed in this chapter is inspired by Bayesian optimization [64], which is a method that exploits approximation of a function. An example of such approximation with the Gaussian process (GP) can be found in [65]. Compared to the established illuminance measurement procedure commonly used in the real-world, the main difference of the proposed solution is the delineation of the CPs based on a virtual model of the measured luminaire and simulated propagation of light emitted from luminaire. The model is based on the GP and trained on simulated illuminance data from the Dialux program [32], which uses the measured luminosity curve of the given luminaire.

The GP enables us to create a nonparametric model that is fitted to match the virtual model. To provide an unrestricted model, the GP exploits a surrogate function that represents the uncertainty of the sensor's measurement in

a computationally tractable way. The possibility to exploit the nonparametric model also makes the GP a popular choice in many research fields, e.g., an indoor localization system using a Wi-Fi signal [66], localization and mapping of magnetic fields [67], representing the probability of grasping an object in multi-finger object grasp planning [68], or model-based reinforcement learning for model representation in [69] or [70].

The surrogate function $\hat{f}_{lb}(\boldsymbol{x})$, obtained from a GP [71], is used to represent the lower bound of the illuminance value and is used to compute the CP candidates $\mathcal{X}_c$ for the measurements, where $\mathcal{X}_c$ is defined as:

$$\mathcal{X}_c = \{\boldsymbol{x} \,|\, \boldsymbol{x} \in \mathcal{I} \wedge \hat{f}_{lb}(\boldsymbol{x}) \leq \tau\}\,. \tag{5.1}$$

The set $\mathcal{X}_c$ contains all positions $\boldsymbol{x}$ inside an inner area of $\mathcal{I}$ with surrogate function value of $\boldsymbol{x}$ no larger than the threshold τ. These positions are potential candidates for the CPs. We then use an acquisition function (Sec 5.1.4) to select one of the candidates:

$$\boldsymbol{x}^* = g(\mathcal{X}_c). \tag{5.2}$$

The selected candidate is determined as the next CP, where the illuminance is measured, and the value of illuminance is used to update the surrogate function. This process is repeated iteratively until the set of the CP candidates $\mathcal{X}_c$ becomes empty.

5.1.1 Surrogate Function

The key part of determining the CPs for the illuminance measurement is the GP [71] that provides a nonparametric statistical model. The GP approximates the unknown function $f(\boldsymbol{x})$ and provides information about the uncertainty of the estimation on the basis of the collected observations $\mathcal{D}$, which is a database containing tuples of positions and observations:

$$\mathcal{D} = \{(\boldsymbol{x}_1, f(\boldsymbol{x}_1)), \ldots, (\boldsymbol{x}_m, f(\boldsymbol{x}_m))\}\,, \tag{5.3}$$

where m refers to number of observations. Database $\mathcal{D}$ is used to calculate the CPs during illuminance measurements. The GP provides an approximation of the function $f(\boldsymbol{x})$ and is completely specified by its mean and covariance functions:

$$\hat{f}(\boldsymbol{x}) \sim \mathcal{GP}(\text{mean}(\boldsymbol{x}), k(\boldsymbol{x}, \boldsymbol{x}')), \tag{5.4}$$

where $\hat{f}(\cdot)$ is an approximation of the function $f(\cdot)$, and $k(\cdot,\cdot)$ is a covariance function. We use the zero mean function $\text{mean}(\boldsymbol{x}) = \boldsymbol{0}$, from now on. For the covariance function, we use the squared exponential kernel [71], defined as:

$$k(\boldsymbol{x}_p, \boldsymbol{x}_q) = \sigma_a^2 \exp(-\frac{1}{2\sigma_l^2} \|\boldsymbol{x}_p - \boldsymbol{x}_q\|^2) + \delta_{pq}\sigma_n^2\,, \tag{5.5}$$

where σ_a, σ_l, and σ_n are hyperparameters representing amplitude, length scale and noise of the kernel, and δ_{pq} is the Kronecker delta function. We describe

the approach for selecting the hyperparameters in Sec. 5.1.2. A modified version of the squared exponential kernel that is used to handle occlusions caused by room walls is described in Sec. 5.1.3, thus respecting the walls of the room by the surrogate function.

The posterior probability density of the approximation function given test point $\tilde{\boldsymbol{x}} \in \mathbb{R}^2$ from database $\mathcal{D}$ is calculated as:

$$p(\hat{f} \,|\, \tilde{\boldsymbol{x}}\,,\, \mathcal{D}) = \mathcal{N}(\mu(\tilde{\boldsymbol{x}}), \sigma^2(\tilde{\boldsymbol{x}}))\,, \tag{5.6}$$

where $\mathcal{N}$ represents the normal distribution with mean μ and variance σ^2. The mean and the variance are computed as [71]:

$$\mu = \boldsymbol{k}_{\mathcal{D}}^{\top} K_{\mathcal{D}}^{-1} \boldsymbol{f}_{\mathcal{D}}\,, \tag{5.7}$$

$$\sigma^2 = k(\tilde{\boldsymbol{x}}, \tilde{\boldsymbol{x}}) - \boldsymbol{k}_{\mathcal{D}}^{\top} K_{\mathcal{D}}^{-1} \boldsymbol{k}_{\mathcal{D}}\,, \tag{5.8}$$

where $\boldsymbol{k}_{\mathcal{D}}$ and $\boldsymbol{f}_{\mathcal{D}}$ are vectors with the i-th entry computed from the i-th database point:

$$k_{\mathcal{D}}^{i} = k(\boldsymbol{x}_i, \tilde{\boldsymbol{x}}), \quad f_{\mathcal{D}}^{i} = \boldsymbol{f}(\boldsymbol{x}_i), \quad \boldsymbol{x}_i \in \mathcal{D}, \tag{5.9}$$

and the ij-th entry of matrix $K_{\mathcal{D}}$ is computed as:

$$K_{\mathcal{D}}^{ij} = k(\boldsymbol{x}_i, \boldsymbol{x}_j), \quad \boldsymbol{x}_i, \boldsymbol{x}_j \in \mathcal{D}. \tag{5.10}$$

We can therefore compute a prediction of the mean and the uncertainty at any point. A visualization of these values (mean and uncertainty) for a particular one-dimensional GP is shown in Fig. 5.1. Fig. 5.1 shows a visualization of the surrogate function for a one-dimensional example where the surrogate function (green) is computed. The measurements (black dots) are used to predict the mean value (blue, dashed) along with the 4σ confidence area (blue, shaded). The predicted illuminance value tends to approach zero if there is no close measurement. This behaviour is caused by the zero mean function, ensuring that the predicted value represents the lower bound.

Mean μ and two standard deviation σ are used to compute the proposed surrogate function, that is defined as a lower bound estimate:

$$\hat{f}_{lb}(\boldsymbol{x}) = \mu(\boldsymbol{x}) - 2\sigma(\boldsymbol{x})\,. \tag{5.11}$$

The probability that the function lies below the true value is based on the normal (Gaussian) distribution [28, 26], where 2σ correspond to 95% probability of occurrence of the searched value. Thus, this function is exploited to compute candidates for the next CP according to Eq. (5.1). The visualization of the surrogate function is shown in Fig. 5.2. In this figure (Fig. 5.2), the dashed black line represents the threshold value τ and divides the room into areas above the threshold τ (red) and areas below the threshold τ (blue). The color changes from dark red (representing maximum with 1000 lx) to light red (above threshold τ 500 lx) and then below the threshold τ from light blue (below 500 lx) to dark blue (minimum 0 lx). The same color scale is used for all figures in this section.

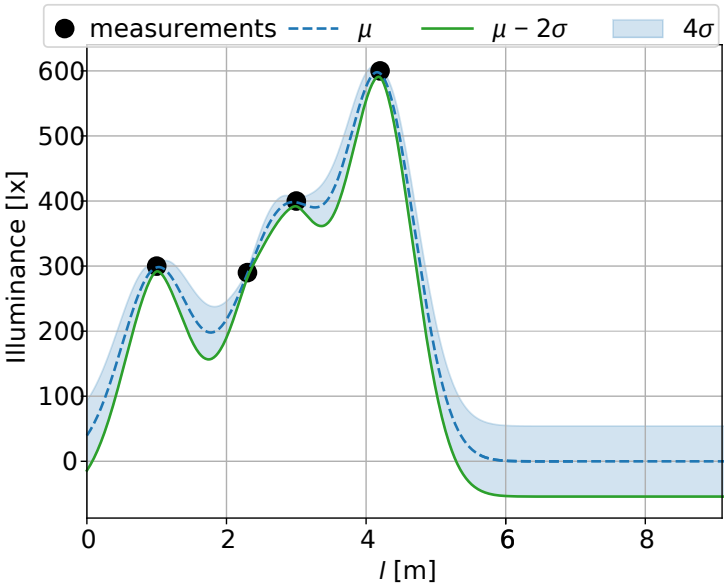

Figure 5.1: Example of 1D GP [15].

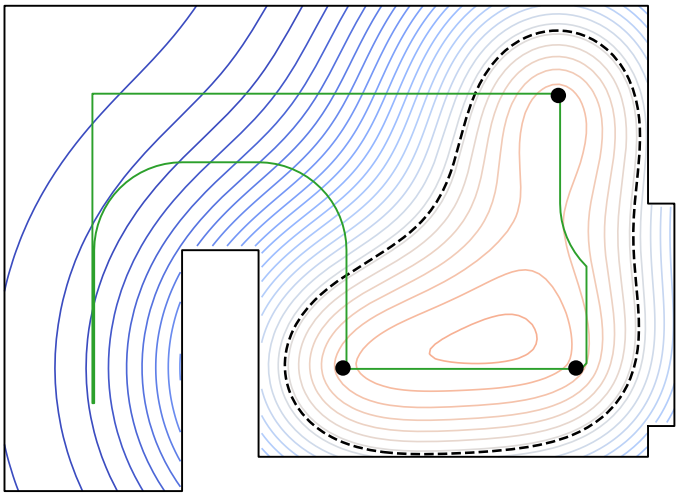

Figure 5.2: The two-dimensional surrogate function is visualized without handling occlusions [15].

5.1.2 Selecting Hyperparameters

Hyperparameter values, i.e., amplitude, length scale, and noise, are required for computing the surrogate function. The noise of the kernel is estimated manually based on the uncertainty of the photometer used in our experiments. The amplitude and the length scale are found by maximizing the marginal log likelihood [71] of data generated from the simulation of the illuminance via Dialux simulation program [32]. The simulated data are produced by placing a single luminaire in an empty space, i.e., a room without walls. In the Dialux program [32], a room is configured as a space with one luminaire and black walls that do not reflect any light, to obtain illuminance values emitted by the

luminaire. The illuminance values collected from the simulation are stored in database $\mathcal{H}$, as follows:

$$\mathcal{H} = \{(\boldsymbol{x}_1, f(\boldsymbol{x}_1)), \ldots, (\boldsymbol{x}_n, f(\boldsymbol{x}_n))\}, \tag{5.12}$$

where $f(\boldsymbol{x}_i)$ is the simulated illuminance value obtained for position $\boldsymbol{x}_i$. Positions $\boldsymbol{x}$ are selected in the room so that they form a rectangular network, i.e., similar as Fig. 2.1. Database $\mathcal{H}$ is used for training a virtual model of the measured luminaire. From database $\mathcal{H}$, the logarithmic probability of the model for given hyperparameters can be calculated as:

$$\log p(\boldsymbol{f}_\mathcal{H}|\sigma_a, \sigma_l) = -\frac{1}{2}\boldsymbol{f}_\mathcal{H}^\top K_\mathcal{H}^{-1}\boldsymbol{f}_\mathcal{H} - \frac{1}{2}\log|K_\mathcal{H}| - \frac{n}{2}\log 2\pi, \tag{5.13}$$

where terms $\boldsymbol{f}_\mathcal{H}, K_\mathcal{H}$ are obtained from Eq. (5.9) and Eq. (5.10), while assuming $\mathcal{H} = \mathcal{D}$. The derivation of this equation can be found, for example, in [71]. The hyperparameters are found by maximizing the logarithmic probability (5.13) via a numerical optimization technique [72]. Hyperparameter values that maximize the probability are used later for the experiments. The luminaire during the simulation is assumed to correspond to the real room luminaires. Therefore, the hyperparameters specify prior knowledge about the illuminance variation in the environment.

5.1.3 Handling Occlusion

The squared exponential kernel measures the similarity of the illuminance value based on the Euclidean distance between two positions. Therefore, the walls that lie in between these positions are ignored, as only distance is considered. This results in a situation where the value measured on one side of the wall affects the value obtained by surrogate function on the other side as visualized in Fig. 5.2. To resolve this issue, we use a modified kernel matrix that uses a ray tracing function to check if there is direct visibility between two points:

$$k'(\boldsymbol{x}_p, \boldsymbol{x}_q) = \begin{cases} k(\boldsymbol{x}_p, \boldsymbol{x}_q), & \text{if there is direct visibility,} \\ 0 & \text{otherwise,} \end{cases} \tag{5.14}$$

where $k(\cdot,\cdot)$ is the square exponential kernel defined in Eq. (5.5). This modification results in the surrogate function considering the room wall as shown in Fig. 5.3 and not ignoring the wall as in Fig. 5.2.

5.1.4 Acquisition Function

The acquisition function selects the location of the CP from candidates in set $\mathcal{X}_c$. In practical applications, special attention is given to the boundary of the measurement area $\partial\mathcal{I}$, because the boundary $\partial\mathcal{I}$ is closest to the obstacles (walls $\partial\mathcal{P}$), the measured illuminance values on $\partial\mathcal{I}$ are most affected by the reflections from the obstacles and are thus different from the illuminance values in the inner part of the measurement area $\mathcal{I}$. Therefore the CPs

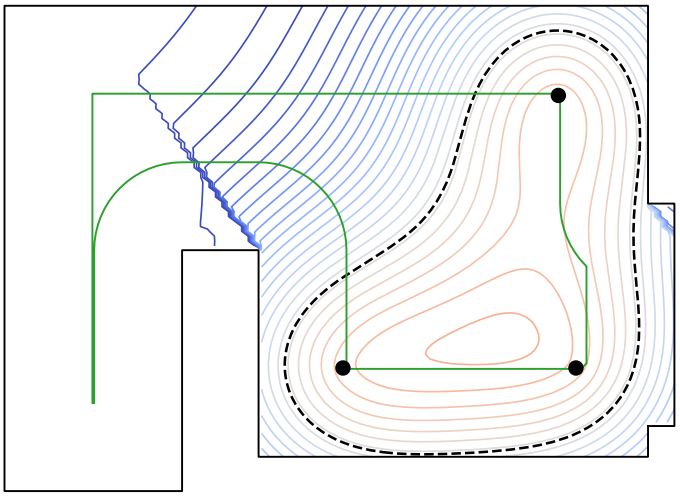

Figure 5.3: The two-dimensional surrogate function is visualized with occlusion handling [15].

are selected first on the boundary $\partial\mathcal{I}$ by filtering the CP candidates. After the illuminance value along the entire boundary $\partial\mathcal{I}$ has been verified, the algorithm continues with the remaining candidates.

The acquisition function that uses the illuminance propagation model selects the new CP so that it is at the maximum distance from the CPs that have already been collected (measured):

$$\boldsymbol{x}^* = \arg\max_{\boldsymbol{x}_i \in \mathcal{X}_c} \min_{\boldsymbol{x}_j \in \mathcal{D}} d(\boldsymbol{x}_i, \boldsymbol{x}_j)\,, \tag{5.15}$$

where $d(\cdot,\cdot)$ represents the Euclidean distance. The proposed heuristic selection results in a small number of the CPs, but it requires the mobile platform to travel a large distance. The heuristic is based on the assumption that the speed of the mobile robot is faster than the measurement process. Another heuristic can be designed to take the measurement/travelling trade-off into account. For example, one can select the CP candidate that is closest to the location of the last the CP. The distance to be traveled will then be small, but more the CPs will be required for the validation process.

5.2 Proposed algorithm

This section provides an illustrative explanation of the proposed solution for automatic determination of the CPs, where autonomous measurement of illuminance in the interior is performed. The developed method of determining the CPs for illuminance uses a statistical model built based on the observations as visualized by the contour graph in Fig 5.4. Fig. 5.4a shows collected observations (black dots) by the mobile platform in the third iteration of automatic illuminance measurement via the robotic platform. From the virtual model of the measured luminaire and a simulated propagation of light emitted from this luminaire, we predict which parts of the room have a high

probability of satisfying the illuminance level requirement (red). The next the CP (red cross) to be measured is selected in an area which has not yet satisfied the requirements (blue). The robotic platform plans a collision-free trajectory (purple dashed curve) to the selected point and moves to the desired location. Fig. 5.4b shows the automated measurement proceed in the next (fourth) measurement iteration. A new observation is collected and is used to update the model for the next iteration.

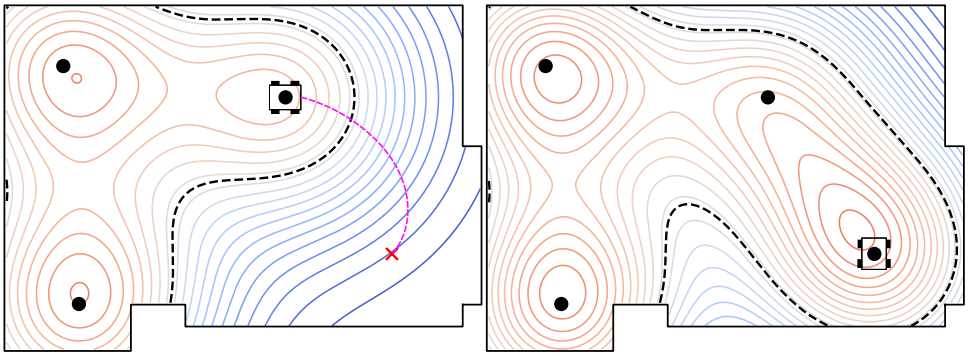

(a) : 3rd iteration. **(b) :** 4th iteration.

Figure 5.4: The overview of one iteration in the measurement process of illuminance [15].

The virtual model of the measured luminaire is represented by the surrogate function of the GP, with lower bound $\hat{f}_{lb}$ defined by the Eq. (5.11) subtracting two standard deviations σ from the mean μ. This model is part of the proposed (novel) solution. Two versions of the novel solution (algorithm) for measurement the illuminance have been designed.

The first version of the algorithm checks if the measured illuminance is above the required threshold τ everywhere in the measured area $\mathcal{I}$ of the room. If this is satisfied, the room passes the verification audit. However, if there exist is the CP where the illuminance is below the threshold τ, the algorithm terminates, and the measured room does not pass the verification audit.

An example of the first algorithm determining the CPs in a one-dimensional environment is shown in Fig. 5.5 where a green curve represents the lower bound $\hat{f}_{lb}$ of the model, the blue dashed line represents the model's mean μ and an expanding standard deviation σ of the model, and black dashed line specifies threshold τ (100 lx). Fig. 5.5 shows the state reached by the algorithm in the fourth iteration in which the illuminance at the CP is measured to be of value 600 lx. Moreover, as the virtual model is updated, it can be seen that the following the CP is placed in the red cross location as this is the place where the illuminance requirements are not met for the first time in the direction of the measuring the measurement area $\mathcal{I}$. In this example, the acquisition function from Sec. 5.1.4 does not apply.

The first version of the algorithm in a two-dimensional environment follows the same principle as in the one-dimensional environment by first verifying that there is no point below the specified threshold τ at the boundary of the

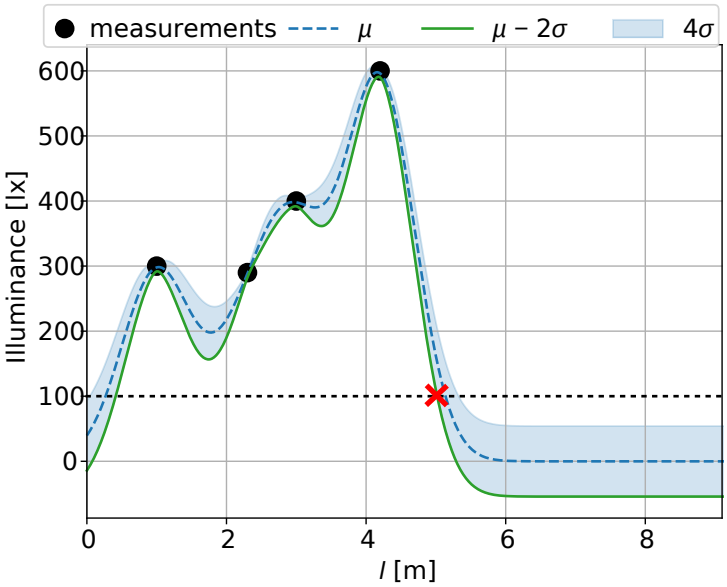

Figure 5.5: Example of determining the CPs for the first version of the algorithm in a 1-D environment.

measurement area of the room defined by the $\partial\mathcal{I}$. Subsequently, the inner part of the measurement area $\mathcal{I}$ is verified. If there is no the CP where the illuminance value is measured below a specified threshold τ, the verification process ends successfully; otherwise the room does not pass the audit.

The second version of the algorithm terminates when the maximal standard deviation σ in the virtual model is below a specified threshold of the standard deviation τ_σ. Note that standard deviation σ in the model represents the uncertainty of the model itself. Therefore, when standard deviation σ decreases, the uncertainty about the illuminance value in the measured area $\mathcal{I}$ decreases as well. By a proper setting of threshold τ_σ, the accuracy of the measurement can be adapted to the client's audit requirements. Apart from this termination condition, the second algorithm terminates if the measured average value of the illuminance is above the required threshold τ, thus, passing the verification audit. Similarly as in the first algorithm, the second algorithm starts measuring at the $\partial\mathcal{I}$ until the standard deviation σ of the virtual model is below τ_σ, then it continues measuring in the area denoted by the inner part of the measurement area $\mathcal{I}$.

Fig. 5.6 shows an example of determining the CP in the fourth iteration for the second version of the algorithm in a one-dimensional environment, where the acquisition function from Sec. 5.1.4 does not apply. After the fourth iteration, the lower bound $\hat{f}_{lb}$ decreases below 0 lx. Moreover, it is clear that the standard deviation of the model increases by moving further away from the existing the CPs. This is clearly seen by moving from the fourth the CP from left to right by increasing l. Thus, by considering l of 6 m or more meters, we can see a high increase in the standard deviation σ, above the τ_σ (equal to 10 lx in this example). Therefore, the second algorithm places next

the CP to the first distance (l) where this threshold τ_σ is exceeded, as can be seen from the red cross at $l = 6$ m. This process continues until one of the terminating conditions it met.

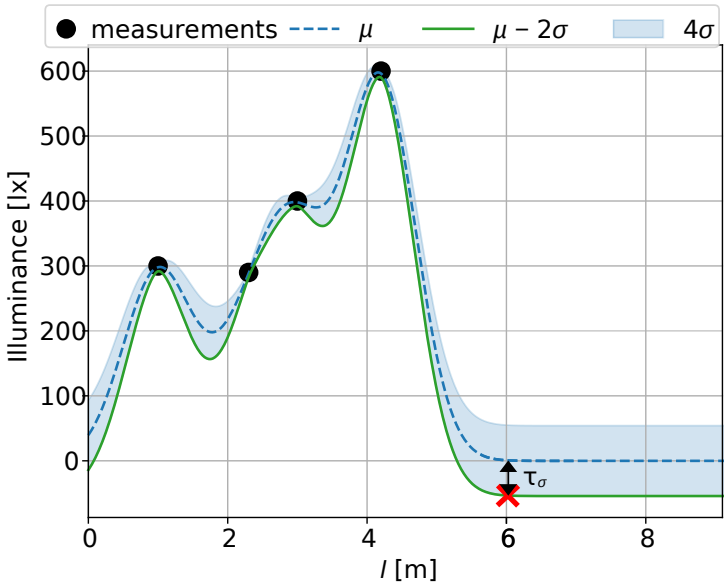

Figure 5.6: Example of determining the CPs for the second version of the algorithm in a 1-D environment.

For further use, it is advisable to define of the algorithm values, called input parameters for each version, that are necessary to calculate the CPs. The first version of the algorithm uses as input parameters the measured value of the illuminance at the CP, obtained from the photometer. Another input parameter is the set threshold τ for all the CPs in the measurement area $\mathcal{I}$, determined by the standard [1]. Further input parameters are the polygon of the measured room $\mathcal{P}$, which is obtained by mapping the room using a mobile platform, and the distance of the measurement area boundary $\partial\mathcal{I}$ from the wall (boundary of the polygon $\partial\mathcal{P}$) determined by the standard [1]. The second version of the algorithm uses as input parameters the measured value of the illuminance at the CP, a set threshold τ for the measured average value of the illuminance in the entire measurement area $\mathcal{I}$ determined by the standard [1]. Furthermore, it is the polygon of the measured room $\mathcal{P}$, the distance of the boundary of the measurement area $\partial\mathcal{I}$ from the wall (boundary of the polygon $\partial\mathcal{P}$) and the set threshold of the standard deviation τ_σ.

5.2.1 Estimating the Number of Control Points

The number of the CPs required for verifying the illuminance level is unknown for the proposed method, because the CPs are selected on the basis of the previous measurements. Nevertheless, it may be useful to make at least a rough estimate of the number of the CPs required to pass the audit. We can estimate this number during the verification process (during the measurement

process) by assuming that the illuminance value in the room does not change significantly. This assumption is often satisfied in real environments because humans do not desire a sudden change in the illuminance value in the room. Based on this assumption, in each iteration of the verification process, the number of required the CPs is estimated as follows: initially, the average illuminance value from the previously measured values is computed in the current verification process. Then the positions of the virtual the CPs are iteratively computed, and the computed average illuminance is assumed to be measured at this the CP. The virtual the CPs are added to the virtual model until the room passes the audit, i.e., the room passes the audit when the conditions imposed by either the threshold or the average illuminance value are met. The number of required iterations correspond to the estimated number of the CPs required to pass the audit.

5.2.2 Implementation of the Proposed Solution

The proposed solution for determining the CPs at which the illumination measurements are performed is implemented to a program that is run in the control computer of the robotic units. The program was implemented for each version of the algorithm. The first version was programmed and tested to verify the correctness of the proposed solution. Part of this version was a new method of determining the CPs using the virtual model of the measured luminaire and a simulated propagation of light emitted from this luminaire. This model is created based on the GP and simulated lighting data from the Dialux program [32]. The TensorFlow library [73] was used to implement the first version, and the algorithm was loaded into the first robotic unit for testing.

The second version uses the same tools as ExactGPModel [74] and FixedNoiseGaussianLikelihood [75], but the second version uses the newer PyTorch library [76], which is more suitable for the python programming environment. The second version was tested on the second robotic unit. The second robotic unit was also equipped with software for extracting the floor plan of the map and its approximation to obtain the polygon of the measured room [14]. This created a comprehensive measurement process, which consisted of mapping the room, processing this map into a polygon of the measured room and finally measuring this room.

The difference between the program versions is only in the termination conditions, as stated in Sec. 5.2. Therefore the program can be described by a simplified diagram, which contains the main functions, which are shown in Fig. 5.7. The diagram provides an overview of the main functions and their interconnection as the program passes from one function to another.

The proposed program starts when the robotic unit is placed in the room and loads the virtual model of the measured room, e.g., room dimensions, luminaire model. In the *Measured room* function, the robotic unit initiates the measurement, establishes communication with the photometer, and verifies that the photometer is set to send data. It also creates a database of candidates for the CPs. After initialization, the program continues with the

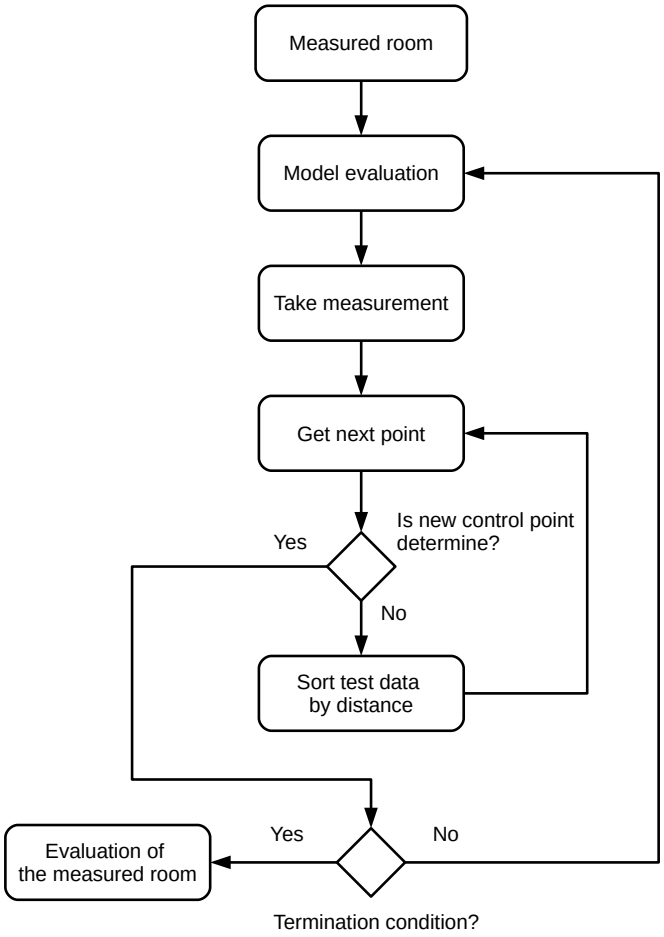

Figure 5.7: Implementation of the program for measurement of illuminance.

Model evaluation function, which controls the entire measurement process. The *Model evaluation* function evaluates whether the terminating condition has not occurred for the end of the entire measurement process. It also initiates the movement of the robotic unit with the measurement device to the new CP. When the robotic unit reaches the new CP, function *Take measurement* is called to process the measurement. The *Take measurement* function obtains the illuminance value from the photometer and uses the obtained illuminance value to update the model. The updated model is used to calculate the next CP.

Two functions provide the process of determining the next CP. The first function called *Get next point* determines the next CP first from the boundary of the measurement area $\partial\mathcal{I}$ and then from the inner measurement area $\mathcal{I}$. In order for the program to select another the CP, the candidates for the CPs must be sorted. The *Sort test data by distance* function is used for sorting, which sorts candidates for the CPs according to the distance from already determined the CPs. The *Get next point* function then selects the candidate for the CP that has the greatest distance and declares it the next CP. The program then switches to the *Model evaluation* function, and the

entire process is repeated.

5.3 Experimental Evaluation of the First Version of the Algorithm

The proposed solution for determining the CPs is evaluated via various experiments. The experiments are divided into simulated experiments and real robotic experiments. The experiments use the first version of the algorithm, which verifies that the illumination in the measurement area of the room is above a set threshold. This section also includes a description of the robotic units, estimation of the time required for completing the audit of the room (verification of the room light system) and an estimate of the number of the CPs determined by the proposed solution.

5.3.1 Simulated Experiments

The verification of the proposed solution is done at first by simulated experiments. The simulated experiments use Dialux software [32] for simulating the light emitted from the luminaires. The type of the luminaires is the same for all of the simulated experiments: a *Modus LLX 236 AL* [77] fluorescent tube, which are installed in the real measured rooms. The threshold of illuminance τ is set to 500 lx for all experiments. This value is the required average illuminance value for office environments, as specified in [5]. Nevertheless, in simulated experiments, it is verified that the measured illuminance in the measurement area of the room is above the threshold value, not only the average illuminance. Several simulated experiments have been carried out:

- four experiments in a real room visualized in Fig. 2.3. The dimensions of this simulated real room correspond to the real dimensions of the room with an area of 39 m^2 (7.5×5.5 m), and
- one experiment in a larger room with an area of 235 m^2 (15×17.5 m).

In all the simulated rooms, the boundary of the measurement area $\partial\mathcal{I}$ is set to 1 m from the wall or column as specified by the standard [7].

The Initial Experiment of the Algorithm

The verification that the algorithm correctly determines the CPs at the boundary of the measurement area $\partial\mathcal{I}$ using the acquisition function (Sec. 5.1.4) is depicted in Fig. 5.8, where the left subfigure shows the top view of the tested room view and the right subfigure shows the measured illuminance on the inner ring, i.e., $\partial\mathcal{I}$. In Fig. 5.8a, the green dot is the first CP, the blue curved line shows the room's boundary $\partial\mathcal{P}$, and the orange curved line shows the boundary of the measurement area $\partial\mathcal{I}$. In Fig. 5.8b the x-axis represents the distance from the first CP, while the measurement area boundary $\partial\mathcal{I}$ being called the inner ring in this experiment because it is a closed curved

line. The blue curved line is mean μ, the orange curved line is the lower bound $\hat{f}_{lb}$, the green line is the illuminance threshold τ, the black crosses are the measurement points (the CPs) and the blue shaded curved line is the confidence area 4σ.

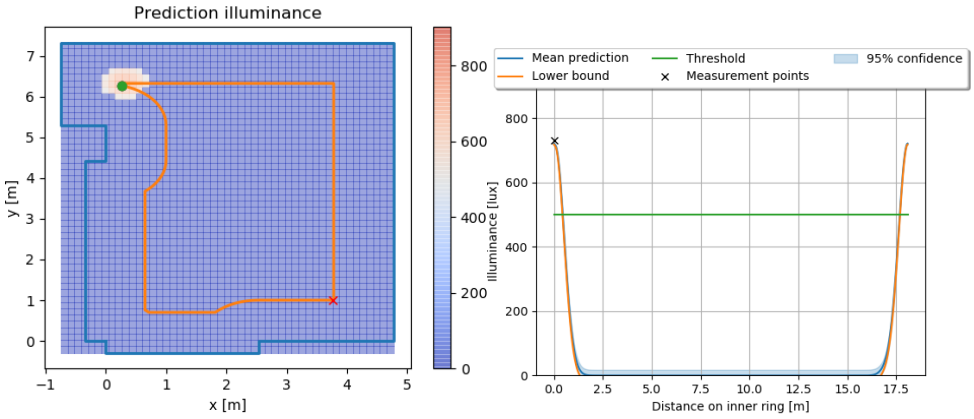

(a) : The surrogate function visualization on the tested room.

(b) : The surrogate function value on the inner ring.

Figure 5.8: The initial experiment of the algorithm with a partial measurement process – 1st iteration.

Fig. 5.9a shows the surrogate function of the simulation of for the eighth iteration of the measurement at the boundary of the measurement area $\partial\mathcal{I}$. The CPs are located at the Measurement points (black crosses) and it is clearly visible that the longest distance between two consecutive measurements is between the second and third measurement, i.e., the second and the third black cross from the left. Therefore the algorithm should add the CP between these two the CPs according to Eq. (5.15). The situation, after adding the CP to the designated position is shown in Fig. 5.9b, that shows the ninth iteration.

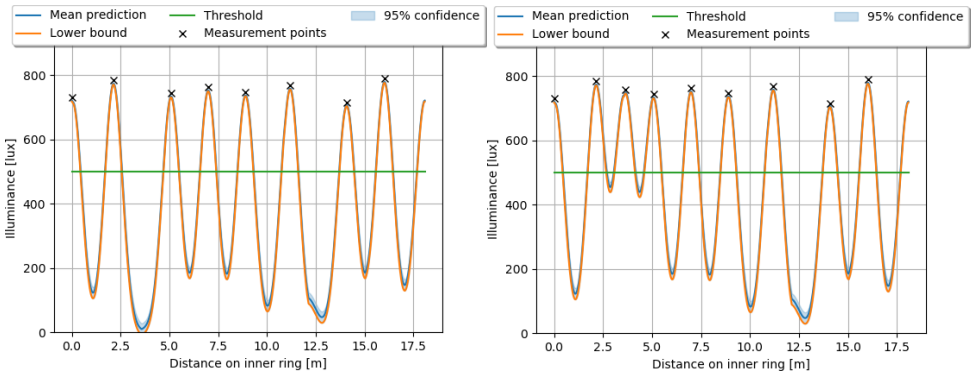

(a) : 8th iteration.

(b) : 9th iteration.

Figure 5.9: The initial experiment of the algorithm with a partial measurement process – 8th iteration and 9th iteration.

Fig. 5.10 shows the process end in the twentieth iteration. The right subfigure shows that the surrogate function (lower bound $\hat{f}_{lb}$) is above a specified threshold τ (500 lx) in the entire inner ring. The left subfigure also shows a colored background above the set threshold of illuminance τ.

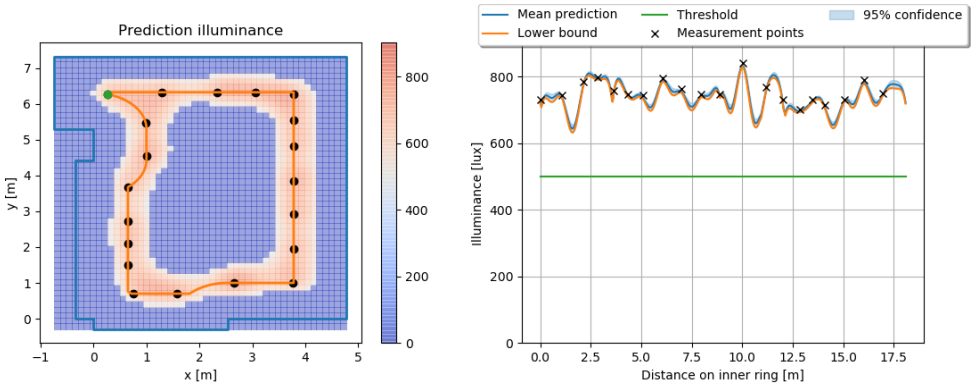

Figure 5.10: The initial experiment of the algorithm with a partial measurement process – 20th iteration.

The experiment proved that the algorithm determines the CPs according to Eq. (5.15), described in Sec 5.1.4. If the algorithm decides only based on measurements at the boundary of the measurement area $\partial\mathcal{I}$, the room passes the audit. This simulation of the surrogate function view is used only during this experiment. Subsequently, only the room view is used in all other experiments.

Evaluation of the Algorithm in Ideal Conditions

In this section, we verify that the algorithm works according to Sec. 5.2.2 and determines the CPs according to Sec. 5.1.4. The verification is done by checking, that the algorithm first determines the CPs at the boundary of the measurement area $\partial\mathcal{I}$ and then in the inner part of the measurement area $\mathcal{I}$. Furthermore, the algorithm has to decide whether the measured room passes or not the audit.

The verification is done via two experiments in which we vary the position of the luminaires. In the first experiment, nine luminaires are distributed uniformly in the room, creating the basic (first) scenario of illuminance distribution. The locations correspond to the distribution of the luminaires in the room visualized in Fig. 5.11 where red rectangles indicate the luminaires. The proposed verification algorithm determines the surrogate function (Fig. 5.12), where the simulated illuminance values from program Dialux [32] are shown in Fig. 5.12a. It is worth noting that the illumination distribution in Fig. 5.12a is created by an algorithm based on illumination data from the Dialux program [32] that corresponds to the illumination distribution in Fig. 5.11. The following figures (Fig. 5.12b to Fig. 5.12d) show the surrogate function (the lower bound $\hat{f}_{lb}$) where the CPs are determined on the boundary of the measurement area $\partial\mathcal{I}$. The calculation of new the CPs at the boundary

ends after the lower bound $\hat{f}_{lb}$ is above the threshold τ (Fig. 5.12e). The threshold τ is set to 500 lx in the entire boundary of the measurement area $\partial\mathcal{I}$. The CPs are determined inside the measurement area $\mathcal{I}$ in Fig. 5.12f and Fig. 5.12g until the entire measurement area $\mathcal{I}$ is verified (Fig. 5.12h). As no value below the threshold τ is observed, the room passes the audit. As already described in Sec. 2.1.1, there are three standardized reasons to perform an audit of the lighting system.

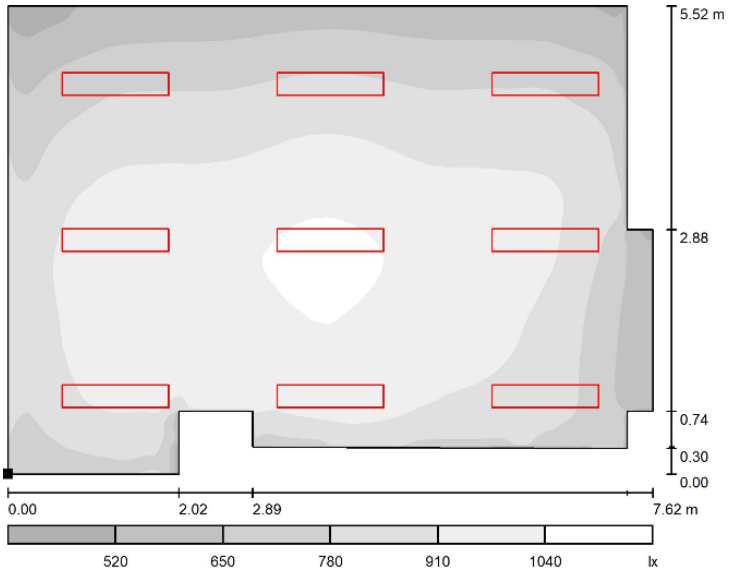

Figure 5.11: Placement of the luminaries in the Dialux program [32] for the evaluation of the algorithm in ideal conditions.

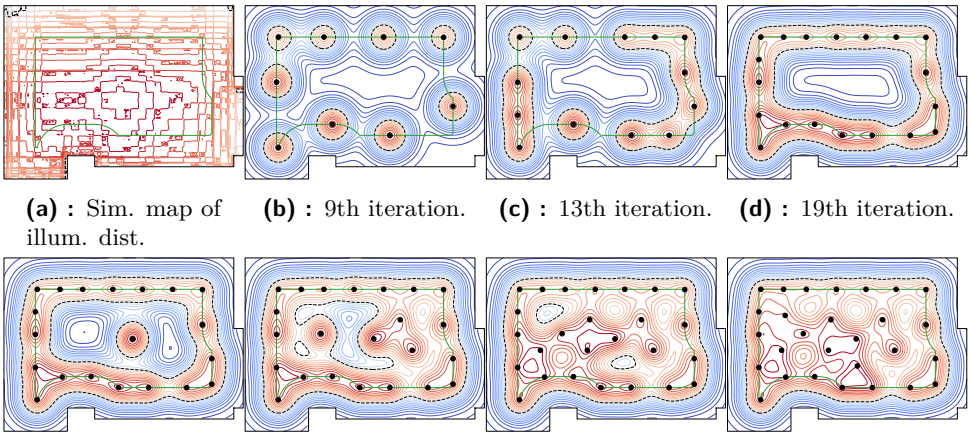

(a) : Sim. map of illum. dist. **(b) :** 9th iteration. **(c) :** 13th iteration. **(d) :** 19th iteration.

(e) : 20th iteration. **(f) :** 23rd iteration. **(g) :** 26th iteration. **(h) :** 28th iteration.

Figure 5.12: Experiment of the algorithm evaluation in ideal conditions. The room passes the audit [15].

The results of this experiment validate the correct implementation of the first version of the algorithm according to Sec. 5.2.2. It can be seen from Fig. 5.12 that the CPs are placed according to the logical sequence. This

means that the algorithm always determines a new CP, that is furthest from the already determined CPs (see Sec. 5.1.4). The new CPs are first determined at the boundary of the measurement area $\partial\mathcal{I}$, until the boundary is covered by the CPs. Then the new CPs are determined in the inner part of the measurement area $\mathcal{I}$. Further description is given in Sec. 5.2. Also, one part of this experiment was to check the algorithm to see if it could determine the CPs even in a more complex room. Therefore, the polygon shown in Fig. 2.3 was intentionally used for the first experiment to obtain a more complex room corresponding to real conditions.

Evaluation of the Termination Condition

To evaluate the functionality of the terminal conditions two luminaries from the previous experiment are turned off, and thus a modified (second) scenario for the distribution of illuminance is created, which is shown in Fig. 5.13. This creates a large area extending into the inner (measurement) area, where the illuminance is below the threshold τ of 500 lx. The illuminance distribution is shown in Fig. 5.14a. Fig. 5.14b shows the start of the measurement process, i.e., the first iteration, when the measured illuminance value is much higher than the set threshold τ. Fig. 5.14c shows the second iteration where the measured value of illuminance approaches the set threshold because the black dashed line (representing the threshold) is much closer to the CP than in the first iteration. This can also be seen in Fig. 5.14a, where higher illuminance values above a set threshold τ change to dark red. The first version of the algorithm found that the value was below the threshold τ in the third iteration (Fig. 5.14d) and reported that the room should not pass the specified audit.

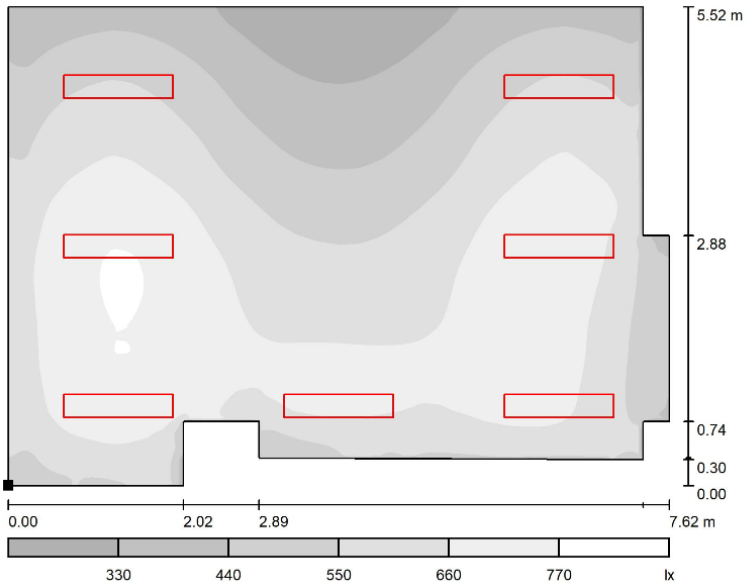

Figure 5.13: Placement of the luminaries in the Dialux program [32] for the evaluation of the termination condition.

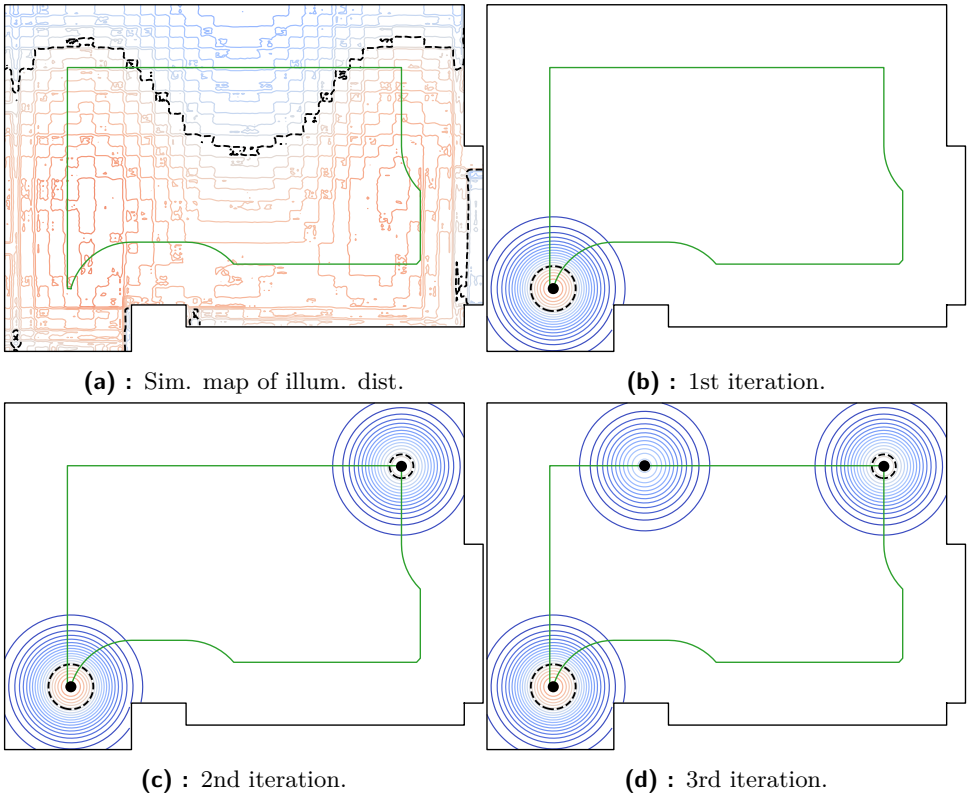

(a) : Sim. map of illum. dist. **(b) :** 1st iteration.

(c) : 2nd iteration. **(d) :** 3rd iteration.

Figure 5.14: The third simulated illuminance experiment. The room therefore does not pass the audit [15].

Evaluation of the Control Points Placement Adaptation

In the fourth simulated experiment, a more challenging scenario (third) is created, as shown in Fig. 5.15. Only a small area inside the inner (measurement) area $\mathcal{I}$ is below threshold τ in this scenario, which is shown in Fig. 5.16a. In addition, many measured values are close to the threshold. The algorithm determines fewer the CPs in the area where the illuminance value is high (vertical boundaries of the measured area $\partial\mathcal{I}$). However, more the CPs are determined where the value is closer to the threshold τ (horizontal boundaries of the measured area $\partial\mathcal{I}$) a more detailed description is given in Sec. 5.2. The algorithm successfully adapted the distance between the CPs based on the measured value of illumination and the set threshold τ to verify the illuminance distribution in this challenging scenario. The locations of the CPs and the visualization of the lower bound $\hat{f}_{lb}$ are visualized in Fig. 5.16b and Fig. 5.16c. Finally, as shown in Fig. 5.16d, the illuminance value is found to be below the threshold τ, suggesting that the room should not pass the audit after the thirty-seventh iteration.

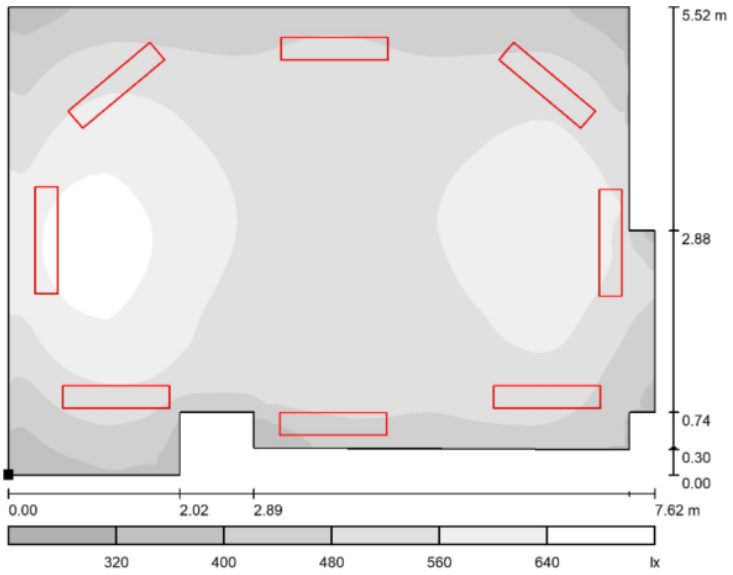

Figure 5.15: Placement of the luminaries in the Dialux program [32] for the evaluation of the CPs placement adaptation.

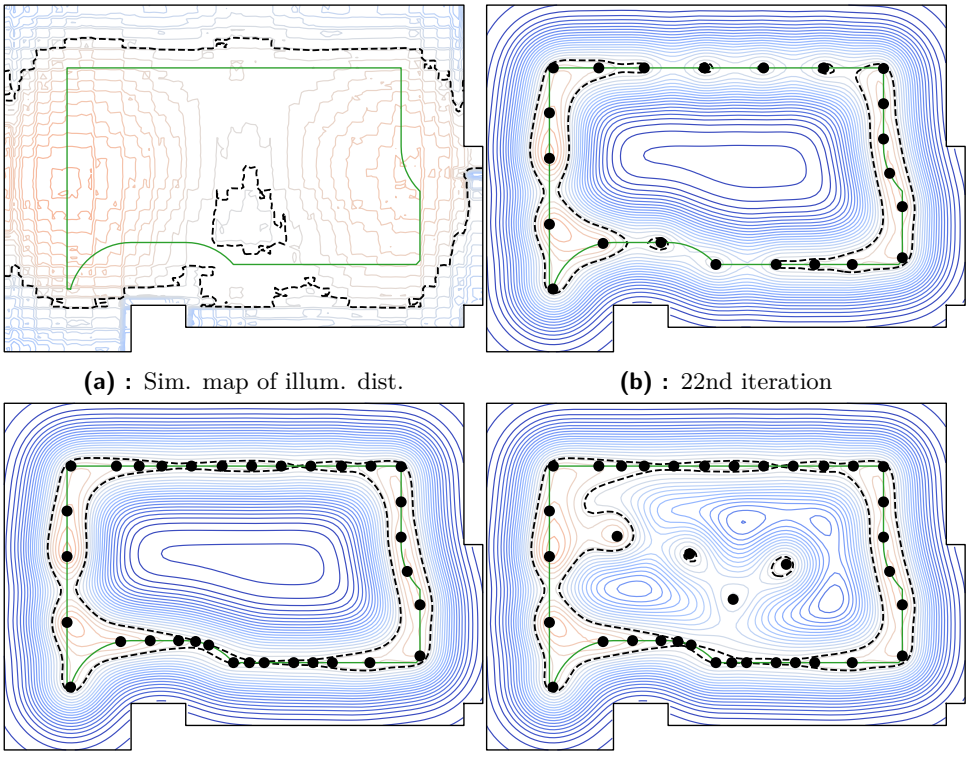

(a) : Sim. map of illum. dist. **(b) :** 22nd iteration

(c) : 33rd iteration **(d) :** 37th iteration

Figure 5.16: The fourth simulated illuminance experiment. The room therefore does not pass the audit [15].

Evaluation of the Algorithm in a Complex Floor Plan

The algorithm has been evaluated in the smaller room without any obstacle. However, in the real-world in the rooms some obstacles can be found. Therefore, a larger room with a multifaceted floor plan is selected and evaluated. In the larger room a column is added to test if the algorithm properly adapts to the presence of a column in the calculation. This room is used for evaluation of the algorithm in a complex floor plan, which is shown in Fig. 5.17. The luminaires are evenly distributed in the room (Fig. 5.17), the illuminance distribution is created via the Dialux program [32], as shown in Fig. 5.18a. Fig. 5.18b shows how the program first determined the CPs at the boundary of the measurement area $\partial\mathcal{I}$, and then Fig. 5.18c shows how the algorithm determines the CPs in the inner part of the measurement area $\mathcal{I}$. The first version of the algorithm correctly identified the column in the room and took the column into account when determining the individual the CPs. Fig. 5.18d shows how the algorithm has distributed all the CPs around the measurement area $\mathcal{I}$, and at the same time, the algorithm suggests that the room should pass the audit.

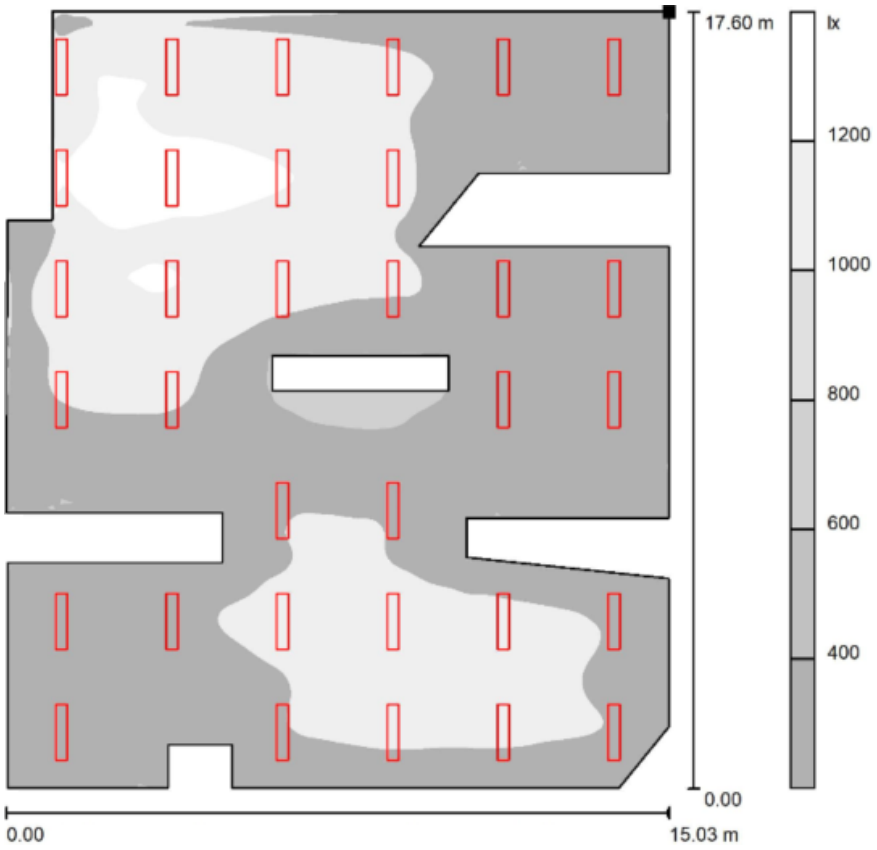

Figure 5.17: Placement of the luminaries in the Dialux program [32] for the evaluation of the algorithm in a complex floor plan.

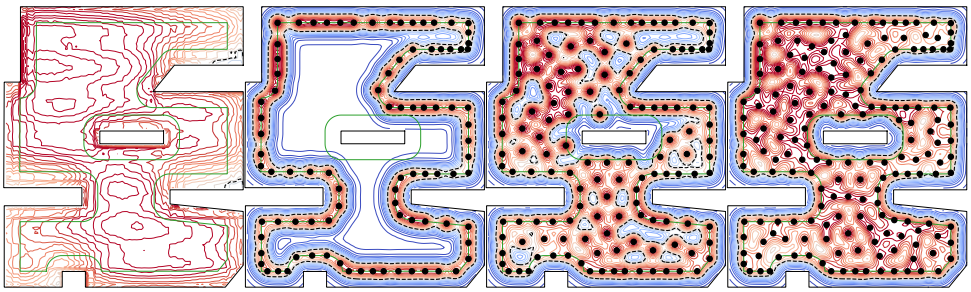

(a) : Sim. map of illum. dist. **(b) :** 89th iteration **(c) :** 134th iteration **(d) :** 177th iteration

Figure 5.18: The simulated experiment in a larger room with a column. The room passes the audit [15].

5.3.2 Robotic Units

The previous experiments were carried by means of simulation. In order to verify the algorithm in a real environment, it is necessary to perform robotic experiments that use a real mobile platform (robotic unit). The robotic unit is equipped with a photometer, moves autonomously in the measured room, and performs measurements of illuminance or noise. Two robotic units were used to test the algorithm. The first robotic unit was loaned for testing and used the first version of the algorithm (program). The second robotic unit, which exploits the second version of the algorithm, was developed during the design of the algorithm and was part of publication [11] and several bachelor's projects [12, 13, 14]. The most important advantage of the second robotic unit is its cost. To provide an insight into the cost of both robots, the first robot, based on the Jackal robotic platform (without sensors), costs € 16,450 [78]. The second robotic unit costs about € 1,550, which is ten times lower.

Although various sensors could be used for localizing the robot within the room [79, 80, 81, 82, 83], the laser rangefinder is the most common choice. Therefore, robotic units were equipped with a laser rangefinder. Both robotic units use SLAM [84, 85] to measure the floor plan of the room. In SLAM, measurements from two sources are combined in order to build the map and to localize the robot in it:

1. robot odometry, which measures the local motion of the robot based on the rotations of the wheels; and

2. the laser rangefinder, which measures the distance to other obstacles.

The robot's location is represented by the robot's location probability in the room represented by an occupancy map. This occupancy map, apart from the robot location probability, contains information about location of obstacles in the room and is created via the laser rangefinder [86]. The probability of the robot's location is updated via data from the odometry. Because the odometry measurements are taken locally, and wheel slips cannot be observed, the uncertainty of the location is increased by this update. After

each laser rangefinder measurement, the occupancy map is updated using the probability of the robot location. The laser rangefinder measurements are also used to update the robot location probability with respect to the reconstructed map. This update reduces the uncertainty of the localization.

Photometer

Both robotic units use the same measurement device - the PRC Krochmann Radio-Lux 111 photometer [31]. Fig. 5.19 shows a separate device, sensor, reduction from the RS-232 serial port to USB for communication with the control computer and an enlarged view of the device display. The device can be used for both outdoor and indoor measurements. Selected device and sensor specifications are listed in Tab. 5.1. As the photometer is subject to calibration, it is necessary to correct each measured illuminance reading to match the actual reading, according to:

$$E_i = K_{\mathrm{dj}} \cdot K_{2856\mathrm{i}} \cdot E_{\mathrm{mes}}\,, \tag{5.16}$$

where E_i is the actual illuminance value, E_{mes} is the illuminance value measured by the photometer, $K_{2856\mathrm{i}}$ is the correction coefficient for the given illuminance range, and K_{dj} is the correction coefficient of the individual source type. From the photometer calibration sheet (Appendix B), it can be seen that $K_{2856\mathrm{i}}$ is 1.029 and K_{dj} is 0.990.

Figure 5.19: The PRC Krochmann Radio-Lux 111 photometer [13].

Table 5.1: Selected specifications of the RadioLux 111 measurement instrument.

Illuminance units	Lux (lx)	
measurement range	Basic Advanced	0.01–300 000 lx 0.001–300 000 lx
Sensor	Receiving area	Diameter 8 mm
Device	Display Range change	4 digits LCD Automatic
Dimensions	Device Sensor Connecting cable	200 × 95 × 40 mm Diameter 35 mm, height 20 mm 3 m
Weight	Device Sensor	approx. 300 g approx. 100 g

First robotic unit

The first robotic unit to be used for testing was the Jackal underground mobile platform (Fig. 5.20) from Clearpath Robotics Inc. The Jackal robotic unit was equipped with a laser rangefinder for mapping and location in room and was also equipped with a Wi-Fi router for remote communication and a measurement device for measurement of illuminance. The robotic unit uses the SLAM [84, 85] to map the space and to determine its location in such a mapped space, the adaptive Monte Carlo localization [87, 88, 89, 90]. The basic parameters of the robotic unit are shown in Tab. 5.2.

Figure 5.20: Underground mobile platform Jackal.

Table 5.2: Parameters of the robotic unit Jackal.

External Dimensions	508 × 430 × 250 mm
Internal Dimensions	250 × 100 × 85 mm
Weight	17 kg
Maximum Payload	20 kg
Max Speed	2.0 m/s
Run Time (Basic Usage)	4 hours
User Power	5V at 5A, 12V at 10A, 24V at 20A

Second robotic unit

The second robotic unit was designed, developed and programmed over several years, leading to three bachelor projects [12, 13, 14]. A detailed description of the robotic unit can be found in [12]. The robotic unit consists of several parts. Fig. 5.21 shows a block diagram of the robotic unit. The control of the robotic unit is handled by the control computer that is connected to lidar, both development kits, and photometer. The lidar UTM-30LX [91] is used for localization and mapping. The complete RD02 [92] system is used for the movement, consisting of the H bridge motor drive MD25 [93] and two EMG30 motors [94]. The photometer [31] and sound level meter [95] are connected to the control computer. Arduino UNO development kits are only used to communicate and transfer information to another type of interface. The basic parameters of the second robotic unit are listed in Tab. 5.3. The robotic unit can be seen in Fig. 6.23a. Fig. 6.23b shows the power supply part and Fig. 6.23c the control part.

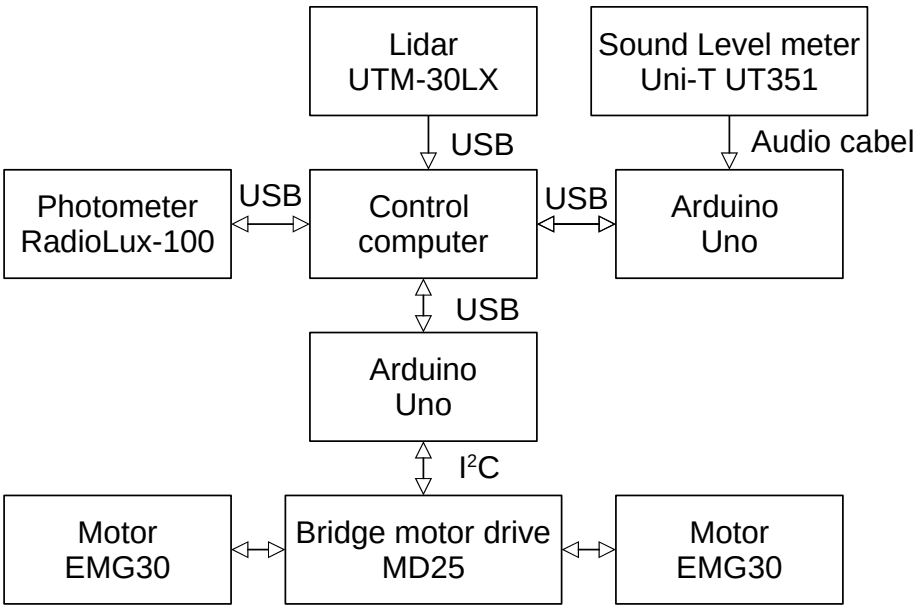

Figure 5.21: Block diagram of the second robotic unit.

Table 5.3: Parameters of the second robotic unit.

External Dimensions	440 × 300 × 180 mm
Internal Dimensions	400 × 260 × 120 mm
Weight	8 kg
Rated Speed	0.89 m/s
Max Speed	1.13 m/s
Run Time (rated load)	6 hours
Run Time (maximum load)	1 hours
User Power	12 V at 2.7 A

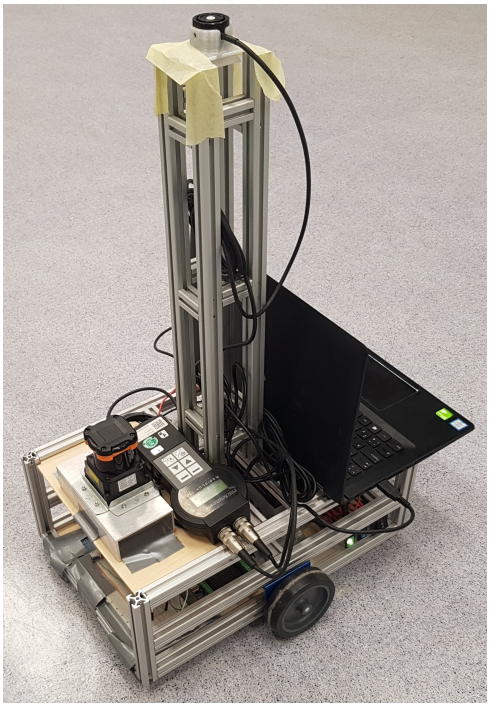

(a) : The entire second robotic unit equipped with a photometer.

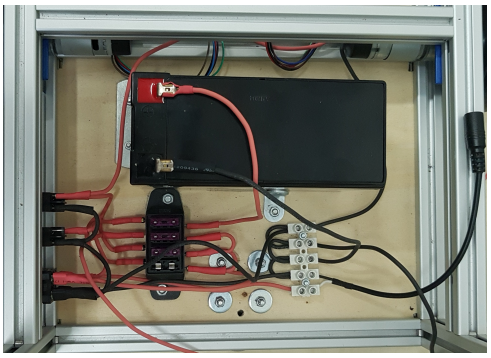

(b) : Power supply part of the robotic unit.

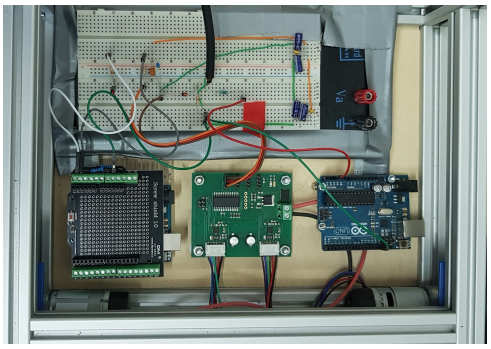

(c) : Control part of the robotic unit.

Figure 5.22: Second robotic unit.

5.3.3 Robotic Experiment

For the first real experiment, the mobile robotic platform Jackal (Sec. 5.3.2) was used. The first version of the algorithm was run in the first robotic unit. The terminating condition was determined according to Sec. 5.2 so that each measured illuminance value must be above a specified threshold τ (500 lx), and at the same time, the lower bound $\hat{f}_{lb}$ is above the threshold τ in the entire measurement area $\mathcal{I}$. The distance between the boundary of the measurement area $\partial\mathcal{I}$ and the wall ($\partial\mathcal{P}$) was set at 1 m.

In the real experiments, neither the floor plan of the room nor the true

illuminance distribution is known. First, the room for the real experiment (Fig. 5.23a) was mapped by a mobile platform equipped with a laser rangefinder. The robotic unit reconstructs a occupancy map of the room with an area of about 40 m^2 using a laser rangefinder and SLAM (Fig. 5.23b). The walls in the map (Fig. 5.23b) are represented by black color and used to construct polygon $\mathcal{P}$. The white area corresponds to the free space, and the grey area corresponds to the unknown values (not observed by the laser because the walls occlude the view).

(a) : Room used in the experiment.

(b) : Constructed occupancy map.

Figure 5.23: The room used for the experiment with mobile platform Jackal [15].

The created map of the measured room is later used for localizing the robotic unit, via an adaptive Monte Carlo localization [87, 88, 89, 90]. Similarly to SLAM, the robotic unit odometry measurements and the laser rangefinder measurements are used to update the probability of the location of the robotic unit. The robotic unit is placed in the room in an unknown position. Initially, the robot's location is unknown and is therefore uniformly distributed throughout the room. Then, based on the data from laser rotary rangefinder and the robotic unit odometry measurements, the robotic unit updates the probability distribution for each location by increasing the probability of where the robotic unit is most likely placed and decreasing the probability for all other locations. Unlike SLAM, the map of the measured room is fixed during localization. Polygon $\mathcal{P}$ is extracted from the map to select the CPs. The hyperparameters of the GP are fitted according to the data simulated by Dialux program [32] for a single luminaire in black space without light reflections. The first version of the algorithm is then used to perform the audit of the lighting system in the measured room.

In each iteration, the location of the next CP is computed by the algorithm. The robotic unit uses the map to plan a collision-free trajectory to reach the computed location of the CP. The planned trajectory is followed by the robot, and after the CP has been reached, the illuminance value is measured via the photometer. The measured value is used by the algorithm to compute the location of the next CP. The process is repeated until the room passes the audit of the lighting system or until the termination condition occurs (Sec. 5.2). The measurement process is visualised in Fig. 5.24.

The first robotic unit starts determining the CPs at the boundary of the measurement area $\partial\mathcal{I}$. Fig. 5.24a to Fig. 5.24d capture this CP determination procedure. The algorithm same determines the CPs as in the simulated experiments. In Fig. 5.24e, the robotic unit moves into the inner part of the measurement area $\mathcal{I}$ because there is no the CP at the boundary of the measurement area $\partial\mathcal{I}$ that has a lower measured value than the set threshold τ, and at the same time, there is no lower bound $\hat{f}_{lb}$ below the threshold τ in the $\partial\mathcal{I}$. Fig. 5.24h shows the thirty-seventh iteration when no measured value below the threshold τ is observed, and the algorithm stopped because the lower bound $\hat{f}_{lb}$ is above the threshold τ in the entire measurement area $\mathcal{I}$. The lighting system in the room, therefore, passes the audit.

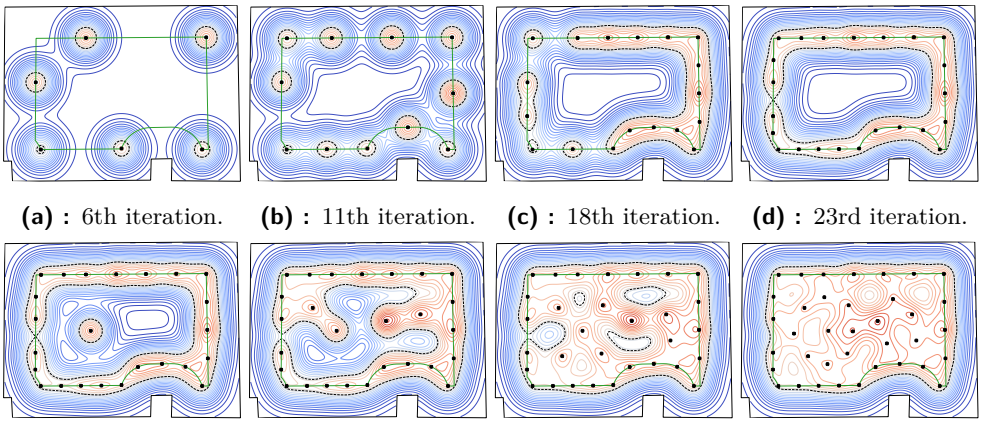

(a) : 6th iteration. **(b) :** 11th iteration. **(c) :** 18th iteration. **(d) :** 23rd iteration.

(e) : 24th iteration. **(f) :** 27th iteration. **(g) :** 31st iteration. **(h) :** 37th iteration.

Figure 5.24: Illuminance measurement via the first robotic unit in the room with dimensions of 8×5 m that passes the audit [15].

5.3.4 Estimation of the Audit Time

We estimate the time required to perform the audit for a human operator and for the first robotic unit, which uses the first version of the algorithm. The audit time required by a human operator is estimated based on a discussion with a professional auditor. The measurement time for the robotic unit is estimated with the assumption of a constant robotic unit speed of 0.1 m/s. We also assume that a single measurement at the CP takes 5 seconds. The estimated values are shown in Tab. 5.4. Note that the time required to map the room is not included in the estimate. However, this time is negligible because the distance travelled is much shorter than the distance travelled during the measurement process.

In real experiment, the measurements took approximately 30 minutes, including preparation of the first robotic unit, the room mapping, and making the final measurements. However, the experiment was performed only as a proof of concept, with a slow robot speed and no optimization of the measurement time. The first robotic units could operate more quickly in

a real application, resulting in a much faster measurement.

Table 5.4: The estimated time required to perform the audit [15].

Room [m×m]	Estimated time [min] Auditor	Robot
Square room 4 × 4	60	4
Large room (Fig. 5.18) 17 × 15	180	130
Real room (Fig. 5.24) 8 × 5	90	15

5.3.5 Estimation of the Number of Control Points

We estimate the number of the CPs required to pass the audit, as presented in Sec 5.2.1. This estimate is done for the first version of the algorithm (Sec. 5.2.2). The estimate is performed for all of the presented experiments that passed the audit, i.e., (i) the simulated experiment for the real room, shown in Fig. 5.12; (ii) the simulated experiment for the larger room (Fig. 5.18); and (iii) the experiment performed by the first robotic unit in the room shown in Fig. 5.24. The estimated number of the CPs and also the number of required the CPs are shown in Fig. 5.25.

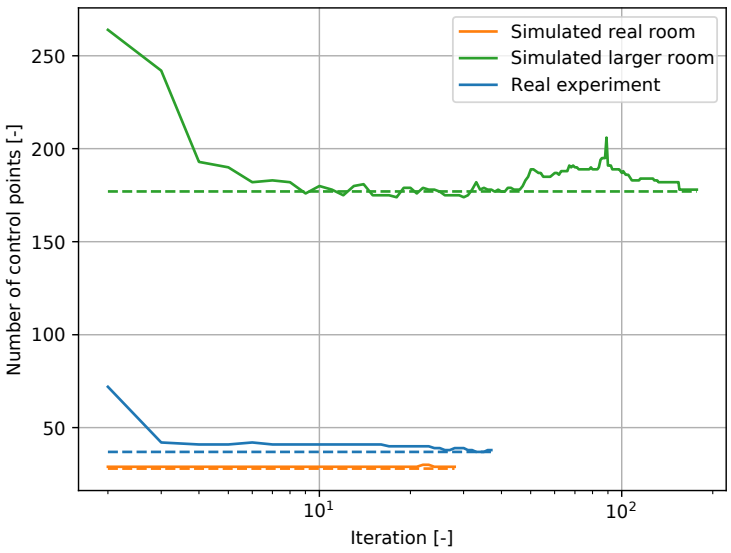

Figure 5.25: The number of CPs for different experiments. The dashed lines show the number of the CPs required to perform the audit. The solid lines show the estimate that was computed at each iteration [15].

The dashed lines in Fig. 5.25 show the number of the CPs required to perform the audit. The solid lines show the estimate that was computed at each iteration. The estimate for the larger room shows the behaviour of the proposed method in a situation with more significant changes in the illuminance value in the room. Although the number of the CPs is estimated accurately after a few measurements, the method overestimates the number after taking measurements in corners where the illuminance is low. The

estimate then improves iteratively after taking measurements that are not on the boundary of the inner area. The results show that the proposed estimation method can provide a rough estimate of the number of measured points.

The proposed estimation method computes the number of the CPs required to pass the audit. For this reason, the experiments where the room did not pass the audit are not included in the analysis. If the room does not pass the audit, the measurement process is stopped when an the illuminance value below the threshold is observed. As a result, the estimated number of the CPs does not correspond to the number of measured the CPs.

5.4 Experiment for the Second Version of the Algorithm

The second version of the algorithm (program) is evaluated in this subsection. The type of luminaires is the same for all simulated and robotic experiments as in the experiments for the first version of the algorithm (Sec. 5.3): *Modus LLX 236 AL* [77]. The threshold τ is set to 500 lx for the average measured illuminance value in the entire measurement area in all experiments. This subsection starts by the definition of the average illuminance value calculation, which is necessary for the second version of the algorithm. In the next part, simulated experiments are presented, to verify performance in more complex scenarios. The central part of this subsection are robotic experiments using the second robotic unit. The last part of this subsection provides a comparison of measurements using the proposed solution with a robotic unit and the measurement methodology established in the current real-world.

5.4.1 Average Illuminance Value

The first version of the algorithm was used in this section, which had a fixed threshold τ for each the CP in the measurement area, as specified by Eq. (2.10). However, this condition is not used in the current real-world measurement method. On the contrary, the current standard [1] stipulates that the average measured value of illumination in the entire measurement area $\mathcal{I}$ must be above the specified threshold τ in order for a room to pass the audit:

$$\frac{1}{|\mathcal{I}|}\int_{\mathcal{I}} f(\boldsymbol{x})\,\mathrm{d}\boldsymbol{x} > \tau\,, \tag{5.17}$$

where $|\mathcal{I}|$ denotes the area of polygon $\mathcal{I}$. This condition is implemented into the second version of the algorithm by the following modifications:

1. surrogate function $\hat{f}_{lb}(\boldsymbol{x})$ is used instead of $f(\boldsymbol{x})$ in Eq. (5.17),
2. the CP candidates are selected based on the uncertainty of the prediction of GP:

$$\mathcal{X}_c = \{\boldsymbol{x}\,|\,\boldsymbol{x} \in \mathcal{I} \wedge \sigma(\boldsymbol{x}) > \tau_\sigma\}\,, \tag{5.18}$$

where τ_σ is the fixed threshold for the uncertainty (threshold of the standard deviation),

3. the procedure stops if Eq. (5.17) is satisfied (the measured room passes the audit), or if there are no more the CP candidates left according to the Eq. (5.18) (the measured room does not pass the audit).

The first modification changes the lower bound $\hat{f}_{lb}$ to be represented by the averaged computed value not decreasing with new measurements. The second modification ensures that the surrogate function approximates the true value of the illuminance better over time, i.e., reduces the uncertainty because the uncertainty of the prediction of the GP must not exceed the set threshold of the standard deviation τ_σ. The third modification can therefore be used to stop the procedure if the average value of the lower bound $\hat{f}_{lb}$ is above the set threshold τ or there are no other candidates for the CP.

5.4.2 Simulation Experiment

Because the second version of the algorithm is based on the first and the difference is only in the termination conditions (see Sec. 5.2), the results of some simulated experiments from the first version of the algorithm are valid for the second version. These are simulated experiments aimed at adapting the location of the CPs (Sec. 5.3.1) and evaluation of the algorithm in a complex floor plan (Sec. 5.3.1) because the termination conditions at these experiments do not affect functionality. The second version of the algorithm (program) is subjected to further verification using multiple simulations created during individual simulated experiments. The first simulated experiment focuses on verifying that the second version of the algorithm can properly calculate the average illuminance value. Then a simulated experiment is created to determine the value of the standard deviation threshold τ_σ suitable for the further simulated and robotic experiments. The last simulated experiment verifies that the algorithm can respond to changes in input parameters. The simulated experiments use Dialux [32] software to simulate the light emitted from luminaires.

Verification of the Average Illuminance Value Calculation

The simulation scenarios for simulated real rooms from Sec. 5.3.1 are used for testing the average illuminance value calculation. The scenario is actually the illuminance distribution for a particular experiment from Sec. 5.3.1, where Fig. 5.12a, Fig. 5.14a and Fig. 5.16a show the illuminance distributions for the three scenarios. In addition to these three scenarios, we create another scenario by subtracting 100 lx from the illuminance function of the fourth scenario (as shown Sec. 5.3.1). The basic assumption of this experiment is that the second version of the algorithm determines the CPs until the lower bound $\hat{f}_{lb}$ average is below a specified threshold τ, or there are no candidates for the CP left according to the Eq. (5.18), where threshold of the standard deviation τ_σ is set to 10 lx.

The estimated average illuminance value during the optimization process is visualized in Fig. 5.26, where the estimated value increases with each new measure of illuminance and approaches the true value (simulated from Dialux [32]) of the average illuminance in the entire measurement area $\mathcal{I}$ (dashed lines). The procedure continues until the estimate (solid line) is below the threshold τ (solid black line). If the procedure does not stop, the dotted lines are obtained. The size of the gap between the true average and the estimate can be controlled by the uncertainty threshold τ_σ (threshold of the standard deviation) Eq. (5.18). The algorithm is not always terminated by reaching the threshold τ, as in some scenarios, in Fig. 5.26 Scenario 4, the average illuminance has to be measured until the σ of the measurement is below the τ_σ. This can be considered to be a more challenging scenario, as more iterations are needed. However, as shown in Fig. 5.26 the proposed algorithm is still able to complete the measurements successfully.

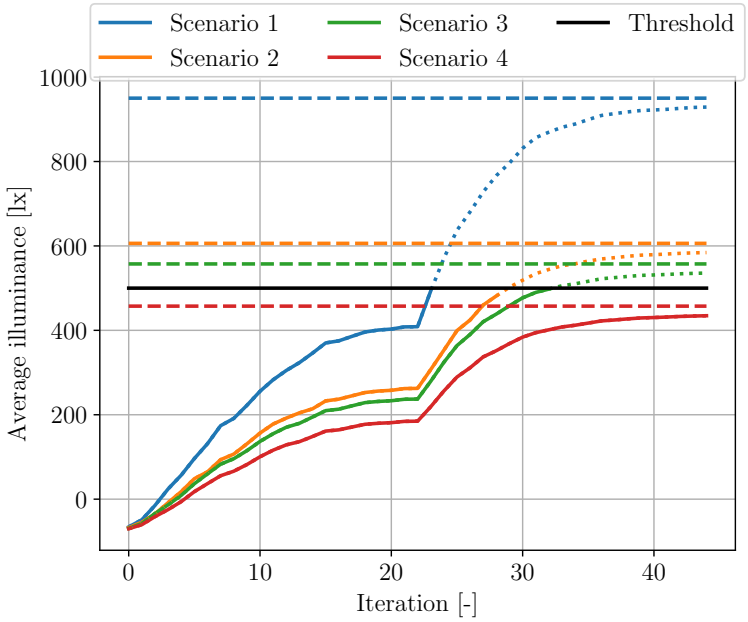

Figure 5.26: The lower bound estimate of the average illuminance value for four different scenarios [15].

The objective of this experiment is to reach the illuminance threshold by the average surrogate function of each scenario. The surrogate function for each scenario that satisfies the objective is shown in Fig. 5.27, where the i-th column corresponds to the i-th scenario. In the first three columns, the top row visualizes the surrogate function for the iteration in which the objective is fulfilled for the first time. The objective is not fulfilled for the fourth scenario (Fig. 5.27d). We, therefore, show the true illuminance distribution for the fourth scenario instead. This part of the experiment verified that the second version of the algorithm works according to the assumption. Thus, if the set objective is not achieved, the algorithm adds the CPs as long as there are candidates for the CPs according to Eq. (5.18). The bottom row (Fig. 5.27e,

Fig. 5.27f, Fig. 5.27g and Fig. 5.27h) shows the last iteration of the process, i.e., there are no the CP candidates for the CP left. It can be seen that the surrogate function approximates the true illuminance distribution reasonably well in the last iteration (see Sec. 5.3.1 for the true illuminance distribution of the first three scenarios).

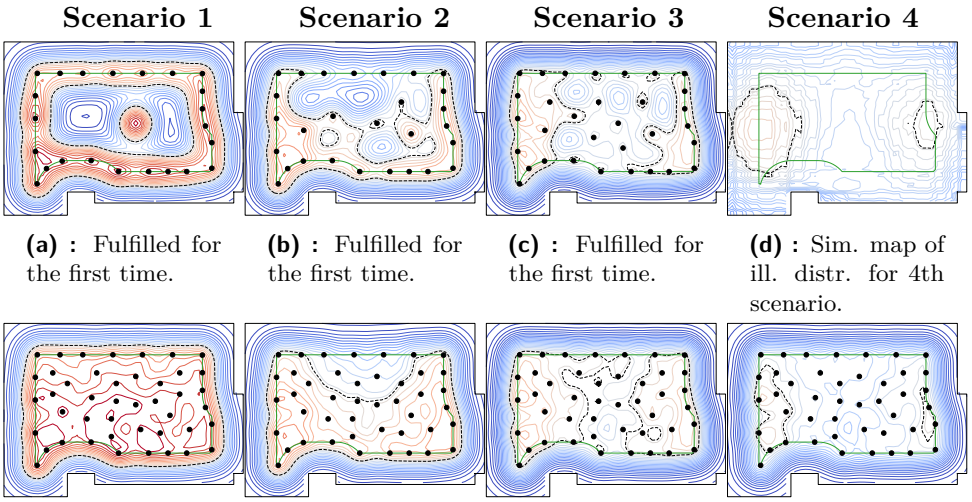

(a) : Fulfilled for the first time. **(b) :** Fulfilled for the first time. **(c) :** Fulfilled for the first time. **(d) :** Sim. map of ill. distr. for 4th scenario.

(e) : Last iteration. **(f) :** Last iteration. **(g) :** Last iteration. **(h) :** Last iteration.

Figure 5.27: The simulated results, where each column represents one of the scenarios. The top row, i.e., subfigures a, b, c and d, shows the surrogate function when the objective has been satisfied or the true illuminance distribution if the objective is not satisfied. The bottom row, i.e., subfigures e, f, g and h, shows the surrogate function obtained in the last iteration [15].

The consideration of the average illuminance value in the entire measurement area instead of the illuminance value at each the CP has been implemented in [13]. This project also contains several experiments to verify the algorithm's functionality with a new condition for fulfilling the audit. The most important experiments are real tests with the help of a second robotic unit.

Simulated Experiment to Determine the Threshold of the Standard Deviation τ_σ

The second version of the algorithm uses the maximum allowed value of the standard deviation σ between the CPs called the standard deviation threshold τ_σ (Sec.5.4.1), as one of the termination conditions. The assumption is that the lower the standard deviation threshold τ_σ value, the more the CPs are located in the measurement area $\mathcal{I}$, as more reliable measurements are necessary. For the experiment to verify this assumption, the second version of the algorithm was modified not to end as soon as it reaches the set threshold τ for the average value of the illuminance. Conversely, the algorithm continues the measurement process as long as there are candidates for the CPs according to the Eq. (5.18). Therefore, only one termination condition is used to end

the measurement process. The result of the modified second version of the algorithm is the average value from the GP corresponding to the real average measured illuminance value in the entire measurement area $\mathcal{I}$. The simulated experiment with real dimensions is used as a simulated room (Fig. 2.3). In the experiment several simulations where the standard deviation threshold τ_σ changes in each simulation are performed. The range of 1 lx to 12 lx was decided, gradually set as the standard deviation threshold τ_σ, because for larger values, the difference between the mean μ and the reference (obtained form the Dialux simulations) is too high. In order to be able to compare the determined average illuminance value from the algorithm, the reference average illuminance value has to be defined first. The reference is obtained from the Dialux program [32], which calculated the average illuminance value of the entire room and determined the illuminance distribution. Therefore, the measurement area $\mathcal{I}$ for the modified second version of the algorithm is extended to the entire room, meaning there is no distance between the boundary of the measurement area $\partial\mathcal{I}$ and the walls ($\partial\mathcal{P}$). The reference is calculated to be 855 lx from the Dialux program. The illuminance distribution data is then added to the modified second version of the algorithm, which uses this data to perform simulated illuminance measurements at the specified the CPs.

Thus, the modified second version of the algorithm gradually sets the specified values of the standard deviation threshold τ_σ and performs a simulation for each entered value. The results of all simulations of this experiment are shown in Tab. 5.5, where the first column contains the total number of CPs that the algorithm calculated before it was terminated by reaching the condition of the maximum standard deviation threshold τ_σ. The second column contains the average lower bound $\hat{f}_{lb}$ value for the last iteration of the measurement process. The third column of the table contains the mean μ value predicted by the GP for the last iteration. The fourth column shows the difference between the calculated the mean μ and the reference value obtained from the Dialux program.

The best results, which are close to the reference, are achieved by the modified second version of the algorithm at the maximum standard deviation threshold τ_σ of 1 lx. However, from a maximum standard deviation threshold of 1 lx to 11 lx, the difference from the reference does not exceed 1%. Selected examples of the calculation during the last iteration are shown in Fig. 5.28, where Fig. 5.28a shows 313 CPs for τ_σ equal to 1 lx. Fig. 5.28b shows 135 CPs for τ_σ equal to 5 lx. Fig. 5.28c shows 78 CPs for τ_σ equal to 10 lx, and Fig. 5.28d shows 60 CPs for τ_σ equal to 12 lx.

The experiment proved the assumption that the lower the standard deviation threshold τ_σ value, the more the CPs are located in the measurement area $\mathcal{I}$. More the CPs result in a more reliable prediction of the mean value. For example, for τ_σ equal to 1 lx, the number of the CPs is the highest and the difference between mean and reference is zero. However, in previous experiments, the τ_σ value of 10 lx was used to calculate the CPs. As can be seen from Tab. 5.5 at $\tau_\sigma = 10$ lx, the difference is only 0.23% while determining

Table 5.5: Determination of threshold of the standard deviation τ_σ.

		CPs [-]	Avr. $\hat{f}_{lb}$ [lx]	Mean [lx]	Diff. [%]
Threshold of the standard deviation τ_σ [lx]	**1**	313	854	855	0.00
	2	215	857	859	0.47
	3	182	857	860	0.58
	4	155	856	861	0.58
	5	135	856	861	0.70
	6	120	855	860	0.58
	7	105	854	861	0.70
	8	97	849	857	0.23
	9	87	844	854	-0.12
	10	78	846	857	0.23
	11	69	834	847	-0.94
	12	60	819	833	-2.57

78 CPs. This experiment clearly shows that a maximum standard deviation threshold of 10 lx is sufficient and will continue to be set to τ_σ.

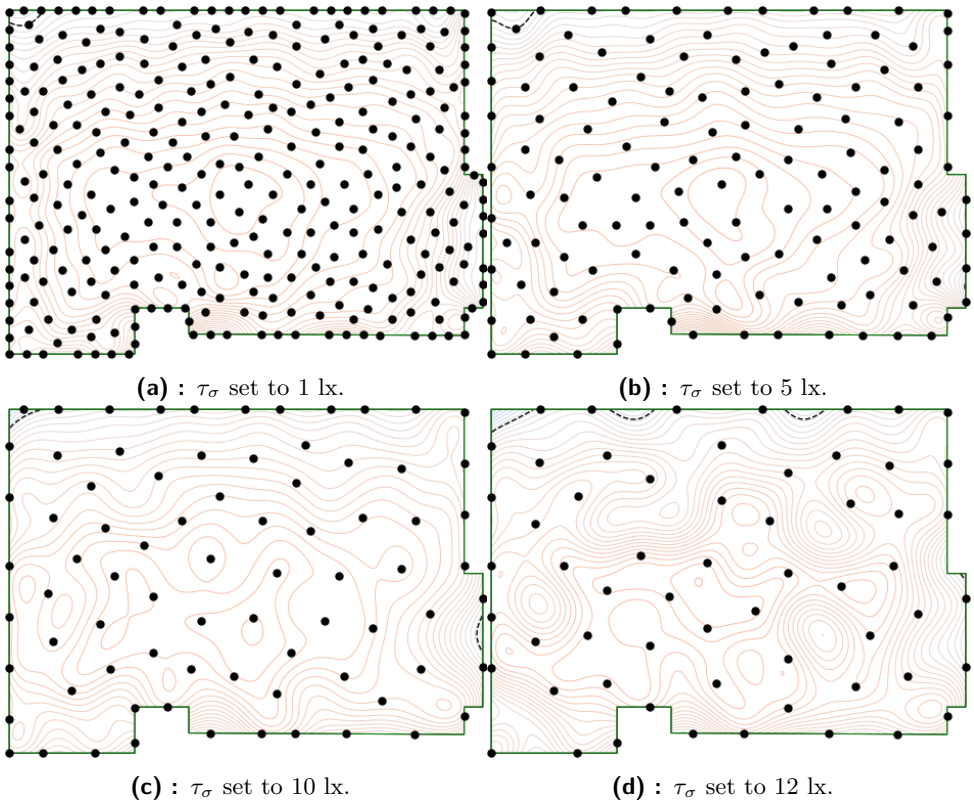

(a) : τ_σ set to 1 lx. **(b) :** τ_σ set to 5 lx.

(c) : τ_σ set to 10 lx. **(d) :** τ_σ set to 12 lx.

Figure 5.28: Simulated experiment for different τ_σ.

Simulated Experiment with Changing Input Parameters

In the simulated experiment evaluation of the CPs placement adaptation (Sec. 5.3.1), it was proven that the algorithm adjusts the spacing between the CPs at the boundary of the measurement area $\partial\mathcal{I}$ based on the measured illuminance value in each the CP. The following experiment focuses on verifying whether the second version of the algorithm can respond to a change in input parameters. The input parameters for the second version of the algorithm are the distance between the boundary of the measurement area $\partial\mathcal{I}$ and the wall ($\partial\mathcal{P}$), the measured illuminance value and a threshold of the standard deviation τ_σ as described in Sec. 5.2. The threshold of the standard deviation τ_σ for this experiment is set to a value of 10 lx. The calculated number of the CPs is monitored in this experiment.

The same spatial polygon $\partial\mathcal{P}$ is used as in Fig. 2.3. The experiment consists of several simulations in which distances of 0 m and 1.5 m between the boundary of the measurement area $\partial\mathcal{I}$ and the wall ($\partial\mathcal{P}$) are tested. In order to be able to compare individual simulations, the second parameter (measure value of illuminance at a specific the CP) is changed to a uniform value of measure illuminance at all the CPs. The second version of the algorithm ends the process of measurement if the average lower bound $\hat{f}_{lb}$ is in the entire measurement area above specified threshold τ, which is set at 500 lx for this experiment.

The results of the experiment are shown in Tab. 5.6, which shows that the larger the measurement area $\mathcal{I}$, the higher the number of the CPs at the same measured illuminance value in each the CP. Conversely, the higher the measured illuminance at all the CPs, the lower the number of the CPs in the entire measurement area $\mathcal{I}$. The experiment shows that the second version of the algorithm can adapt the calculation of the CPs for the entire measured area $\mathcal{I}$ based on various input parameters.

Table 5.6: The number of the CPs depending on the illuminance value obtained from the Dialux program and the distance of the inner measurement area from the wall.

Number of the CPs [-]		**Illuminance [lx]**		
		600	**800**	**1000**
Distance between $\partial\mathcal{I}$ and $\partial\mathcal{P}$ [m]	**0.0**	39	25	20
	0.5	27	19	15
	1.0	20	14	11
	1.5	13	9	7

Fig. 5.29 shows the last iteration, when the average lower bound $\hat{f}_{lb}$ exceeded the specified threshold τ (500 lx), of the individual simulations with different input parameters. In all simulations, the measured illuminance value at all the CPs is set to 600 lx. Fig. 5.29 shows that increasing the distance between the boundary of the measurement area $\partial\mathcal{I}$ and the wall ($\partial\mathcal{P}$) cannot be done indefinitely due to the dimensions of the room, which are 7.5×5.5 m. Therefore, the upper limit of the experiment was set at only 1.5 m. However,

Fig. 5.29, where the distances are 0 m to 1.5 m, shows that the algorithm can adapt to any input parameters.

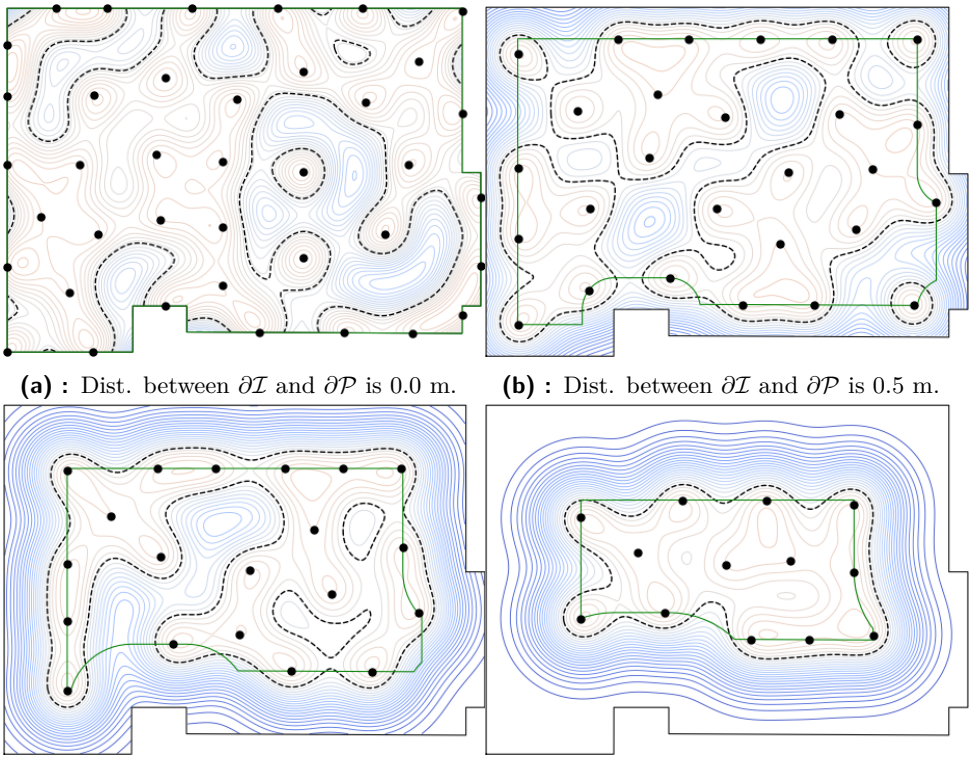

(a) : Dist. between $\partial\mathcal{I}$ and $\partial\mathcal{P}$ is 0.0 m. **(b) :** Dist. between $\partial\mathcal{I}$ and $\partial\mathcal{P}$ is 0.5 m.

(c) : Dist. between $\partial\mathcal{I}$ and $\partial\mathcal{P}$ is 1.0 m. **(d) :** Dist. between $\partial\mathcal{I}$ and $\partial\mathcal{P}$ is 1.5 m.

Figure 5.29: Simulated experiment with different input parameters.

5.4.3 Robotic Experiments

The second algorithm version has been tested in [13] in the second robotic unit with consideration of the real conditions. From real experiments, it is clear that the closer the second robotic unit approaches the wall, the higher the demands on the safe trajectory calculation. The control computer of the second robotic unit is not powerful enough for the trajectory planning program used, which is needed when the robotic unit is around 1 m and closer to the wall ($\partial\mathcal{P}$) (more information can be found in [13]). Due to the low computing power of the control computer and the safety of the robotic unit, the operator must be present in the measured room. Therefore, the distance between the boundary of the measurement area $\partial\mathcal{I}$ and the wall ($\partial\mathcal{P}$) is set to 1.5 m for all experiments. This distance is acceptable since the second robotic unit can safely measure determined the CPs at this distance without the operator in the room, thus saving operator time. Also, the second version of the algorithm has shown by simulation experiment (Sec. 5.4.2) that it adapts to the specified distance between the boundary of the measurement area $\partial\mathcal{I}$ and the wall ($\partial\mathcal{P}$).

Evaluation of second robotic unit limitations

The second robotic unit is more accessible to general public due to its much lower cost. However, due to the lower price the robotic unit has some limitations that are described in this subsection. The limitations have been found and evaluated in [13]. Two limitations that have been found are accuracy of approaching the CPs during the measurement process and the distance between $\partial\mathcal{I}$ and $\partial\mathcal{P}$. The experimental evaluation of the limitations consists of several real tests, in which three different distances (between $\partial\mathcal{I}$ and $\partial\mathcal{P}$) are tested, namely 1 m, 1.5 m and 2 m. Different tolerances on accuracy of reaching the required the CPs, represented by a circular deviation from the required CP have been evaluated. The results of the experiment are shown in Tab. 5.7. This experiment proves that the robotic unit can not ride safely 1 m from the wall ($\partial\mathcal{P}$) at any selected tolerance due to the second robotic unit limited control computer's computing power. Testing of the robotic unit tolerance of reaching the CPs has been evaluated for 0.2 m, 0.1 m and less than 0.1 (tested by setting tolerance to 0.05 and 0). The testing has shown that the robotic unit can meet the tolerance of reaching the CPs for tolerances of 0.2 and 0.1. However, when the tolerance is set to less than 0.1 m, that robotic unit is incapable of reaching the CPs correctly and, thus, it is not possible to exploit tolerances below 0.1 m.

Table 5.7: Distance of the robotic unit from the last CP in the measurement process depending on the approach tolerance [13].

Distance from the last CP [cm]		**Distance between $\partial\mathcal{I}$ and $\partial\mathcal{P}$ [m]**		
		2.0	**1.5**	**1.0**
Tolerance [m]	**<0.1**	-	-	-
	0.1	8	2	-
	0.2	16	8	-

Evaluation the Termination Condition of the Second Version of the Algorithm

Another experiment in [13] focuses on evaluating the termination condition of the second version of the algorithm in real environments when the measured room passes the audit. The assumption is that the algorithm terminates as soon as it reaches the termination condition for the successful audit. For the second version of the algorithm, the audit of the lighting system is successfully completed when the mean value of the lower bound $\hat{f}_{lb}$ in the entire measured area $\mathcal{I}$ reaches the required threshold τ, in this case, 500 lx. The experiment is evaluated in two real rooms using the second robotic unit with a tolerance (a circular deviation from the required CP) set to 0.1 m and a distance of 1.5 m between the boundary of the measurement area $\partial\mathcal{I}$ and the wall ($\partial\mathcal{P}$).

In the first room, the second version of the algorithm gradually calculates 12 CPs, determining in the twelfth iteration that the mean value of the lower

bound $\hat{f}_{lb}$ is above the set threshold τ and terminated the measurement with the result that the room passed the audit. Fig. 5.30 shows the course of measurements in individual iterations. In the second room, the same algorithm gradually calculated 16 CPs, when in the sixteenth iteration terminates the measurement. It can be seen in Fig. 5.31 that the CPs are determined only at the boundary of the measurement area $\partial\mathcal{I}$ (1.5 m from the wall), with this number of the CPs being sufficient to measure room passes the audit. The robotic experiment in two rooms confirmed the assumption that the algorithm will end the measurement as soon as it reaches the end condition for the successful audit.

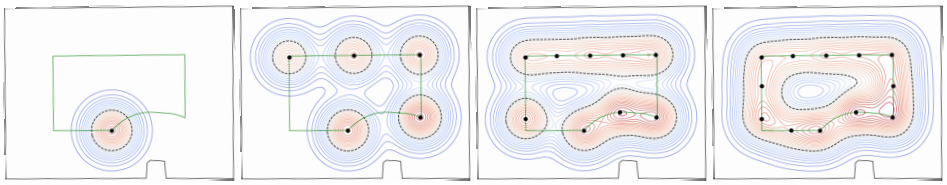

(a) : 1st iteration. **(b) :** 5th iteration. **(c) :** 9th iteration. **(d) :** 12th iteration.

Figure 5.30: Measurements in the first room. The room passes the audit. The room has dimensions of 8×5 m [13].

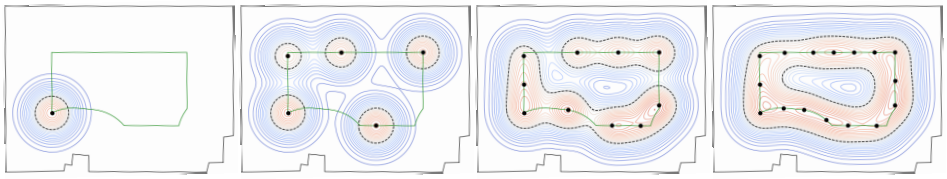

(a) : 1st iteration. **(b) :** 5th iteration. **(c) :** 10th iteration. **(d) :** 16th iteration.

Figure 5.31: Measurements in the second room. The room passes the audit. The room has dimensions of 8×5 m [13].

5.4.4 Comparison Between Manual Measurement and the Proposed Solution

The most important experiment is to compare measurements in the real world done by a specialist and measurements using a second robotic unit running the second version of the algorithm. The second robotic unit uses a modified second version of the algorithm to compare these measurements, which is described in Sec. 5.4.2. The second version of the proposed solution is modified so as not to stop when the required mean measured illuminance value in the measurement area $\mathcal{I}$ is reached. Therefore, the modified algorithm continues until there is no other candidate for the CP with the threshold of the standard deviation τ_σ greater than 10 lx according to Eq. (5.18). It is expected that the calculated mean μ of the illuminance value corresponds to the value found during the manual measurement.

In order to compare the measurements, the second robotic unit starts 1.5 m from the walls ($\partial\mathcal{P}$), following the measurements described in previous

sections. The measurement sensor of the measurement device is at 1 m from the floor. Before the measurement, the room is cleared of furniture, and then the lighting system is put into a state of regular operation, i.e., the luminaires are lit for at least 20 minutes before the start of the measurement, in order to stabilize the luminous flux (Sec. 2.1.3). First, the room is measured by a robotic unit, and then it is measured by a method established in real-world measurements by a specialist with the difference that the boundary of the measured area $\partial\mathcal{I}$ is extended to 1 m from the wall ($\partial\mathcal{P}$). In the manual measurement method, the measurements are done in a grid array with distance between $\partial\mathcal{I}$ and $\partial\mathcal{P}$ set to 1 m. As the measurements are done in a rectangular grid, where the next row/column is for distance between $\partial\mathcal{I}$ and $\partial\mathcal{P}$ of 1.74/1.68 m in respective axes. These measurements roughly represent the distance between $\partial\mathcal{I}$ and $\partial\mathcal{P}$ and are exploited for comparison to robotic unit measurements for this distance. The specialist in the illuminance measurement carried out the manual measurement and supervised the correct measurement methodology established in practice.

The robotic measurement is first started by mapping the room space with the second robotic unit. Subsequently, the robotic unit measures the room in approximately 20 minutes and determines 23 CPs. Fig. 6.25 shows the robotic unit during the measurement. Note, that there is no human operator in the room.

Figure 5.32: Example of the procedure of measurement of illuminance using the second robotic unit.

Fig. 5.33 shows several important iterations from determining the CPs. One of the iterations of interest is when the algorithm completes the measurement at the boundary of the measurement area $\partial\mathcal{I}$ or the next iteration (Fig. 5.33c) as the measurement continues in the inner part of the measurement area. Fig. 5.33d shows the end of the measurement, followed by the algorithm determining that the measured room passes the audit.

The algorithm receives the measured value that is processed (corrected) to match the actual (correct) illuminance value. The correction follows Eq. (5.16)

from the calibration sheet of the given measurement instrument. The calibration sheet of the exploited illuminance measurement device (photometer) is given in Annex B. Once the measurement process in the room (shown in Fig. 5.33d) is complete, the algorithm determines the corrected mean μ of the illuminance value from the measured values. In the measured room, the mean μ illuminance value of 841 lx is obtained.

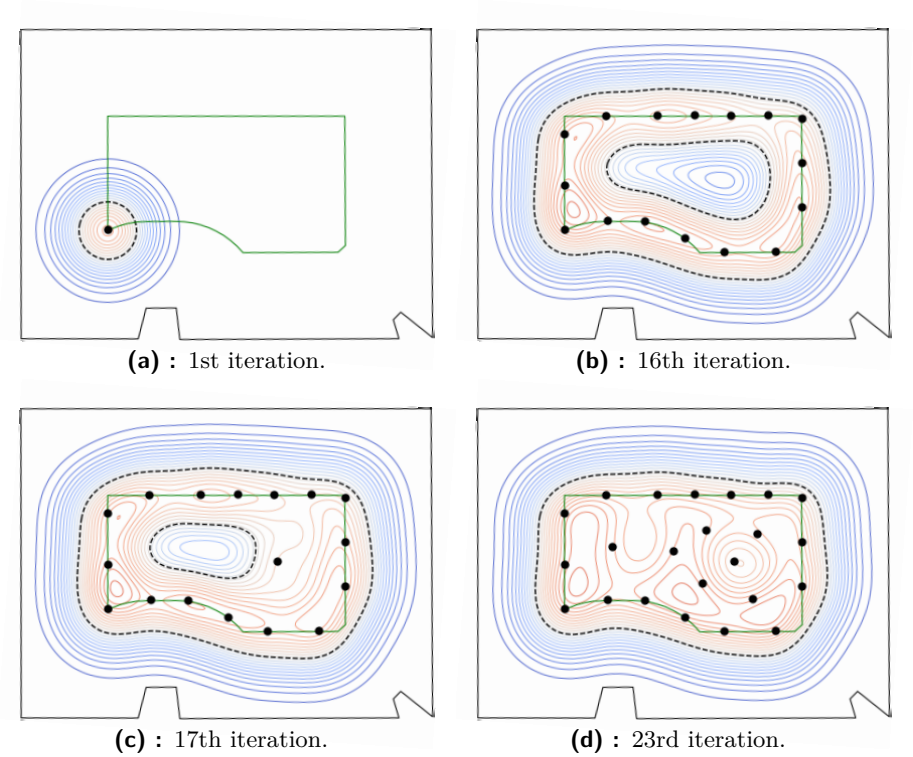

(a) : 1st iteration. **(b) :** 16th iteration.

(c) : 17th iteration. **(d) :** 23rd iteration.

Figure 5.33: Measurement to determine the mean illumination value with the measurement area of 1.5 m from the wall. The room has dimensions of 7×5 m.

The same room is measured manually by the specialist who have used a tripod with the photometer for the measurement. First, the dimensions of the room are measured manually, which are then used in the equation (2.3), to determine the minimum spacing of the CPs on the x-axis (height) and y-axis (width) in the measured room. The spacing differs because the room dimensions are 7.15 m in x-axis and 5.40 m in y-axis. Subsequently, the individual the CPs are placed at the calculated spacings, where the tripod equipped with a sensor of the measurement instrument is placed and the illuminance is measured. Fig. 5.34 shows an example of such a procedure. Manual measurement by two persons takes about an hour.

The results from the manual measurement are shown in Tab. 5.8. The measured illuminance values marked in blue are used to compare measurements using the second robotic unit with the measured area $\mathcal{I}$ 1.5 m from the wall. The mean corrected illuminance value from the manual measurement is calculated from the measured and corrected values, which is 809 lx. The correction of the measured illuminance values is again determined accord-

Figure 5.34: Example of the process from manual measurement.

ing to Eq. (5.16) from the calibration sheet (Annex B). The difference in the corrected measured values between the manual measurement and the measurement via the second robotic unit is 5.89%.

Table 5.8: Manually measured corrected illuminance values. The room has dimensions of 7×5 m.

Length [cm]	**100**	**174**	**247**	**321**	**394**	**468**	**541**	**615**
100	711.9	737.2	749.9	786.0	760.6	713.8	705.0	630.9
168	783.0	812.3	799.6	822.1	818.2	787.9	787.9	701.1
236	855.2	878.6	863.0	897.1	896.2	860.1	854.2	765.5
304	796.7	822.1	821.1	857.2	830.8	782.1	768.4	677.7
372	717.7	748.9	749.9	779.1	751.8	721.6	707.0	627.0
440	557.8	571.4	–	595.8	582.2	550.0	530.5	480.7
	Illuminance [lx]							

Based on the knowledge from the last experiments, where a limitation of the minimal distance between $\partial\mathcal{I}$ and $\partial\mathcal{P}$ was set to 1.5 m, the second robotic unit program has been modified to reduce the computation complexity and enable the robotic unit to approach the CPs located 1 m from the wall. Therefore, this software makes it possible to prepare another experiment, where the measurement takes place in the measurement area $\mathcal{I}$ set to 1 m from the wall ($\partial\mathcal{P}$).

The experiment is performed in the same room, and the robotic unit

identifies 35 CPs. Fig. 5.35 shows the gradual filling of the measurement area with the CPs. It can be seen from Tab. 5.8 that the manual method determines 47 CPs based on the spacings that are calculated using the Eq. (2.3) and dimensions of the measured room.

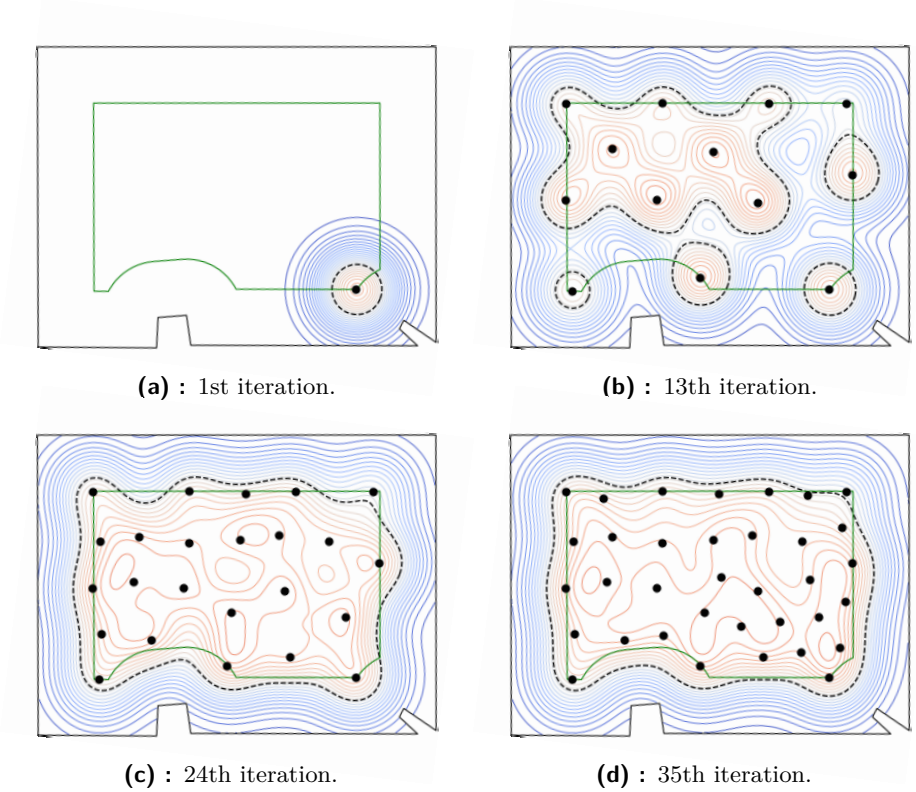

(a) : 1st iteration. **(b) :** 13th iteration.

(c) : 24th iteration. **(d) :** 35th iteration.

Figure 5.35: Measurement to determine the mean illumination value with the measurement area of 1 m from the wall. The room has dimensions of 7×5 m.

The corrected mean μ illuminance value from the proposed solution was 806 lx, and the mean corrected illuminance value from manual measurement was 745 lx. The difference between these values is 8.16%. If the differences between the last two experiments are compared, it is evident that the results from the last experiment show a deterioration.

The deterioration of the result is caused by the fact that the measured illuminance values at the boundary of the measurement area $\partial\mathcal{I}$ have lower illuminance values than the measured values from the inside of the measurement area $\mathcal{I}$, as can be seen in Tab. 5.8. At the boundary of the measurement area $\partial\mathcal{I}$, 9 out of 35 CPs were determined by the algorithm. On the contrary, in the manual measurement, 23 CPs were determined at the boundary of the measurement area $\partial\mathcal{I}$ and 24 CPs in the inner part of the measurement area $\mathcal{I}$. Determination the CPs is based on the measured illuminance values measured by the second robotic unit, altogether with the virtual model of the luminaire. In the virtual model of the luminaire, the walls are not affecting the light emitted form the luminaire, i.e., the walls are non reflective and also non absorbing, but in the real measurement, the walls are affecting the

emitted light (reflection and absorption). This is the cause of the difference in the measured values. However, the estimation of the wall reflection and absorption is a complex problem, that requires time-consuming measurements [96]. Thus, in the future work, we propose to modify the proposed algorithm to place a higher number of the CPs at the boundary $\partial\mathcal{I}$ to reduce the difference in the measured values, while keeping time complexity low.

5.5 Calculation of Illuminance Measurement Uncertainties

An integral part of each measurement process is the determination of the uncertainties of the measurement. To determine the uncertainties of the proposed measurement solution, we select the last robotic experiment, where the distance of $\mathcal{I}$ to walls ($\partial\mathcal{P}$ is 1 m, as this is the most similar experiment to the established measurement process in practice. Since less than ten measurements are made at each the CP, type A uncertainty (u_A) is not very reliable and will therefore not be determined. The focus of this section is the calculation of type B uncertainties (u_B) for each identified source of error, with a total of five sources identified. The calculation of the individual standard uncertainties of type B for each identified source of error is inspired by article [27], which dealt with the determination of uncertainties in the modernization of the goniophotometer.

5.5.1 The Uncertainty of the Control Points Location in the Interior – u_{Bl}

The location of the second robotic unit is based on values from the UTM-30LX laser rangefinder [91] and odometry calculation. The documentation of the used RD02 system [92] does not contain any detailed information about uncertainties, errors or accuracies of the system. Determining the uncertainty of turning the motor to the correct position is beyond the scope of this work, as it is extremely complicated and not one of the thesis goals. Therefore, it was decided that the uncertainty would be based only on data provided from laser rangefinders UTM-30LX documentation [91].

The partial standard uncertainty u_{Bl} caused by the inaccuracy of the laser rangefinder used can generally be determined from:

$$u_{Bl} = \frac{\triangle p}{X \cdot \sqrt{3}} \cdot 100\%, \tag{5.19}$$

where $\triangle p$ is the accuracy of the UTM-30LX laser rangefinder used, the documentation states that for a distance of 0.1 m to 10 m, the usual range for measurement distances in experiments, the accuracy is ± 30 mm. X is the minimum measured distance. In the last experiment, the second robotic unit measured a minimum distance of 1 m because it must not get closer to the wall. From this accuracy data, u_{Bl} can be calculated for:

$$u_{Bl} = \frac{0.03}{1.0 \cdot \sqrt{3}} \cdot 100 = 1.73\%. \tag{5.20}$$

The calculation of this partial uncertainty is usable for the location of the second robotic unit in room, but not for the uncertainty within the illuminance measurement because for typically measured rooms, we consider the spatial illumination gradient small enough to allow the contribution of partial uncertainty of the CPs location in the interior to the total uncertainty to be neglected.

5.5.2 The Uncertainty of the Measurement Device – u_{Be}

The robotic unit used a Radio-Lux 111 photometer [31] to measure illumination. The partial standard relative uncertainty for a photometer can generally be determined as:

$$u_{Be} = \frac{\frac{\delta_1}{100} + \frac{N \cdot R}{X}}{\sqrt{3}} \cdot 100\%, \tag{5.21}$$

where δ_1 is a photometer error in percentage, X is a measurement read out from the device (lx), N is the number of significant digits with an error, R is the value of significant digits with the least weight (lx).

The manufacturer of the digital photometer states for measurement ranges of 0.01 to 29.99 lx, 0.1 to 299.9 lx, etc. up to 100 to 299900 lx in the documentation that the measurement error is 0.5% ± 1 valid digit, i.e., $P = 0.5\%$ and $N = 1$. When measuring on a robotic unit, the lowest possible photometer reading is assumed, approximately $X = 0.3$ lx and at the same time, $R = 0.001$ lx. Thus, the partial standard relative uncertainty of u_{Be} is:

$$u_{Be} = \frac{\frac{0{,}5}{100} + \frac{1 \cdot 0{,}001}{0{,}3}}{\sqrt{3}} \cdot 100 = 0.48\%. \tag{5.22}$$

5.5.3 The Uncertainty of Influence of the Final Dimensions – u_{Bk}

Part of the primary sources of possible errors for the measurement of illuminance, which are listed in Tab. 2.1, is the partial standard uncertainty u_{Bk}. Due to the final dimensions of the measured luminaires and the sensor, this partial standard uncertainty is determined according to [97] as:

$$u_{Bk} = \frac{\left| 1 - \left(\frac{r_0}{\sqrt{r_0^2 + (a+b)^2}} \right)^3 \right|}{\sqrt{3}} \cdot 100\%, \tag{5.23}$$

where r_0 is the axial distance of the light center of the luminaire (source) from the center of the sensor receiving surface (m), a is half the characteristic

dimension of the luminaire, b is the radius of the sensor receiving surface, which is 0.004 m according to the manufacturer's catalog. Due to the dependence on the distance between the luminaire and the sensor, the lowest (worst) distance, which is 2.34 m, will be considered. The measured luminaires are all the same and have a characteristic dimension a equal to 0.6 m. Based on the above parameters, the partial standard uncertainty u_{Bk} can be determined:

$$u_{Bk} = \frac{\left|1 - \left(\frac{2.34}{\sqrt{2.34^2+(0.6+0.004)^2}}\right)^3\right|}{\sqrt{3}} \cdot 100 = 5.32\%, \tag{5.24}$$

This uncertainty is also calculated in the measurement used in the current real-world measurement method.

5.5.4 The Uncertainty of Instability of Used Devices – u_{Bs}

The uncertainty of the instability of the devices u_{Bs} used corresponds to the influence of the instability of the devices used, such as the instability (fatigue) of the sensor, the light sources and the power supply. It is not possible to identify individual effects on the overall instability of the equipment used. Therefore, the partial standard uncertainty u_{Bs} is calculated from the change in the photometer reading during time T, which corresponds to the measurement time:

$$u_{Bs} = \frac{\left|\frac{Y_{max}}{Y_{min}} - 1\right|}{\sqrt{3}}, \tag{5.25}$$

where Y_{max} is the maximum measured value of the photometer during the measurement period, Y_{min} is the minimum measured value with a photometer for the measurement time. Long-term measurement of illuminance in one place was not performed, and therefore, the value of 0.5% of the results of laboratory measurements given in [97] is used.

5.5.5 The Uncertainty of Positioning the Sensor in the Correct Position – u_{Bv}

The partial standard uncertainty u_{Bv} of setting the position of the sensor on the vertical is determined by the formula:

$$u_{Bv} = \frac{1 - \cos\beta}{2} \cdot 100\%, \tag{5.26}$$

where β is the angle of the sensor offset from the vertical measured in the degrees, it can be assumed that the sensor offset angle does not exceed 2^o. Then the partial standard uncertainty u_{Bv} is:

$$u_{Bv} = \frac{1 - \cos 2}{2} \cdot 100 = 0.03\%. \tag{5.27}$$

5.5.6 Calculation of Combined and Expanded Uncertainty

The combined standard uncertainty u_C is calculated from Eq. (2.8), for which it is necessary to calculate the total standard uncertainty of type A and the total standard uncertainty of type B. The standard uncertainty of type A u_A is not determined due to the small number of measurements at one CP. Conversely, all calculated partial standard uncertainties of type B are listed in Tab. 5.9. However, the first partial uncertainty u_{Bl} is not used to calculate the total type B uncertainty because we neglect it.

Table 5.9: Summary of calculated partial standard uncertainties type B when measurement of illuminance using the second robotic unit.

Error number	Source of error	Label	Calculated partial uncertainty [%]
1	Location of the CPs in the interior	u_{Bl}	1.73
2	The uncertainty of the measurement device	u_{Be}	0.48
3	Instability of used devices	u_{Bs}	0.5
4	Influence of the final dimensions of the radiating surface of the luminaire (source) and the receiving surface of the sensor	u_{Bk}	5.32
5	Position the sensor in the correct position	u_{Bv}	0.03

Based on Eq. (2.5), only the total standard uncertainty of type B u_B is calculated:

$$u_B = \sqrt{u_{Be}^2 + u_{Bs}^2 + u_{Bk}^2 + u_{Bv}^2} = 5.37\%. \tag{5.28}$$

Since the uncertainty of type A is not determined, it is possible to state that $u_B = u_C$. The expanded uncertainty U is determined from the Eq. (2.8) and calculated as:

$$U = k_u \cdot u_C = 2 \cdot 5.37 = 10.73\%. \tag{5.29}$$

If this expanded uncertainty U were to be considered appropriate, it could be compared with the accuracy requirements in Sec. 2.1.1. The expanded measurement uncertainty U corresponds to the requirements for carrying out the measurements, irrespectively, whether it is done via a robotic unit or by an operator with a tripod.

5.6 Conclusions

In this chapter, we have presented a novel approach that makes lighting audits autonomous. We have used a GP to model the illuminance distribution in a room. The distribution is updated iteratively after each measurement to incorporate new observations. The lower bound estimate is built from the model, and it is used to select the CP for the next measurement. The process continues until the room passes the audit or until a measurement violating the objective is observed.

Two versions of the algorithm were implemented and subjected to simulated and real experiments. The first version of the algorithm was created to verify the proposed solution, and with the help of the first robotic unit, the algorithm was tested in real conditions. The second version of the algorithm was created to provide a measurement closer to the established measurement procedure in the current real-world. Additional simulated experiments were created with this version, which show the generality of the proposed approach. The algorithm was again tested in real conditions with the help of a second robotic unit. By modifying the second version of the algorithm and software of the second robotic unit, it was possible to perform a final test, which compared the measurement values from the established procedure in real-world and the values obtained from the proposed solution. The algorithm showed that the difference is 8.16%. An integral part of the last experiment was determining measurement uncertainty when the expanded measurement uncertainty was 10.73% and thus met the requirements for operating measurement. The result of the comparison and the calculated expanded uncertainty show that the difference between the stated results of the established illuminance measurement procedure in the current real-world and the proposed solution of the illuminance measurement is not statistically significant.

The first robotic unit is able to measure the illuminance in the measurement area $\mathcal{I}$, defined by 1 m from the wall ($\partial\mathcal{P}$), without any problems. The second unit enables the same, but due to its low computing power, it must be under the visual control of the operator to avoid any issues during the measurement process. The proposed solution has demonstrated through experiments that it can operate on various robotic platforms and can respond to changes in input parameters. Therefore, the proposed solution is not limited to the two robotic units, as it is independent on the exploited robotic platform. The robotic platform itself specifies which measurements can be done and which cannot. Therefore, it is possible to do measurements even between the boundary of the measurement area $\partial\mathcal{I}$ and the wall $\partial\mathcal{P}$ (1 m according to the standard [1], or even 0.5 m according to the standard [5]). However, this is not possible on the two robotic platforms used in this thesis and is therefore not shown.

Although the experiments have demonstrated the applicability of the proposed solution, there are two limitations of the proposed approach. The first limitation is the assumption that the parameters of the light emitted from the luminaire used in the room need to be known. This, however, does not pose a severe limitation, as this is obtained from the program

Dialux [32] simulation in advance of the measurement process. The second limitation is the assumption of a occupancy map, i.e., a map of the room that is unchanged during the measurement process. However, this is necessary even in the common measurement procedure in the real-world. Further limitations are connected with the hardware capabilities of the robotic units. The robotic units that were used in the experiments were equipped with a two-dimensional rangefinder. This sensor is not able to measure and map complex three-dimensional objects such as tables and chairs. In addition, the used robotic units were able to move only on a flat floor (without stairs) [15].

Chapter 6

Acoustic Noise Measurement

This Chapter describes the proposed solution for indoor acoustic noise measurement to perform acoustic noise audits. The acoustic noise audits check the compliance of the indoor environment with the hygienic requirements specified in the regulation [98] where people live or work. It is, therefore, possible to assume an environment that does not support the formation of dominant standing waves.

There are several methods of acoustic noise measurement. One of the methods is the measurement of noise in the network of the CPs, which is performed similarly to measurement of illuminance. The acoustic noise measurement process can be automated with the help of a robotic unit equipped with a measurement device. The robotic unit is designed to move autonomously around the room and perform noise measurements in the CPs. This solution thus eliminates the need for the presence of human operators.

The proposed solution is in line with the established procedure of determining the CPs in practice, where the individual CPs are determined based on the dimensions and shape of the room. After calculating all the CPs where acoustic noise measurements are to be performed, the robotic unit plans its trajectory and traverses the individual CPs while performing the acoustic noise measurements. This chapter contains a description of the proposed solution for the measurement of two types of acoustic noise sources, e.g., factory and tram. Furthermore, the proposed solution is verified by means of simulations and real-world experiments. This research has been published, and the text in this chapter is based on [25].

6.1 Proposed Approach

The entire noise measurement process is time-consuming because the acoustic noise measurement is performed over the course of several hours, as each measurement needs to be done over a time long enough to account for the dynamics of the acoustic noise in time. Therefore, it is advisable to automate at least some steps of the process [99]. The proposed solution for acoustic noise measurement aims to design automatic algorithms for placing the CPs in the measured room while respecting all the restrictions set by the standard [4]. The measurement of the acoustic noise level is then performed in these CPs.

The international and national standards [7, 4], for which the proposed solution is designed, do not distinguish different measurement purposes and only specify general rules for the location of CPs. In this work, two different algorithms are created for two types of acoustic noise sources, which are divided into:

1. continuous - long-term stationary noise and
2. recurring - short-term recurring noise.

The algorithm can continuously measure the first type (continuous) acoustic noise source because the acoustic noise is continuous, i.e., always present in the measured room. The measurement of the recurring acoustic noise has to be done over a long time period, as the short-term recurring noise occurs randomly in the measured room. Therefore, the algorithm places the CPs in a way that each determined CP covers the maximum area to estimate the acoustic noise distribution in the room, even in a case, when the acoustic noise occurs rarely and is measured only at some of the CPs.

The contribution of this chapter is the acoustic noise measurement methodology consisting of the design and testing for purposes of living condition verification for a long-term stationary noise and living condition verification for a short-term recurring noise. The CPs are determined to meet the conditions based on the standard [4]. The algorithms for calculating CPs need to be designed in a way that the only information about the room to the robotic unit is the created floor plan via the SLAM [84, 85]. Therefore, individual elements (windows, openings in the wall, etc.) cannot be identified in the proposed solution. For this reason, the condition is set that the CPs are located closest to 1 m from the wall. This condition is based on the requirement for distance from significantly sound-transmitting elements and is specified in [7].

The floor plan notation of the measured room is described in Sec. 2.5.2 and is the same as for the illuminance measurement. Both algorithms start in the same way by determining the measurement area $\mathcal{I}$ and the boundary of this area $\partial\mathcal{I}$. Subsequently, the algorithms go through this boundary point by point, looking for corners. The corner is defined in this chapter as a location where the angle (direction) of the wall changes while this angle is below 180 degrees. For the purpose of the proposed solution, we introduce corner priority classes, defined by the corner angle. Class two is for corners with an angle between 60 and 120 degrees, and class one is for corners with angles above 0 degrees and the corners with an angle of 0 or 180 degrees. The corners are selected as follows: if there are corners from class two, all these corners are selected. If there are only corners from class one, all these are selected. Otherwise no corners are selected.

As with illuminance measurements, it is useful (for evaluation) to define the input parameters that are necessary to calculate the CPs for measurement of acoustic noise. The proposed solution for both algorithms has the same input parameters. The static input parameter that is given by the room itself, is

the floor plan of the measured room. Dynamic input parameters that are set based on the measurement requirements (measurement standards [7]), are:

1. distance of the boundary of the measurement area from the wall (obstacles) and
2. the boundary of the area around each CP where no other the CPs are located.

6.1.1 Long-term Stationary Noise

The sources of the long-term stationary noise is, for example, a running factory or a construction site nearby to the measured room. The acoustic noise measurements are done by starting at one CP and determining all other CPs from this given starting position. This creates a set χ^v of the CPs where the first CP is the starting position and also defines index v from the set V that contains indices of all determined variants. This set χ^v is denoted as a variant. To determine the variant that provides the most accurate acoustic noise map, starting point changes, i.e., it is selected as another CP, and the successive CPs are determined from this starting point. In each CP, the measurement takes place for a time duration long enough to ensure a sufficiently long and high-quality noise measurement. The proposed algorithm searches for the maximum number of the CPs according to the specified input parameters for maximum acoustic noise capture in a given space that meets the following:

$$\chi^* = \max_{v \in V} |\chi^v| \,, \tag{6.1}$$

where χ^* is the maximum number, i.e., set cardinality, of the CPs in a measured room.

The algorithm uses recursion and creates a list of the CPs for each such recursion (variant) by following these steps:

- To meet the condition of at least one CP in a corner (Sec. 2.2.1), place the first CP in a corner.
- From the already determined CPs, the algorithm draws circles with a radius of 0.7 m. The intersections with other circles give the new CPs.
- If such an intersection does not exist, and there is an intersection with $\partial\mathcal{I}$, the algorithm places the CP at this intersection.
- If there are any other intersections with limit cases, e.g., measurement area boundaries $\partial\mathcal{I}$, columns, obstacles, the algorithm places the CP at these intersections.
- If the algorithm does not find any new CP in the iteration, it terminates the recursion and saves the total number of found CPs (this number is called a list) for the given variant.

The algorithm provides the list of the best results (set), i.e., the maximum list of the CPs covering the entire measurement area, according to Eq. (6.1).

Implementation of the Algorithm for Long-term Stationary Noise

The proposed solution for the calculation of the CPs for long-term stationary noise was implemented. The main parts of the algorithm with individual points can be seen in a simplified version in Fig. 6.1. At the beginning the algorithm prepares lists for the evaluation of possible variants, e.g., a list of the corners. Then, the algorithm determines all corners in the measurement area and adds them to the list of the corners. This is followed by the recursive determination of the CPs.

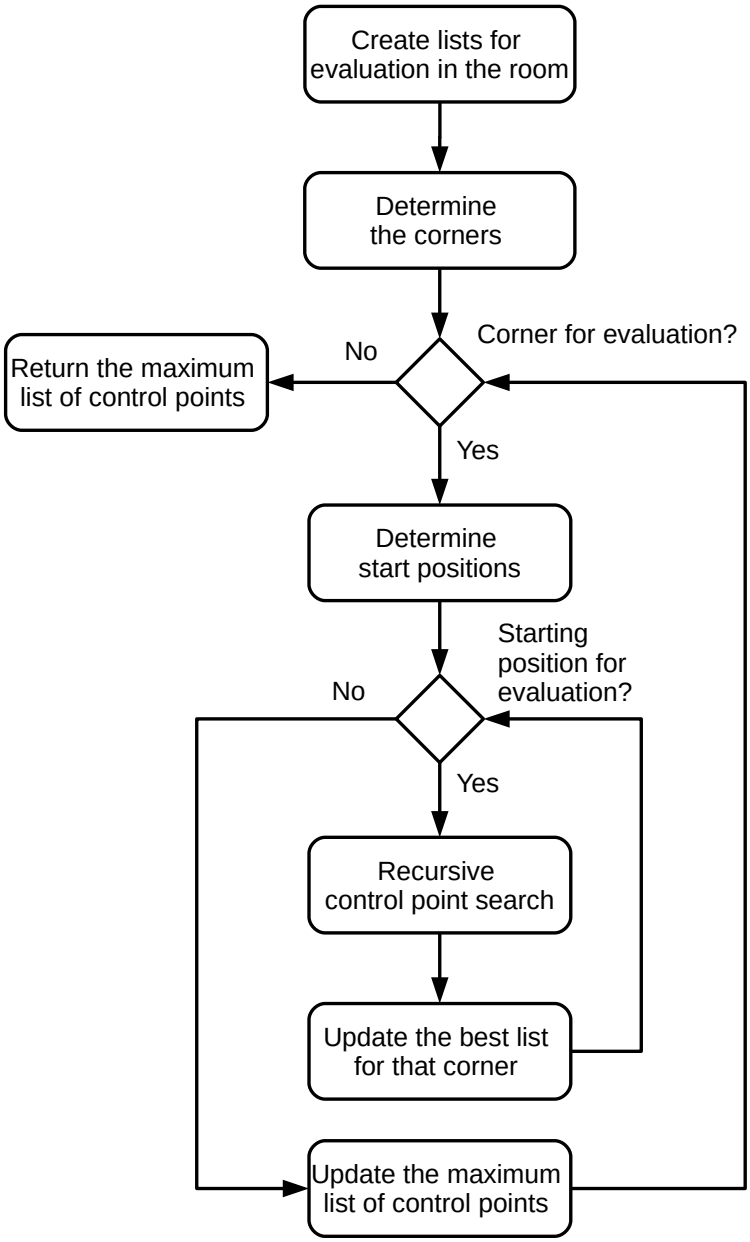

Figure 6.1: Implementation of the long-term stationary noise algorithm.

The CP location request according to Sec. 2.2.1 states that one of the CPs have to be located in the corner of the measurement area. Therefore, it is decided that the first CP is always placed in the corner of the measured area. This defines the first CP in each of the calculated variants.

In the next iteration, a second CP is determined based on a distance of 0.7 m from the first CP and the intersection with the measurement area boundary $\partial\mathcal{I}$. However, more CPs can be obtained in this iteration. Therefore, it was decided that the algorithm would create variants, selecting the first CP and one of the second CPs in each. Note that the first two CPs define a so called starting position of a variant.

The goal of the algorithm is to find the maximum list of the CPs covering the entire measured area $\mathcal{I}$. Therefore, the algorithm tries to sequentially calculate the CPs from each determined starting position. Thus, each just evaluated corner has at least two variants for the calculation of CPs.

The algorithm calculates the list of all possible starting positions and determines the maximum number of CPs for each of them. The algorithm returns the best variant for the evaluated corner. This ends the evaluation of the selected corner.

Fig. 6.2 shows the determination of the CPs by the algorithm. This is shown via an example, represented by the determination of the CPs in a case of the best variant. Fig. 6.2a shows the first calculated starting position from the list of all possible starting positions. From the first starting position, the algorithm determined 42 CPs, as shown in Fig. 6.2b. Fig. 6.2c shows the second calculated starting position from the list of all possible starting positions. From the second starting position, the algorithm determined 42 CPs, as shown in Fig. 6.2d, the algorithm did not calculate the next possible starting position. The algorithm returns the first variant as the best variant because the second variant did not calculate more CPs.

The best variant of the selected corner is compared with the best variant, which was calculated for the previously evaluated corners. After evaluating all corners, the algorithm obtains the variant in which the maximum number of CPs covers the entire measured area $\mathcal{I}$. The list of the CPs of this variant is used to measure acoustic noise.

Another example shows the calculation of the best variants of the evaluated corners. In total, the algorithm identified four corners that met the conditions of the corners. Fig. 6.3 shows an example during the algorithm's calculation when the calculation from two different starting positions (corners and intersections) for two the best variants can be seen. Fig. 6.3a shows the second iteration when the algorithm places the first two CPs (starting position) in the measurement area. The last iteration in determining the maximum number of the CPs for the same starting position can be seen in Fig. 6.3b. Fig. 6.3c and Fig. 6.3d show the same situation but for the different starting positions. When the calculation of the current variant is finished, the algorithm compares it with the best existing one so far and keeps the best.

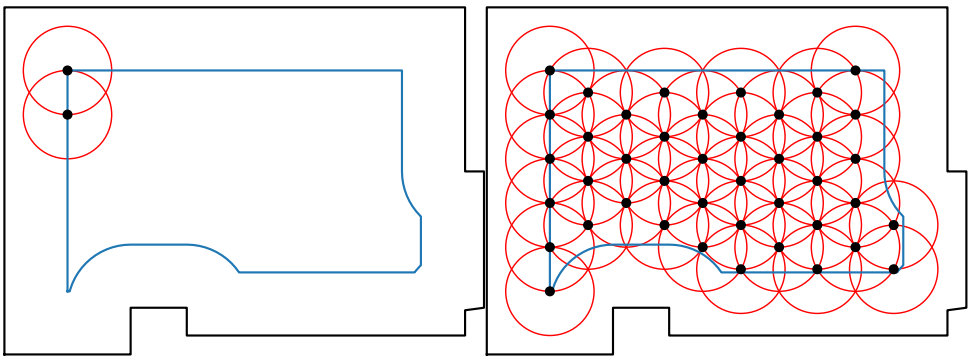

(a) : 2nd iteration (starting position). **(b) :** 42nd iteration.

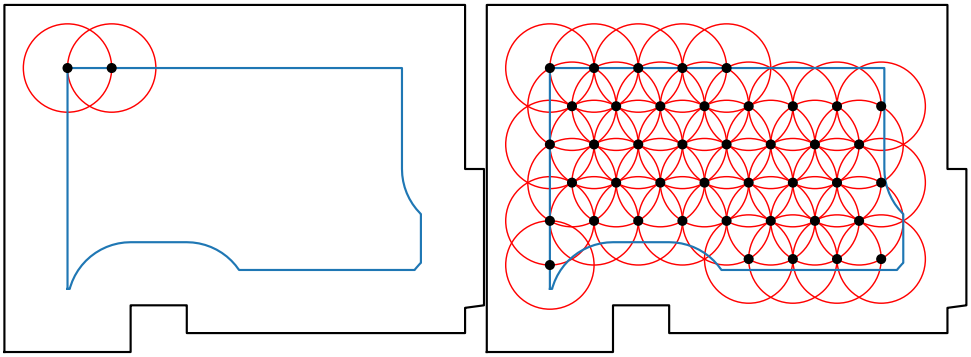

(c) : 2nd iteration (starting position). **(d) :** 42nd iteration.

Figure 6.2: Example of calculation of the starting positions for the evaluated corner when measurement of long-term stationary noise.

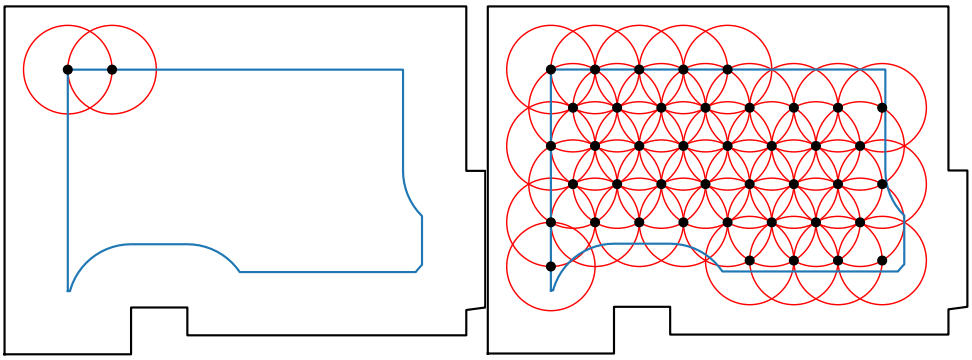

(a) : 2nd iteration (starting position). **(b) :** 42nd iteration.

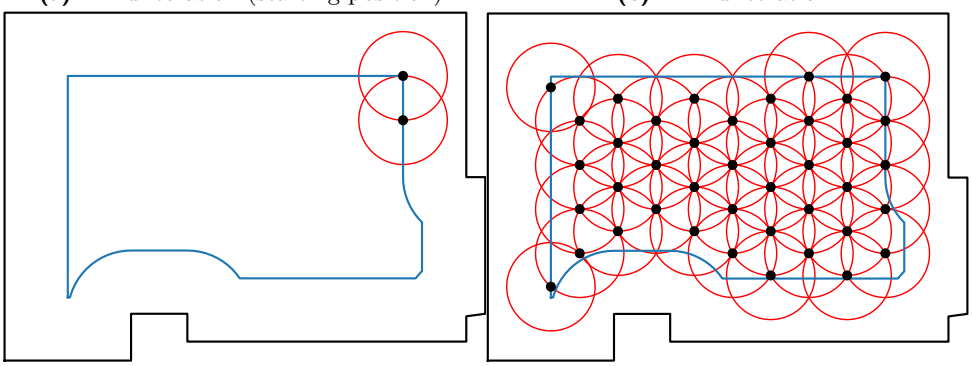

(c) : 2nd iteration (starting position). **(d) :** 41st iteration.

Figure 6.3: Example of calculation of the CPs for long-term stationary noise.

6.1.2 Short-term Recurring Noise

The short-term recurring noise is a type of acoustic noise that is caused, for example, by public transport (trams, buses) at the place of residence, workplace, or school. Measurements of this type of acoustic noise are made in such a way that the measurement instrument is located at the specific CP until the acoustic noise level exceeds a specified threshold. Subsequently, the measurement device is moved to the new CP, and the entire process is repeated. Due to the lack of knowledge of the number of occurrences exceeding the specified acoustic noise level, the algorithm looks for the best location distribution of the CPs in each iteration in order to cover as much measurement area of the measured room as possible. After measuring the given CP, the next CP is selected to have the maximal distance to all previous CPs in the measurement area $\mathcal{I}$:

$$\boldsymbol{x}^* = \underset{\boldsymbol{x}\in\mathcal{I}-\mathcal{P}}{\arg\max} \sum_{p\in\mathcal{P}} d(\boldsymbol{x}_i, \boldsymbol{x}_p)\,, \tag{6.2}$$

where $\boldsymbol{x}_p \in \mathcal{P}$ is the position of the CPs positions selected in previous iterations from the set $\mathcal{P}$ of all previously determined CPs, and $\boldsymbol{x}_i$ are the candidates of the CPs in the measurement area $\mathcal{I}$.

The entire algorithm was designed to obtain maximum coverage of the measurement area by the minimum number of the CPs in as few iterations as possible. The algorithm uses the method of splitting the measurement area into imaginary individual triangles to calculate the ideal candidate for the next CP in each iteration. The entire process is repeated until one of the conditions is satisfied:

- There shall be at least one candidate for the new CP that meets the conditions specified in the standard [7] (minimum distance from walls and other CPs).
- The noise measurement does not exceed the specified level at the measured CP.
- The time interval defined by the standard [100, 101] for the measurement ends.

Implementation of the Algorithm for Short-term Recurring Noise

The proposed solution for the calculation of the CPs for short-term recurring noise was implemented. The algorithm can be divided in a simplified version into several points, and Fig. 6.4 shows how these points are interconnected. The algorithm first creates lists that are used during the evaluation of the measured room. The required list is, for example, a list of the corners, a minimum list of the CPs, and a list of the local maxima. The algorithm then determines the corners for evaluation and adds each corner to the appropriate list. Since the measurement of the acoustic noise must take place at least in one corner according to Sec. 2.2.1, the first CP is located in the

corner of the measured area. This first CP defines the starting position of the algorithm for short-term recurring noise and represents the first iteration.

The goal of the algorithm is to find a minimum list of the CPs covering the entire measured area. Therefore, the algorithm tries to gradually calculate the CPs covering the entire measured area from each corner. This process, when the algorithm tests every corner, is called a variant. Thus, each variant has the starting position, which is located in the currently evaluated corner.

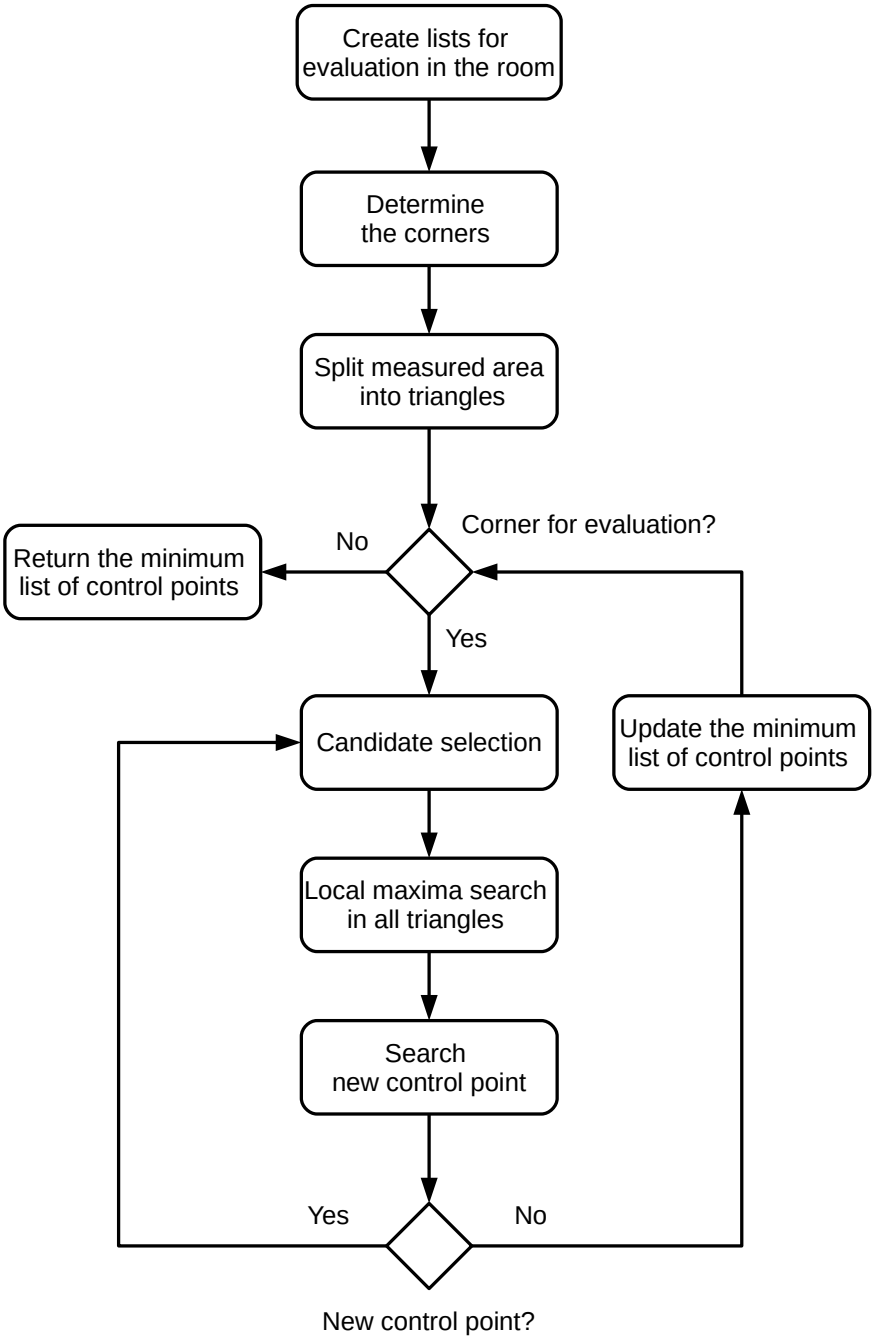

Figure 6.4: Implementation of the short-term recurring noise algorithm.

The algorithm then uses a method that splits the measured area into imaginary individual triangles [102]. This method can determine triangles based on [103] even in the field of measurement, where there are various obstacles. This division of the measured area into imaginary triangles makes it possible to identify the outermost candidates for the new CP from the already determined CPs in the measured area.

The algorithm places the starting position in the selected corner and starts calculating additional CPs in the measured area for the given variant. In each iteration, the algorithm covers the measured area with possible candidates for the new CP and creates a colored background based on the objective function defined in Eq. (6.2). The colored background, thus, changes based on the distance from each already determined CP. Thanks to this colored background, the algorithm calculates local maxima (the outermost candidates for the new CP from already specified CPs) in each imaginary triangle and stores them in the list of current local maxima.

Fig. 6.5 shows the current description of the algorithm. Fig. 6.5 shows the current calculation of the CPs during the third iteration. The black points represent the CPs, the red circles the distance of 0.7 m from each CP and the red points are local maxima. The colored background in Fig. 6.5 changes its color from light to dark based on the distance from each CP.

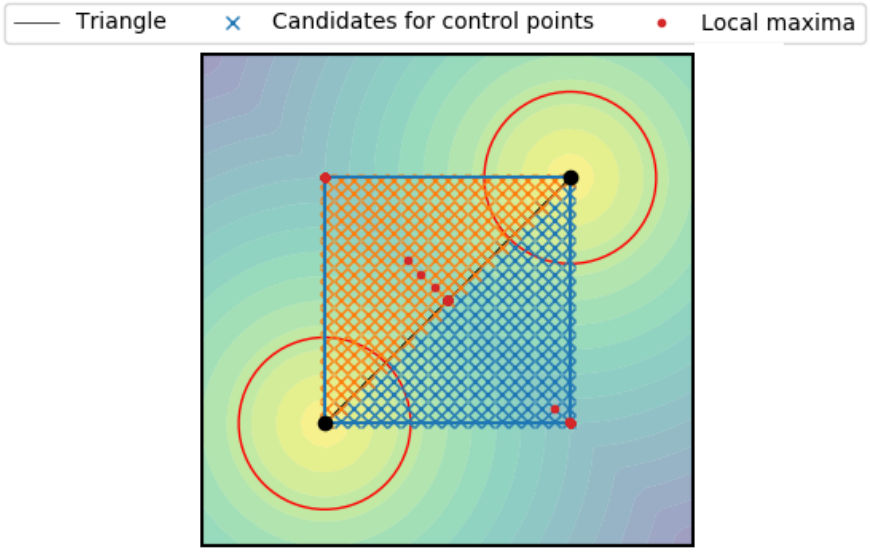

Figure 6.5: The current calculation of the CPs during third iterations for short-term recurring noise.

After finding all local maxima, the algorithm selects from the list the local maximum that has the greatest distance from the already determined CPs in the measurement area. The selected local maximum is declared the new CP if it meets a distance of at least 0.7 m from each already determined CP. The new CP is added to the current list of the CPs. If the algorithm does not find the new CP. The CPs calculation is completed. The algorithm compares the current list of the CPs with the minimum list of the CPs and keep the

smaller one.

The algorithm continues to evaluate the next corner until it evaluates all the corners in the measurement area. Each time the lists are compared, the algorithm overwrites the minimum list of the CPs if it finds the variant in which the smaller number of the CPs is calculated. After evaluating all corners, the algorithm obtains the list containing the minimum number of CPs that cover the entire measured area.

The entire procedure of the algorithm is shown in Fig. 6.6, where the first two iterations and the last iteration of determining CPs for measurement short-term recurring noise are shown. A room was chosen for the example, which is based on Fig 2.4. The algorithm splits the entire measurement area into imaginary individual triangles.

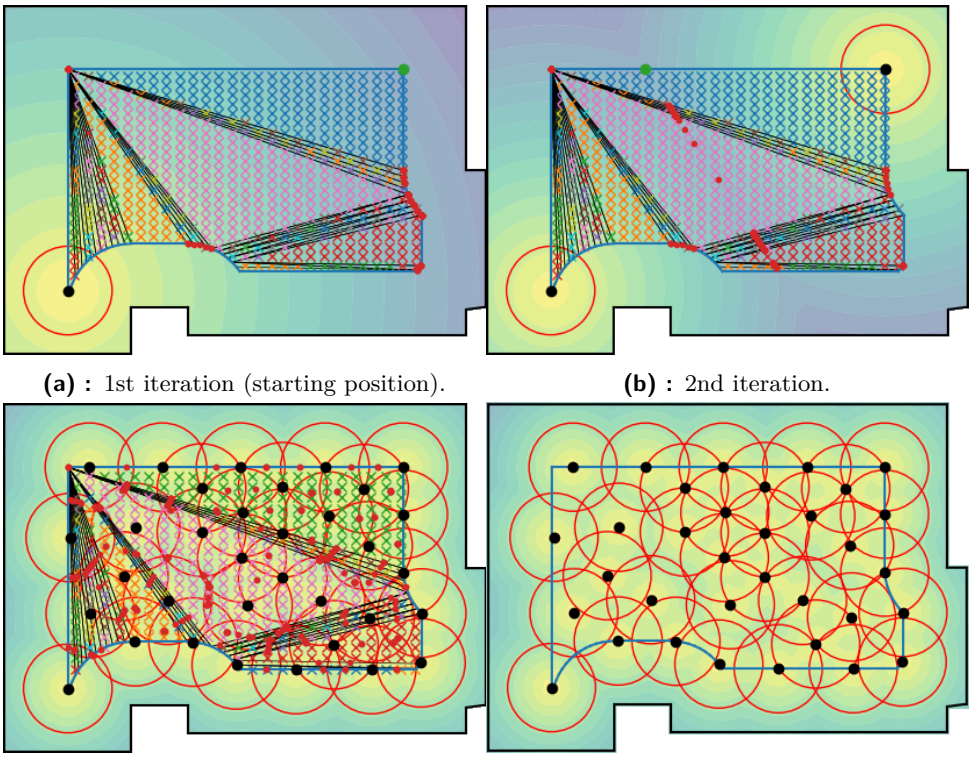

(a) : 1st iteration (starting position). **(b) :** 2nd iteration.

(c) : 33rd iteration. **(d) :** 33rd iteration [16].

Figure 6.6: Example of calculation of the CPs for short-term recurring noise.

Fig. 6.6a shows the calculation of the new CP in the first iteration, where the red dots are local maxima and the green dot is the selected new CP from all local maxima. Fig. 6.6b shows the second iteration's calculation, where the colored background changes based on the already placed CPs from previous iterations. Fig. 6.6c shows the last iteration when it is not possible to place another CP. Fig. 6.6d shows the same iteration but without plotting the supporting parts of the calculation (triangles, candidates for the CPs, and local maxima). This plotting is used further in this Chapter.

6.1.3 Illustration of the Proposed Solution

Similar to the measurement of illuminance, it is possible to create an illustration of the entire proposed solution of acoustic noise measurement using a robotic unit. An example of such an illustration can be seen in Fig. 6.7, where the black dots show the CPs where the previous noise measurement was performed. The blue curved line shows the boundary of the measurement area $\partial\mathcal{I}$. The red circles show the boundaries of the areas in which the acoustic noise measurement will no longer be performed. The red cross shows the future measurement point (the CP). After planning the trajectory without collisions (purple dashed curve), the mobile platform equipped with a sound level meter moves to the new CP. Fig. 6.7a and Fig. 6.7b show an algorithm for long-term stationary noise, which searches for the maximum number of CPs in the measurement area $\mathcal{I}$. Fig. 6.7c and Fig. 6.7d show an algorithm short-term recurring noise, which in each iteration looks for the new CP furthest from the already determined CPs. The colored background shows the distances from the already measured points (the CPs).

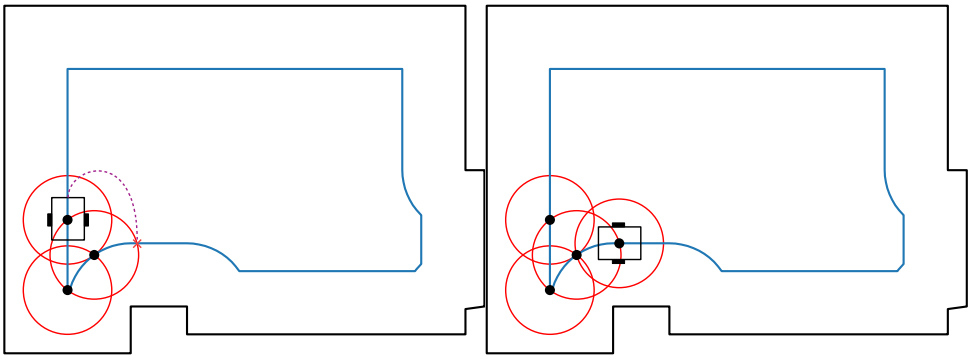

(a) : 3rd iteration. **(b) :** 4th iteration.

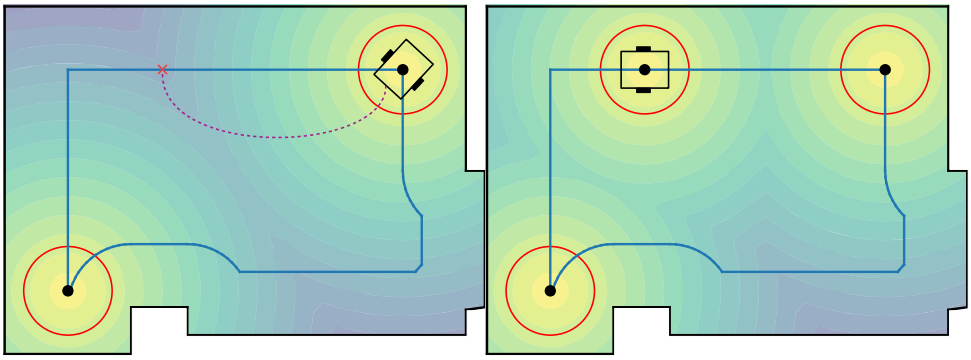

(c) : 2nd iteration. **(d) :** 3rd iteration.

Figure 6.7: The overview of one iteration in the measurement process of acoustic noise using a robotic unit.

6.2 Experimental Evaluation of the Proposed Solution

In order to verify that the proposed solution for the acoustic noise measurement works correctly, the algorithm for measurement long-term stationary noise and the algorithm for measurement short-term recurring noise are experimentally tested. This experimental testing consists of simulations and real measurements, where the second robotic unit is used to move the measurement device to each determined CP within the measurement area $\mathcal{I}$. The simulated experiments focus on the testing of both algorithms to monitor the correct evaluation of the measured rooms. During the most simulated experiments, the total number of CPs and the calculation time of these CPs for both algorithms are recorded. The number of the CPs and the calculation time are then compared between the individual simulated experiments and both algorithms. The results of this comparison show number of the CPs calculated by each algorithm for the best variant and the time required to calculate all the CPs in the best variant in the measurement area $\mathcal{I}$ of the given experiment. Robotic experiments verify the maturity of both algorithms in real conditions, which includes the determination of measurement uncertainties.

6.2.1 Simulated Experiments

In this section, the evaluation of the proposed solution for acoustic noise measurement is described for simulated experiments. The acoustic noise measurement is divided into two types according to the acoustic noise source: long-term stationary and short-term recurring noise. Both types are considered in the experiments. Each simulated experiment is divided into two simulations. First, the algorithm for long-term stationary noise (1st alg.) is simulated, and then the algorithm for short-term recurring noise (2nd alg.). Seven simulated experiments are performed to verify both algorithms. The first six simulated experiments focus on verifying the correct implementation of the 1st alg. and the 2nd alg. by changing the static input parameter (see more in Sec. 6.1) for the calculation of the CPs (floor plan of the measured room). The seventh simulated experiment is focused on changing the dynamic input parameters. The simulated experiments focus on the change of the static input parameter are gradually performed in:

- a simple geometric room which has a floor plan with an area of 16 m^2 (4×4 m),
- a real room which has a floor plan with an area of 39 m^2 (7.5×5.5 m),
- a large room which has a floor plan with an area of about 235 m^2 (15×17.5 m),
- a larger room with one column which has a floor plan with an area of 64 m^2 (8×8 m), and

- a large room with many obstacles which has a floor plan with an area of 144 m^2 (12 × 12 m).

The dynamic input parameters for the first six simulated experiments are:

- The distance between the walls ($\partial\mathcal{P}$) and the boundary of the measurement area $\partial\mathcal{I}$ or column/obstacles as specified by the standard [7] and set to 1 m.
- The radius of a circle representing the boundary of the forbidden area from each the CP in which no other CPs may be located set to 0.7 m (Sec. 2.5.2).

Evaluation of the Algorithms in Simple Room

The first experiment verifies the correctness of the implementation of both algorithms by comparing them with the proposed solution described in Sec. 6.1.1 and Sec. 6.1.2. According to Sec. 6.1.1, the 1st alg. calculates the maximum number of the CPs in the measured room. The 2nd alg. calculates the minimum number of the CPs covering the entire measured room according to Sec. 6.1.2. The experiment is performed in the room with the simple geometric floor plan, for which both algorithms calculate and determine the CPs. The experiment is divided into two simulations.

Fig. 6.8 shows the first simulation where the algorithm determines the CPs for long-term stationary noise. The 1st alg. found four positions located in the corners of the room. For each of these positions, the 1st alg. calculates the list of the CPs. Since this is the very simple geometric room, the result is always the same and the 1st alg. determines 11 CPs as the maximum list. Fig. 6.9 shows the distribution of the CPs over the measured area $\mathcal{I}$, with the first CP in the given variant being shown by a gray point. Fig. 6.9 shows the square room, which is centrally symmetrical. It can be seen from the results that the CPs are equally distributed for all variants but rotated centrally depending on the selected variant.

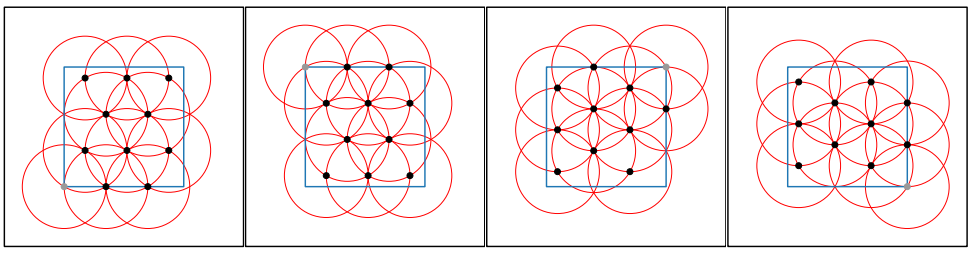

(a) : 1st variant. **(b) :** 2nd variant. **(c) :** 3rd variant. **(d) :** 4th variant.

Figure 6.9: Simulated results of four variants, where the first CP in a given variant is shown by a gray point.

The first iteration of the 1st alg. is shown in Fig. 6.8a, where the algorithm placed the first CP in the lower-left corner. Fig. 6.8b shows the fifth iteration when the 1st alg. determines the CPs in the inner part of the measurement

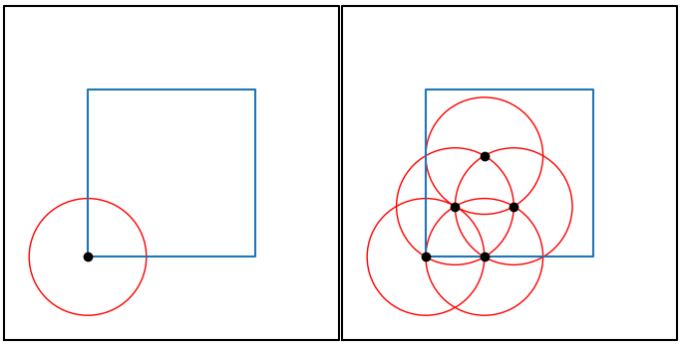

(a) : 1st iteration. **(b) :** 5th iteration.

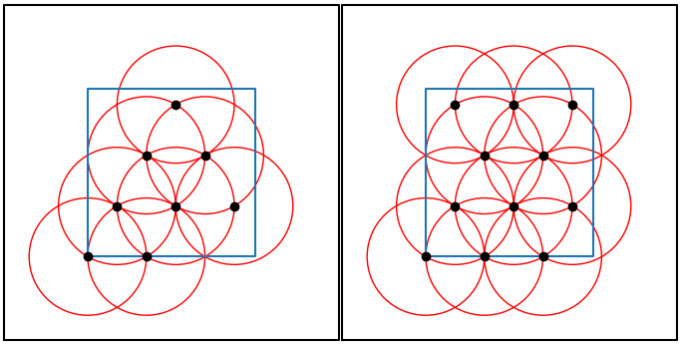

(c) : 8th iteration. **(d) :** 11th iteration.

Figure 6.8: Simulation of long-term stationary noise for simple geometric room [16].

area $\mathcal{I}$. Fig. 6.8c shows the 1st alg. in the ninth iteration, when most of the measurement area $\mathcal{I}$ is covered by the CPs. Fig. 6.8d shows the last, eleventh iteration when the entire measurement area $\mathcal{I}$ is covered by the CPs, and it is not possible to add another CP. It can be seen from the results that the 1st alg. proceeded according to the first step of determining the CPs as described in Sec. 6.1.1. The CPs are determined at the intersections of red circles that define the boundary of the area where the CP must not be added. The 1st alg. followed the steps described in Sec. 6.1.1 until no additional CP can be added and all already determined CPs are located at the intersections. Therefore, this first simulation of the simple geometric room experiment can be declared successful.

Fig. 6.10 shows the second simulation of the experiment, where the 2nd alg. is simulated. Since this is a symmetrical simple room, again, the 2nd alg. determines the same number of the CPs from any corner of the room. Total the 2nd alg. determines thirteen CPs in the measured room. Fig. 6.10a shows the 2nd alg. in the first iteration, where the algorithm determines the first CP in the lower left corner. Fig. 6.10b shows how the 2nd alg. always adds the CPs as far as possible from already specified the CPs. Fig. 6.10c shows the measurement area $\mathcal{I}$ covered by the CPs. However, other CPs can still be placed at the intersections of the red circles, and therefore only Fig. 6.10d shows the last iteration.

It can be seen from Fig. 6.10b that the 2nd alg. determines the CPs according to Sec. 6.1.2. It can also be seen from Fig. 6.10d that the 2nd alg. proceeds according to the parameters set in Sec. 6.1.2 and adds the CPs until it fills the entire measurement area $\mathcal{I}$. In this second simulation of the first experiment, it is verified that the 2nd alg. it is correctly implemented, and further experiments of both algorithms can be performed in more diverse rooms.

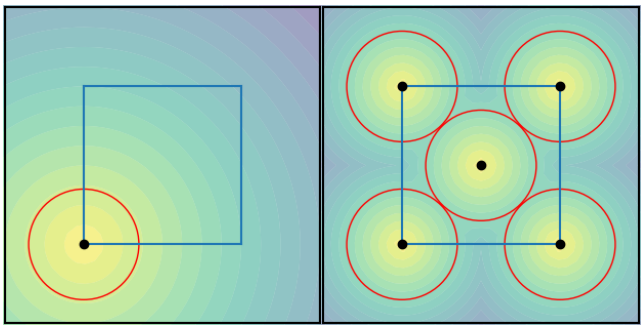

(a) : 1st iteration. **(b) :** 5th iteration.

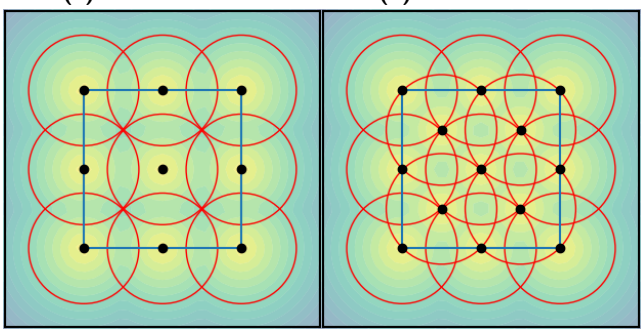

(c) : 9th iteration. **(d) :** Last iteration.

Figure 6.10: Simulation of short-term recurring noise for simple geometric room [16].

Evaluation of the Algorithms in Real Room

This experiment uses a real simulated room for testing. The room has a more complex floor plan than in the first experiment. Both algorithms are evaluated to place the CPs according to the implementation listed in Sec. 6.1.1 for the 1st alg. and in Sec. 6.1.2 for the 2nd alg.

The first simulation of the experiment is shown in Fig. 6.11. Fig. 6.11a shows the second iteration as the 1st alg. determines the starting position from which it is possible to obtain the maximum number of the CPs for this measured room. Fig. 6.11b shows the 24th iteration, where the 1st alg. adds the last CP at the boundary of the measurement area $\partial\mathcal{I}$. Fig. 6.11c shows the 25th iteration, where the 1st alg. has covered with the CPs the entire boundary of the measurement area $\partial\mathcal{I}$, and the 1st alg. further places the CP at the intersection of the red circles in the inner part of the measurement area $\mathcal{I}$. Fig. 6.11d shows the last iteration when the entire measured area $\mathcal{I}$

is covered by the CPs, and it is not possible to add another CP.

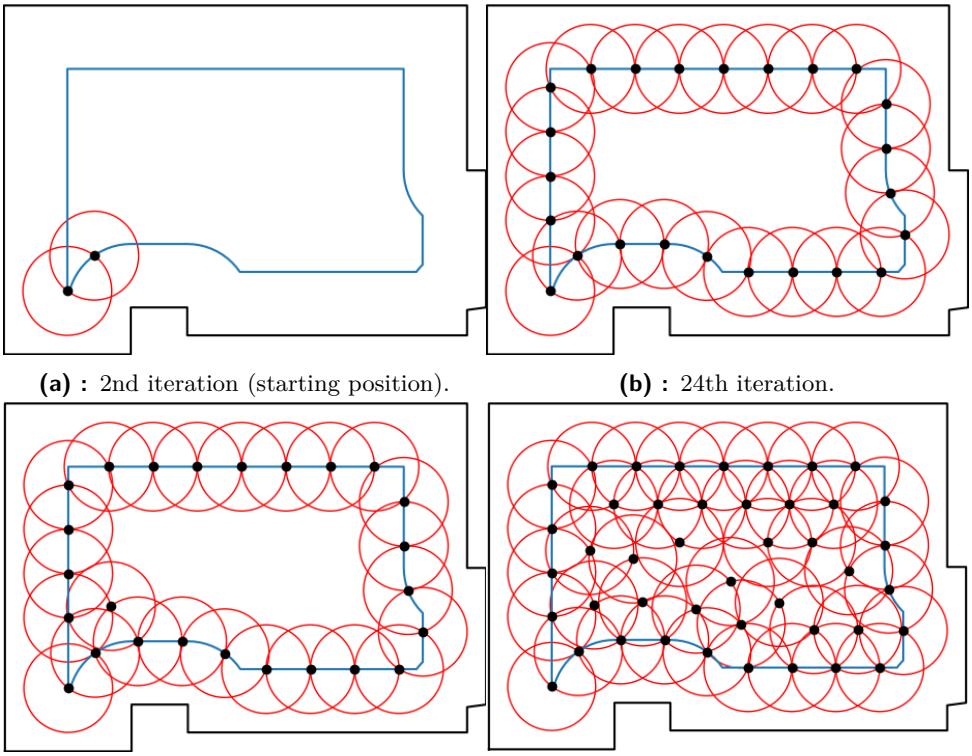

(a) : 2nd iteration (starting position). **(b) :** 24th iteration.

(c) : 25th iteration. **(d) :** 44th iteration [16].

Figure 6.11: Simulation of long-term stationary noise for real room.

It is worth noting that the 1st alg. first determines the CPs at the boundary of the measurement area $\partial\mathcal{I}$, which is evident in Fig. 6.11b. It then passes into the inner area of the measured area $\mathcal{I}$ (Fig. 6.11c). Based on the above results, it can be determined that the 1st alg. determines the CPs according to the implementation mentioned in Sec. 6.1.1.

The second simulation of the experiment is shown in Fig. 6.12, where the 2nd alg. determines a total of 28 CPs as the minimum list of the CPs (covering the entire room), because it is no longer possible to add another CP into this measured area $\mathcal{I}$. Fig. 6.12a shows the starting position for determining the CPs by the 2nd alg. in first variant of the second simulation of the experiment. Fig. 6.12b and Fig. 6.12c show how the 2nd alg. gradually fills the room with the CPs. Fig. 6.12d shows the last iteration of this variant, in which the minimum number of the CPs in the measured area $\mathcal{I}$ is found.

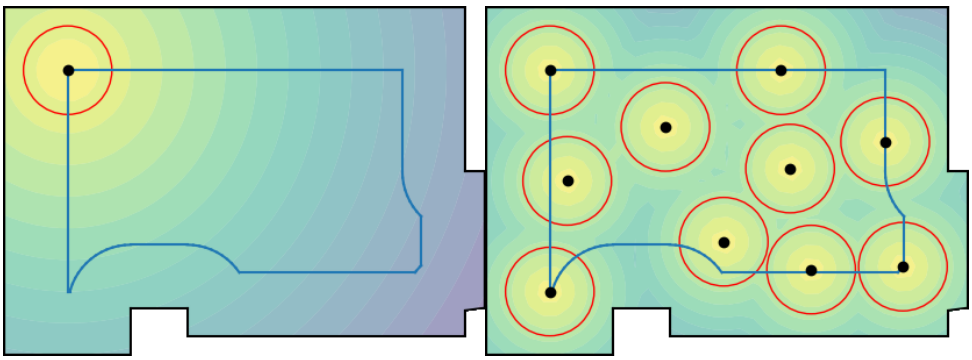

(a) : 1st iteration (starting position). **(b) :** 10th iteration.

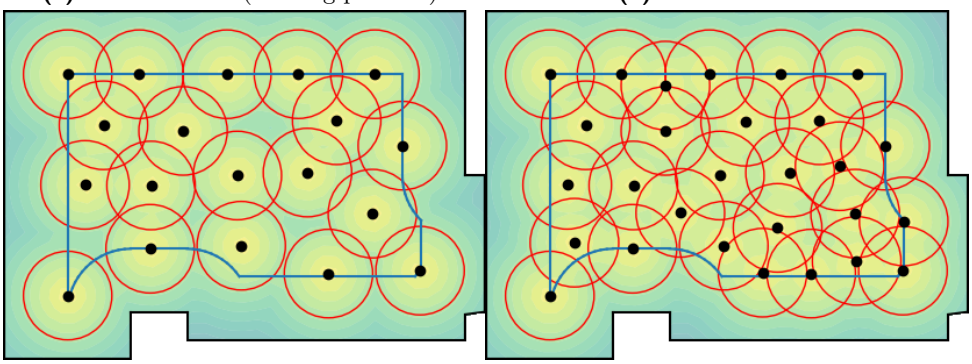

(c) : 19th iteration. **(d) :** 28th iteration.

Figure 6.12: Simulation of short-term recurring noise for real room.

The results of the second simulation of the experiment also show that the 2nd alg. can add the CPs in the measured area $\mathcal{I}$ of a room with more complex geometry. The experiment thus shows from the results that both algorithms can adapt to the floor plan and dimensions of the real room.

Evaluation of the Algorithms in Large Room

The third experiment is focused on verifying the robustness of algorithms in an even more demanding floor plan of the simulated room. The experiment verifies the robustness in the calculation of the CPs in a large geometrically diverse room. This simulated room has larger dimensions than the simulated rooms used in the first two experiments. The experiment is again divided into two simulations, where in the first simulation is tested the 1st alg. and in the second simulation is tested the 2nd alg.

The testing procedure of the 1st alg. is seen in Fig. 6.13, where Fig. 6.13a shows the first iteration of the 1st alg. Fig. 6.13b shows the 1st alg. in 120th iterations, where the 1st alg. systematically finds the CPs in the measurement area $\mathcal{I}$. Fig. 6.13c shows the 1st alg. in 240th iterations, where the room is being mostly covered by the visible CPs. The total number of the CPs is 362, and the final coverage of the room by the CPs can be seen in Fig. 6.13d. From the result of the first test, it is evident that the 1st alg. can determine the CPs in the entire measurement area $\mathcal{I}$ and thus provides the possibility

to obtain the maximum list of the CPs according to Sec. 6.1.1.

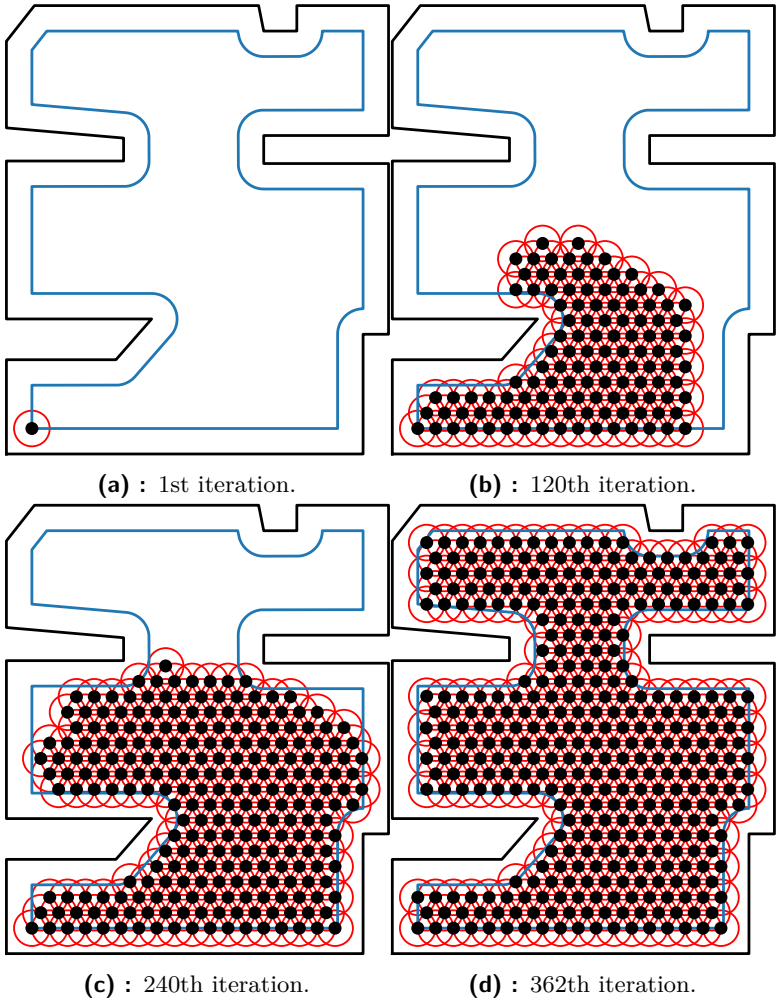

(a) : 1st iteration. **(b) :** 120th iteration.

(c) : 240th iteration. **(d) :** 362th iteration.

Figure 6.13: Simulation of long-term stationary noise for large room.

Fig. 6.14 shows the process of testing the 2nd alg., where Fig.6.13a shows the starting position from which the 2nd alg. found the minimum CPs. The 2nd alg. gradually adds additional CPs (Fig.6.13b and Fig.6.13c) until it fills the entire measured area $\mathcal{I}$. In the 224th iteration (6.13d) the 2nd alg. decides that it is no longer possible to add additional CPs and terminates the variant. From the above results, it is clear that the 2nd alg. found the CPs covering the entire measurement area $\mathcal{I}$ when it is not possible to add another CP in the measured area $\mathcal{I}$. Thus, the 2nd alg. proved that it can also determine the CPs in the large geometrically diverse room. The results of the first three simulated experiments verified that both algorithms determine the CPs according to the implementation in Sec. 6.1.1 for the 1st alg. and in Sec. 6.1.2 for the 2nd alg.

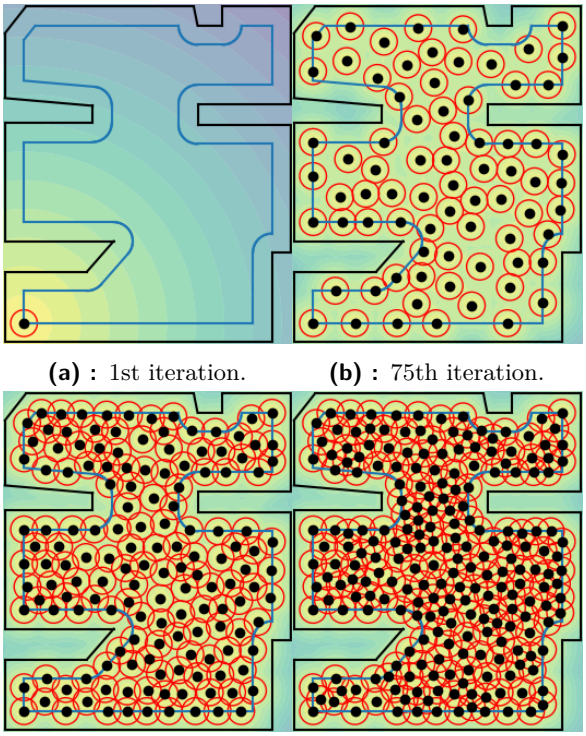

(a) : 1st iteration. **(b) :** 75th iteration.

(c) : 149th iteration. **(d) :** 224th iteration.

Figure 6.14: Simulation of short-term recurring noise for large room [16].

Evaluation of the Algorithms in Larger Room with Column

The next two simulated experiments focus on verifying whether both algorithms can respond to obstacles located in the measurement area $\mathcal{I}$. In a real environment, these obstacles represent, for example, columns and partitions. The first experiment tests algorithms in a simple square environment that contains one column located in the center of the measurement area $\mathcal{I}$. The standard [7] states that no CP may be located at a defined distance from a fixed obstacle. This distance is the same as the distance between the boundary of the measurement area $\partial\mathcal{I}$ and the wall $\partial\mathcal{P}$ of the measured room.

The first simulation of the experiment tests the 1st alg., while the process of testing can be seen in Fig. 6.15. Fig. 6.15 shows a black rectangle in the middle of the measurement area $\mathcal{I}$, which shows the column around which the border of the measurement area $\partial\mathcal{I}$ is marked in light blue. The 1st alg. found the maximum list of the CPs with the first CP located in the upper left corner of the measurement area $\mathcal{I}$, as shown in Fig. 6.15a. Fig. 6.15b shows the 23rd iteration when the algorithm begins to determine the CPs at the inner boundary of the measurement area $\partial\mathcal{I}$ marked by the column. Fig. 6.15c shows the 46th iteration where the algorithm continues to stake out the CPs and safely avoids placing the CPs closer than 1 m from the column. Fig. 6.15d shows the maximum list the CPs for a measurement area $\mathcal{I}$ with

one column in the middle of the measurement area $\mathcal{I}$.

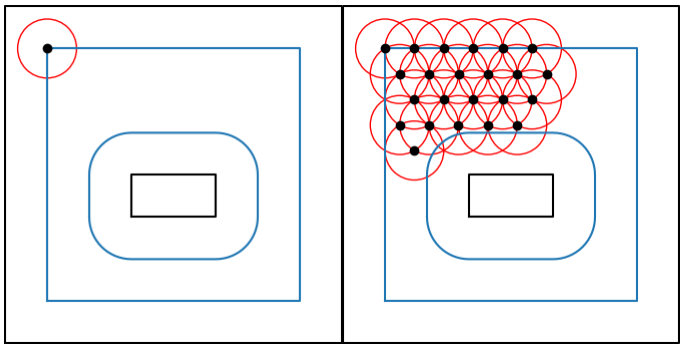

(a) : 1st iteration. **(b) :** 23rd iteration.

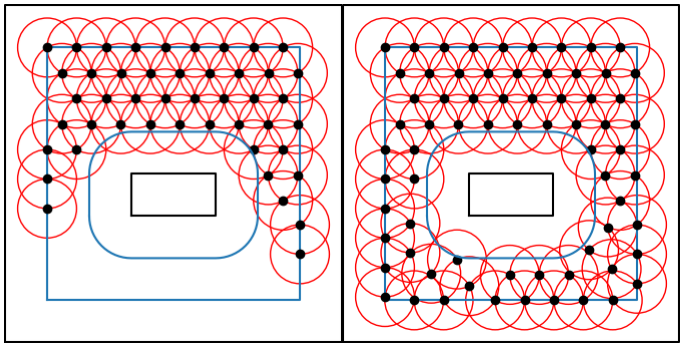

(c) : 46th iteration. **(d) :** 69th iteration.

Figure 6.15: Simulation of long-term stationary noise for larger square room with one column [25].

The results of the first simulation of the experiment show that the 1st alg. can respond to an obstacle in the measurement area $\mathcal{I}$. The 1st alg. correctly marks the boundary of the measurement area $\partial\mathcal{I}$ around this obstacle at a specified distance of 1 m. It can be seen from Fig. 6.15d that the 1st alg. did not place any the CP outside the measurement area $\mathcal{I}$ during the entire CPs calculation. This verified that the 1st alg. can respond correctly to simple obstacles in the inner part of the measurement area $\mathcal{I}$.

The second simulation of the experiment can be seen in Fig. 6.16, where the 2nd alg. is tested on the same room with one column. Fig. 6.16a shows the starting position at which the first CP is located in the lower-left corner of the measurement area $\mathcal{I}$. Fig. 6.16b and Fig. 6.16c show the course of the calculation of the CPs, which are located only in the measurement area $\mathcal{I}$. Fig. 6.16d shows the last iteration, where the 2nd alg. determined 45 CPs and another CP cannot be added to the measurement area $\mathcal{I}$.

It is worth noting the green point in Fig. 6.16, which identifies the next CP in the following iteration. It is thus possible to check from the colored background that the 2nd alg. determines the CP in the measured room correctly. The 2nd alg. uses the colored background in the calculation, which shows the color change based on the distance from the already determined CPs. Fig. 6.16d shows that the 2nd alg. determined all the CPs only in the

measurement area $\mathcal{I}$, which is always defined 1 m from a fixed obstacle or wall. Thus, the second simulation of the experiment proved that the 2nd alg. works correctly and can respond to the column in the measured room.

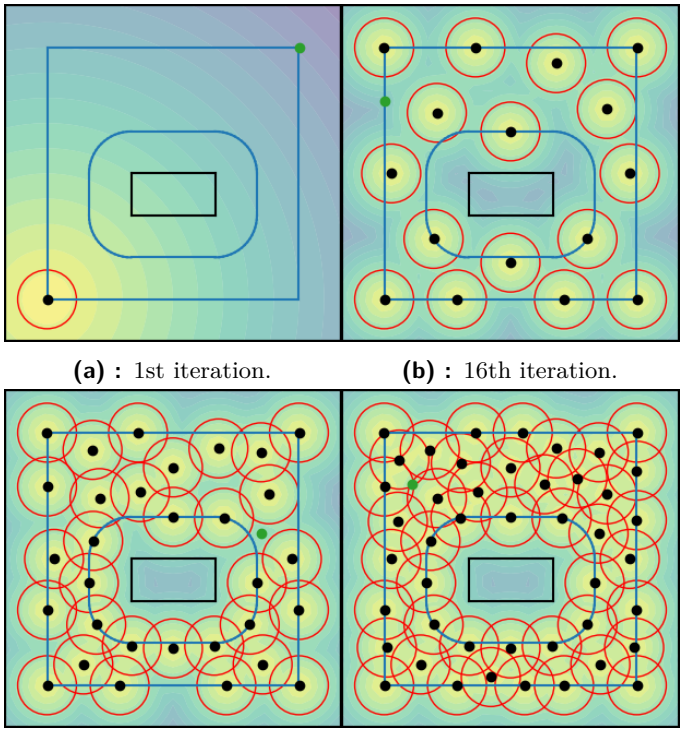

(a) : 1st iteration. **(b) :** 16th iteration.

(c) : 30th iteration. **(d) :** 45th iteration.

Figure 6.16: Simulation of short-term recurring noise for larger square room with one column [25].

Evaluation of the Algorithms in Large Room with Obstacles

In this experiment measured room contains various obstacles inside and outside of the measurement area $\mathcal{I}$. It is assumed that the algorithms also adapt the measured area $\mathcal{I}$ to obstacles that are less than 2 m from the wall $\partial\mathcal{P}$. In this way, the test conditions are determined, and the experiment is again divided into two simulations.

The first simulation of the 1st alg. is shown in Fig. 6.17. The 1st alg. determined the upper right corner as the starting corner, as shown in Fig. 6.17a, from which it calculated the maximum list of the CPs for this measured room $\mathcal{I}$. Fig. 6.17b shows the 62nd iteration, in which the 1st alg. determines the CPs only in the defined measurement area $\mathcal{I}$. The 1st alg. in Fig. 6.17c continues to calculate new CPs and places them in the measurement area $\mathcal{I}$, which is already largely filled with the CPs. At the 187th iteration, the 1st alg. finished calculating the CPs because it is not possible to add another CP to the defined measurement area $\mathcal{I}$.

Fig. 6.17d shows that the 1st alg. correctly determined all the boundaries of the measurement area $\partial\mathcal{I}$. Furthermore, the 1st alg. calculated the maximum

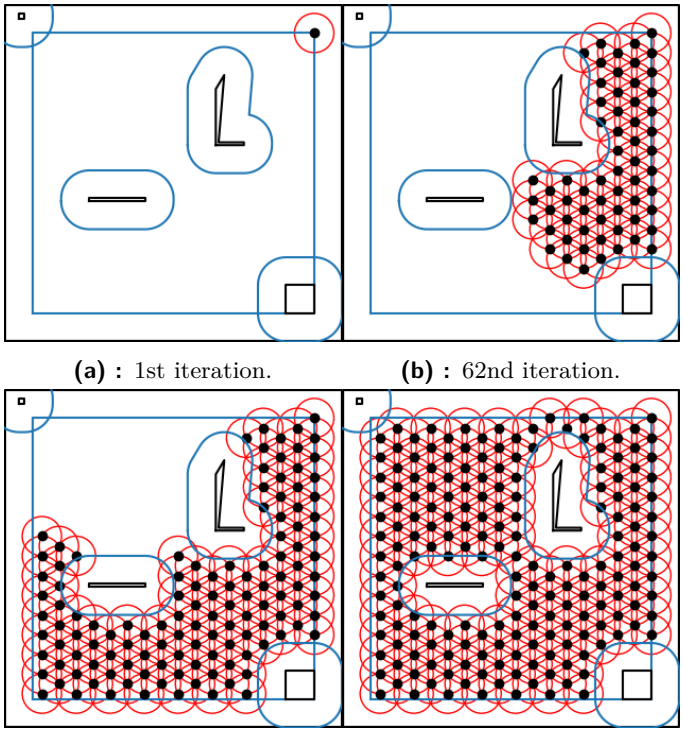

(a) : 1st iteration. **(b) :** 62nd iteration.

(c) : 124th iteration. **(d) :** 187th iteration.

Figure 6.17: Simulation of long-term stationary noise for a large square room with many obstacles [25].

list of the CPs according to Sec. 6.1.1 and determined the CPs only in the measurement area $\mathcal{I}$. Thus, the 1st alg. fulfilled the assumption that it can adapt to more obstacles that are located inside and outside the measurement area $\mathcal{I}$.

The second simulation of the experiment evaluated the 2nd alg. to see if it can respond correctly to various obstacles in the measured room. The process of determining the CPs is shown in Fig. 6.18. The 2nd alg. specified the lower left corner as the starting position for obtaining the minimum number of the CPs, which covers the entire area of measurement $\mathcal{I}$ by the CPs (Fig. 6.18a). Fig. 6.18b and Fig. 6.18c show how the 2nd alg. correctly determines the CPs and gradually fills the measurement area $\mathcal{I}$. Fig. 6.18d shows the last iteration in which the 125 CPs is placed in the measurement area $\mathcal{I}$. The 2nd alg. subsequently determined that it is not possible to add another CP to the room.

The results of the second simulation of the experiment showed that the 2nd alg. correctly determined the boundary of the measurement area $\partial\mathcal{I}$, (1 m from the fixed obstacle and the wall $\partial\mathcal{P}$). It can be seen from the process of determining the CPs (Fig. 6.18) that the 2nd alg. proceeds correctly according to the procedure given in Sec. 6.1.2. From the results shown in Fig. 6.18, it is possible to determine that the 2nd alg. met the assumption and correctly responded to the obstacles distributed throughout the room. The first five

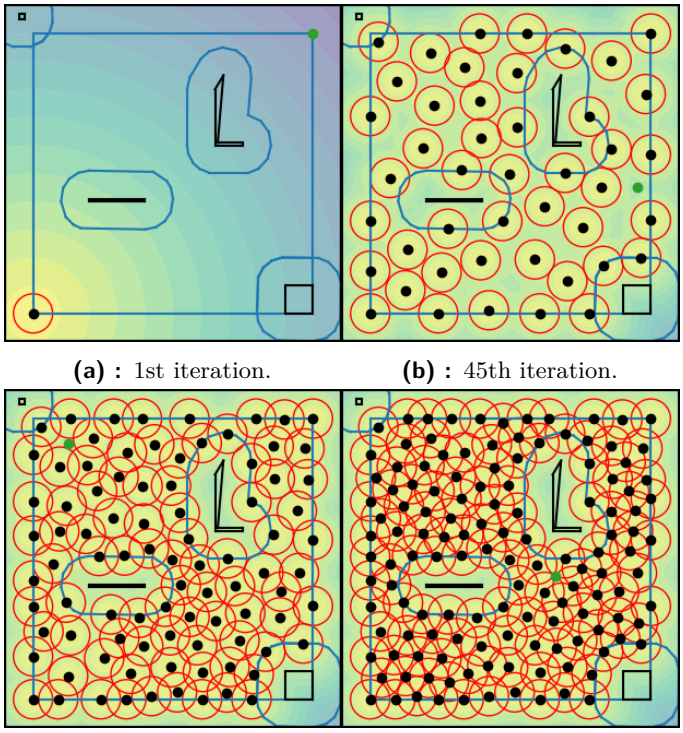

(a) : 1st iteration. **(b) :** 45th iteration.

(c) : 89th iteration. **(d) :** 133rd iteration.

Figure 6.18: Simulation of short-term recurring noise for a large square room with many obstacles [25].

experiments showed that both algorithms are correctly implemented and can respond to different floor plans of rooms, which also contain obstacles.

Simulated Experiment with Comparison of Starting Positions

This experiment aims to verify that both algorithms correctly determine the maximum list of the CPs for the 1st alg. and the minimum list of the CPs for the 2nd alg. with constant input parameters (for example room floor plan). This experiment uses the floor plan, which is also used in the second simulated experiment. This room is selected from all simulated rooms because it most closely resembles spaces that correspond to real conditions. Both priority corner determination classes are canceled for this experiment (see Sec. 6.1). All corners created by defining the measurement area $\mathcal{I}$ are included in the experiment. However, only four selected variants are always displayed, with one of them showing the maximum/minimum list of the CPs found.

This experiment is again divided into two simulations, as in the previous five experiments. Fig. 6.19 shows the selected starting positions from the four variants. Each variant always has the first CP in a different corner. Each column represents one variant, where the top row is the starting position of the variant and the bottom row is the last iteration of the given variant.

Fig. 6.19e shows the last iteration of the first variant, in which the 1st alg.

found 44 CPs in the entire measurement area $\mathcal{I}$. The 1st alg. saves this first variant in the currently largest list, which the 1st alg. uses to store the currently found maximum number of CPs. The 1st alg. continues to the next corner. The currently largest list is then compared with each calculated variant. The third variant can be seen in Fig. 6.19b, where the starting position is located in the upper right corner (the third is determined by the 1st alg. in the measured area $\mathcal{I}$). In this variant, the 1st alg. calculated 41 CPs (Fig. 6.19f). The fourth variant is shown in Fig. 6.19c and Fig. 6.19g, where the 1st alg. calculated 41 CPs. In the seventh corner, at the starting position shown in Fig. 6.19d, the 1st alg. determined 43 CPs (Fig. 6.19h).

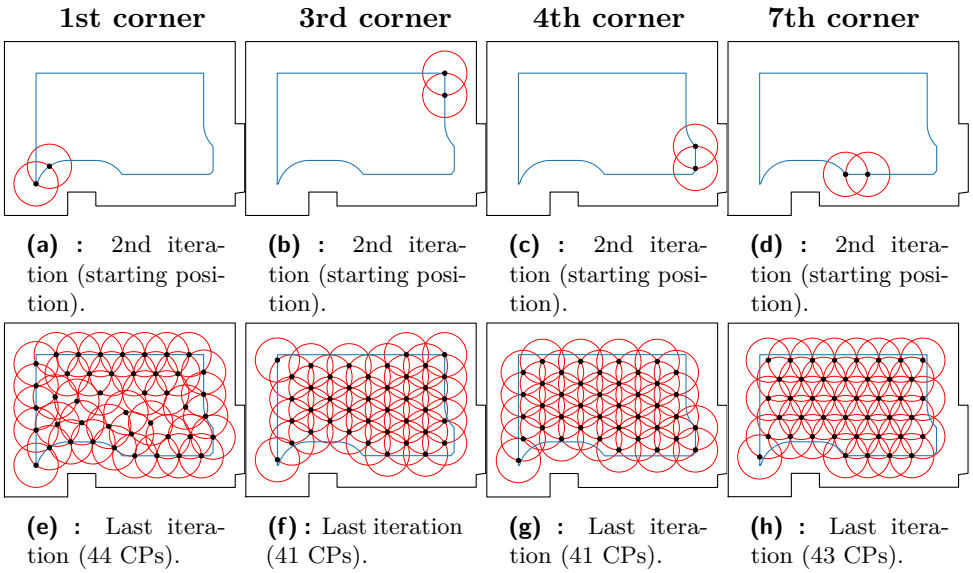

(a) : 2nd iteration (starting position).
(b) : 2nd iteration (starting position).
(c) : 2nd iteration (starting position).
(d) : 2nd iteration (starting position).
(e) : Last iteration (44 CPs).
(f) : Last iteration (41 CPs).
(g) : Last iteration (41 CPs).
(h) : Last iteration (43 CPs).

Figure 6.19: Simulated results for different variants of CPs calculation with the 1st alg. The top row, i.e., subfigures a, b, c and d, show the starting position for the given variant. The bottom row, i.e., subfigures e, f, g and h, show the last iteration with the number of the CPs for the given variant.

The results in Fig. 6.19 show that the first variant, determined by the 1st alg., has the maximum list of the CPs. However, although not all variants of the 1st alg. are listed here, no variant exceeds the first variant by the number of the CPs. Therefore, the first variant is determined as the best variant in which the 1st alg. determined the maximum number of the CPs in the measurement area $\mathcal{I}$. This result is consistent with the result from the first simulation of the second experiment. This proved that the 1st alg. correctly determines the maximum list of the CPs in the measurement area $\mathcal{I}$.

The second simulation of the experiment tests the 2nd alg. to determine whether it correctly determines the minimum list of the CPs in the measured area $\mathcal{I}$. Fig. 6.20 again shows four selected variants with the same column layout as in the first simulation of the experiment. The first starting position of the first variant is determined in the first corner, i.e., the lower-left corner of the measurement area $\mathcal{I}$, as seen in Fig. 6.20a. Fig. 6.20e shows the last iteration of the first variant, when the 2nd alg. determined 32 CPs.

The 2nd alg. saved this variant for further comparison with other variants. Fig. 6.20b, Fig. 6.20c and Fig. 6.20d show other selected variants and their starting positions. In Fig. 6.20f the 2nd alg. calculates 28 CPs that cover the entire measurement area $\mathcal{I}$ and it is not possible to add another CP. Fig. 6.20g shows the last iteration of the third variant of the 2nd alg., in which the 2nd alg. determines 32 CPs. The last selected variant shows 30 CPs in the last iteration in Fig. 6.20h.

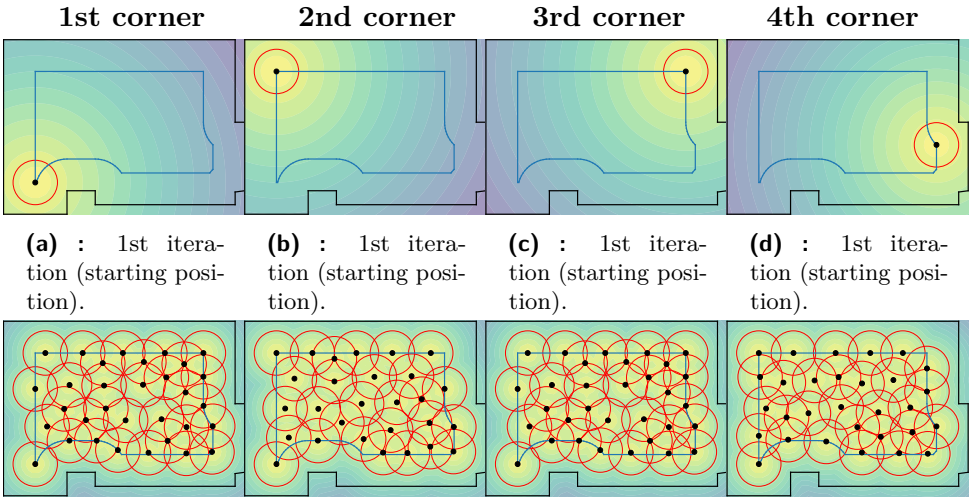

(a) : 1st iteration (starting position).
(b) : 1st iteration (starting position).
(c) : 1st iteration (starting position).
(d) : 1st iteration (starting position).
(e) : Last iteration (32 CPs).
(f) : Last iteration (28 CPs).
(g) : Last iteration (32 CPs).
(h) : Last iteration (30 CPs).

Figure 6.20: Simulated results for different variants of the CPs calculation with 2nd alg. The top row, i.e., subfigures a, b, c and d, shows the starting position for the given variant. The bottom row, i.e., subfigures e, f, g and h, shows the last iteration with the number of the CPs for the given variant.

The results in Fig. 6.20 show four selected variants of the 2nd alg., which searches for the minimum list of the CPs covering the entire measurement area $\mathcal{I}$. After calculating the second variant, the 2nd alg. compared the number of the CPs with the first variant and saved the second variant due to the lower number of the CPs found. This result is not surpassed by any other variant. Therefore, the 2nd alg. determined that the second variant is the best variant from the number of CPs found. This result again agrees with the second simulation of the second simulated experiment. The 2nd alg. proved that it correctly determines the minimum list of the CPs covering the entire measurement area $\mathcal{I}$.

Simulated Experiment with Changing Dynamic Input Parameters

The seventh simulated experiment focuses on verifying that both algorithms can adapt to changes in dynamic input parameters (more about parameters in Sec. 6.1). Several simulations are performed for each algorithm, in which the dynamic input parameters for the calculation of the CPs change. Let us repeat that the first dynamic input parameter is the distance of the measurement

area boundary $\partial\mathcal{I}$ from the wall $\partial\mathcal{P}$. The second dynamic input parameter is the distance of the area boundary around each CP, in which no other CP must be located. The experiment uses the same floor plan of the measured room (static input parameter) for all simulations, which was used in the previous experiment. Recall that for all previously simulated experiments, the dynamic input parameters were set as follows:

1. distance 1 m between the boundary of the measurement area $\partial\mathcal{I}$ and the wall $\partial\mathcal{P}$ and
2. distance of 0.7 m from each CP.

New values are gradually tested for the distance between the boundary of the measurement area $\partial\mathcal{I}$ and the wall $\partial\mathcal{P}$:

- 0.5 m,
- 1.0 m, and
- 1.5 m.

For the distance of the area boundary around each the CP (red circles), the following values are considered in the simulations:

- 0.3 m,
- 0.5 m,
- 0.7 m,
- 0.9 m, and
- 1.1 m.

Simulations using the 1st alg. are shown in Fig. 6.21, which shows the last iterations in calculating the CPs. Fig. 6.21a shows a simulation where the dynamic input parameters are set to a distance of 0.5 m between $\partial\mathcal{I}$ and $\partial\mathcal{P}$ and the boundary around the CP is 0.3 m. The 1st alg. determines the CPs in the entire measurement area and adapts the calculation to the new dynamic input parameters. Fig. 6.21b shows another simulation where a distance of 1.5 m between $\partial\mathcal{I}$ and $\partial\mathcal{P}$ and boundary of 0.3 m around each the CP is set. Fig. 6.21c has as dynamic input parameters again set 0.5 m between $\partial\mathcal{I}$ and $\partial\mathcal{P}$ and 1.1 m around each the CP. Fig. 6.21d shows the last mentioned simulation, in which the distance between $\partial\mathcal{I}$ and $\partial\mathcal{P}$ is set to 1.5 m. The second dynamic parameter is set to 1.1 m around each CP in the measured room. Since each of these simulations was performed correctly, i.e., the 1st alg. determined all the CPs in the measurement area $\mathcal{I}$ by the first dynamic input parameter, and no the CP is located at a distance defined by the second dynamic input parameter. Therefore, the simulations show that the 1st alg. is able to adapt to all new dynamic input parameters.

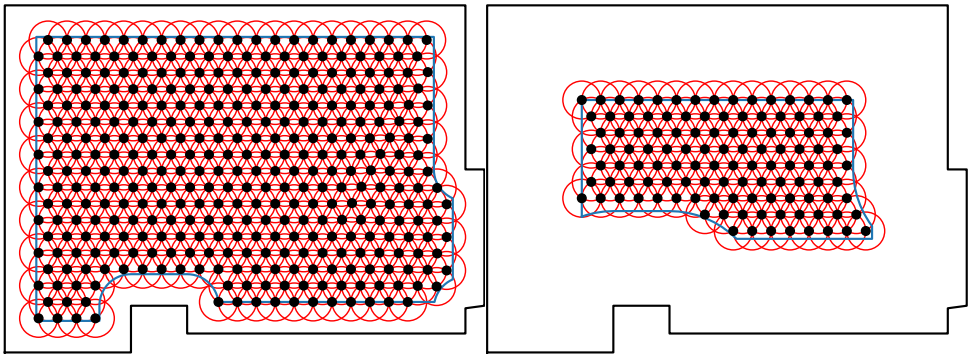

(a) : The distance between $\partial\mathcal{I}$ and $\partial\mathcal{P}$ is 0.5 m, and the boundary around the CP is 0.3 m.

(b) : The distance between $\partial\mathcal{I}$ and $\partial\mathcal{P}$ is 1.5 m, and the boundary around the CP is 0.3 m.

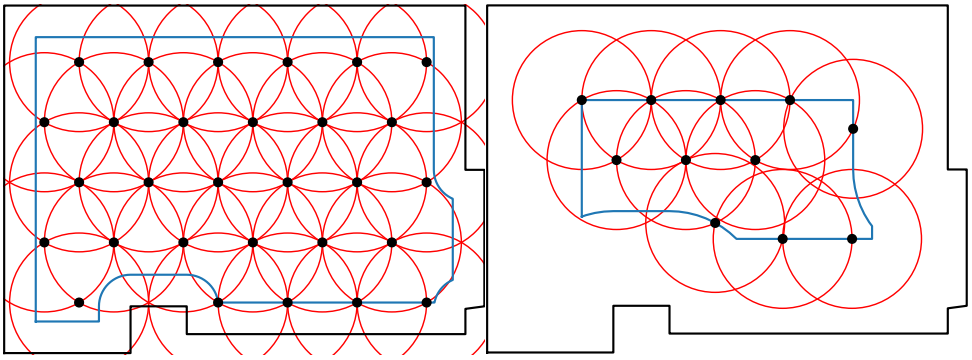

(c) : The distance between $\partial\mathcal{I}$ and $\partial\mathcal{P}$ is 0.5 m, and the boundary around the CP is 1.1 m.

(d) : The distance between $\partial\mathcal{I}$ and $\partial\mathcal{P}$ is 1.5 m, and the boundary around the CP is 1.1 m.

Figure 6.21: Simulated results of the 1st alg. when changing dynamic input parameters.

Fig. 6.22 shows simulations with different dynamic input parameters for the 2nd alg. in the last iteration. These dynamic input parameters are the same for each subfigure as testing the 1st alg. in this experiment. The result of each of these simulations proves that the 2nd alg. is able to respond to both the first and the second dynamic input parameter. Because the 2nd alg. always correctly determined the measurement area $\mathcal{I}$ and calculated all the CPs so that the CPs are located in the measurement area $\mathcal{I}$ and at the correct distances from each other. Overall, the experiment showed that both algorithms can adapt to different dynamic input parameters, even if both dynamic input parameters change at the same time.

The first experiment focused on a simple floor plan, and each following experiment came up with a more difficult environment in which the algorithms were tested. During all simulated experiments, it was shown that the algorithms are able to adapt and respond to various changes in static and dynamic input parameters. The algorithms have also shown that they can adapt the calculation of the CPs even when there are obstacles in the measurement room.

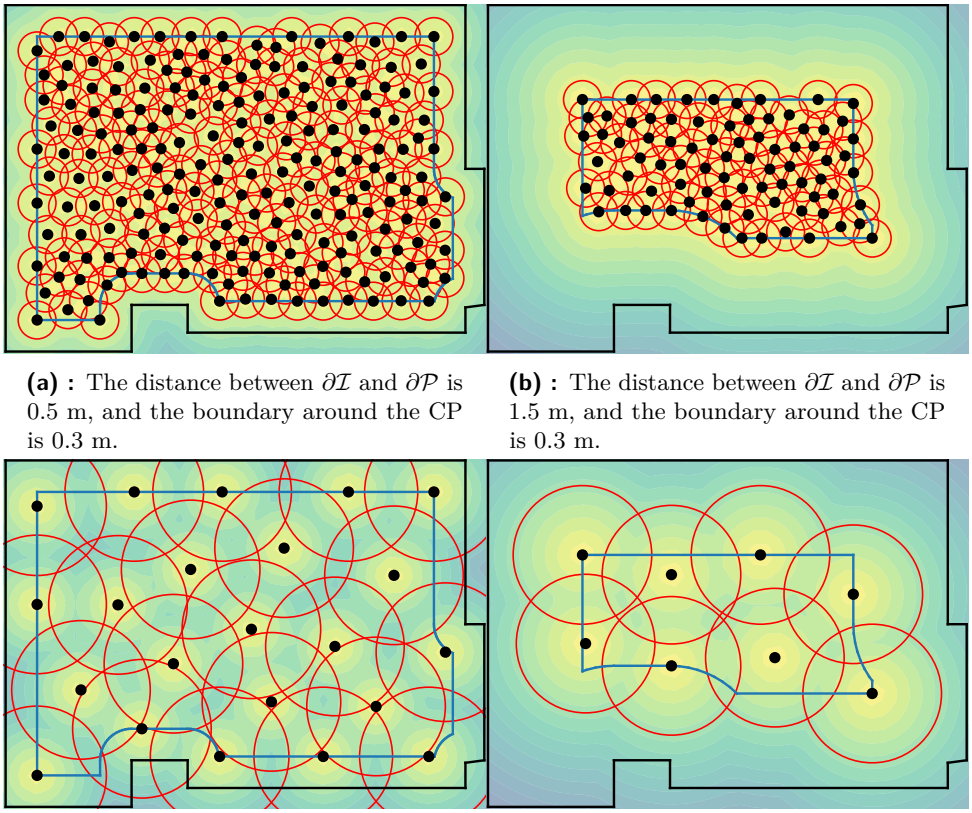

(a) : The distance between $\partial\mathcal{I}$ and $\partial\mathcal{P}$ is 0.5 m, and the boundary around the CP is 0.3 m.

(b) : The distance between $\partial\mathcal{I}$ and $\partial\mathcal{P}$ is 1.5 m, and the boundary around the CP is 0.3 m.

(c) : The distance between $\partial\mathcal{I}$ and $\partial\mathcal{P}$ is 0.5 m, and the boundary around the CP is 1.1 m.

(d) : The distance between $\partial\mathcal{I}$ and $\partial\mathcal{P}$ is 1.5 m, and the boundary around the CP is 1.1 m.

Figure 6.22: Simulated results of the 2nd alg. when changing dynamic input parameters.

6.2.2 Comparison of the Determined Number of Control Points

The simulated experiments showed that the algorithms work according to Sec. 6.1.1 for the 1st alg. and Sec. 6.1.2 for the 2nd alg.. In addition, both algorithms have shown that they can adapt if there are obstacles in the measured room or changes in dynamic input parameters. In addition to the functionality of both algorithms, in addition to the sixth experiment, two other data were monitored during the experiments:

- the number of calculated CPs covering the entire measurement area $\mathcal{I}$, and
- the time required to calculate all the CPs in a given simulation.

This section focuses on the number of the CPs. It is monitored whether the 1st alg. calculates more the CPs than the 2nd alg..

Comparison of the First Five Simulated Experiments

An overview of the number of the CPs covering the entire measured area $\mathcal{I}$ from the first five experiments is given in Tab. 6.1, where the 1st alg. is column A and the 2nd alg. is column B. It is worth noting that the first five experiments were focused on changing the static input parameter. The 1st alg. according to Sec. 6.1.1 finds the maximum list of the CPs covering the entire measured area $\mathcal{I}$. Conversely, the 2nd alg. according to Sec. 6.1.2 determines the minimum list of the CPs that covers the entire measured area $\mathcal{I}$ in the measured room.

Table 6.1: The total number of the CPs for the long-term stationary noise (column A) and short-term recurring noise (column B) [25].

Room	Number of the CPs [-] A	B
Simple geometric room (Fig. 6.8 and Fig. 6.10)	11	13
Real room (Fig. 6.11 and Fig. 6.12)	44	28
Large room (Fig. 6.13 and Fig. 6.14)	362	224
Larger room with column (Fig. 6.15 and Fig. 6.16)	69	45
Large room with obstacles (Fig. 6.17 and Fig. 6.18)	187	133

Surprisingly, in the first experiment, the 1st alg. found two CPs less than the 2nd alg.. This anomaly appeared only in the first experiment and was caused by the simplicity of the simulated room. However, in real conditions, a simple symmetrical room without a diverse floor plan is difficult to find, so this result of the first experiment is negligible.

The second experiment used a room with a real floor plan to verify both algorithms. The assumption is that the 1st alg. determined more the CPs than the 2nd alg. In this room, the 1st alg. determined 44 CPs and the 2nd alg. determined 28 CPs. The results of the experiment show that the algorithms determine the sets of the CPs correctly because it is not possible in any variant to add another CP to the measurement area $\mathcal{I}$. For this reason, it can be stated that both algorithms work correctly as expected.

The third experiment tested both algorithms in a large, diverse room, with the 1st alg. identifying more the CPs than the 2nd alg.. The 1st alg. defined 362 CPs in the measurement area $\mathcal{I}$ of the room, while the 2nd alg. determined 224 CPs in the same area $\mathcal{I}$. The results show that the 1st alg. can find a significantly higher number of the CPs than the 2nd alg..

In the fourth experiment, both algorithms were observed to handle a column in the middle of the room. Again, the algorithms correctly evaluated the measurement area $\mathcal{I}$ and added the CPs so that neither algorithm could add another CP to the measurement area $\mathcal{I}$. The number of the CPs specified

by both algorithms can be seen in Tab. 6.1 for this experiment. The result again shows that the 1st alg. determined more the CPs than the 2nd alg..

The fifth experiment used a simulated room where many obstacles were placed. The 1st alg. determined 187 CPs and the 2nd alg. calculated 133 CPs for the entire measured area $\mathcal{I}$. Although it is a large room with several obstacles, both algorithms compute sets of the CPs corresponding to the implementation.

Comparison of the 1st and the 2nd alg via experiments, apart from the first experiment, shows that the 1st alg. determines a higher number of the CPs than the 2nd alg. This corresponds to the requirements for the long-term static noise measurements as described in Sec. 6.1.1, as the algorithm searches for the maximum number of CPs in the measurement area. On the other hand, the 2nd alg. finds the minimum number of the CPs in the measured area $\mathcal{I}$ of the room. The results of the 2nd alg. correspond to the requirements for measurement of the short-term recurring noise, described in Sec. 6.1.2, as the algorithm searches for the minimal number of CPs in the fewest number of iterations possible. Therefore, it can be stated that the algorithms work correctly for different rooms floor plans (static input parameter).

Comparison of the Results of the Seventh Experiment

This section compares the results of the seventh experiment. A large number of simulations were performed in the experiment where the dynamic input parameters changed. Tab. 6.2 shows the results of these simulations, which differ in the number of the CPs depending on the dynamic input parameters set in each simulation. The experiment used a room with a real polygon $\partial\mathcal{P}$ corresponding to Fig. 2.4 for simulations.

Table 6.2: The number of the CPs depends on the distance between the CPs and the distance of the inner measurement area from the wall. The 1st alg. is column A and the 2nd alg. is column B.

		Distance between the CPs [m]									
		0.3		**0.5**		**0.7**		**0.9**		**1.1**	
		A	**B**	**A**	**B**	**A**	**B**	**A**	**B**	**A**	**B**
Dist. [m]	**0.5**	355	204	129	77	67	52	42	27	29	22
	1.0	220	147	85	49	44	33	28	19	20	17
	1.5	117	81	48	32	24	19	16	11	11	8
		Number of the CPs [-]									

Both algorithms responded correctly to a change in the distance between the CPs and a change in the size of the measurement area $\mathcal{I}$. The 1st alg. always found more CPs than the 2nd alg. in the measured area $\mathcal{I}$ of the room. The results in Tab. 6.2 show that as the measurement area $\mathcal{I}$ decreases, the number of the CPs decreases. Similarly, as the distance between the CPs (red circles) increases, the number of the CPs also decreases. Therefore, the above results show that both algorithms are implemented correctly and adapt the number of the CPs to the dynamic input parameters.

6.2.3 Comparison of the Calculation Time of Control Points

Algorithms differ not only in the sources of the acoustic noise but also in the time they need to determine the CPs for measurement of indoor acoustic noise. Therefore, in experiments were recorded the time required to determine all the CPs in the measurement area $\mathcal{I}$ of the room. The first part of this section focuses on comparing the time of the first five simulated experiments. In these experiments, the static input parameter changed. The second part of this part focuses on the comparison of time between simulations in the seventh experiment, in which the dynamic input parameters changed.

Comparison of the First Five Simulated Experiments

An overview showing the times needed to calculate all the CPs covering the entire measured area from the first five simulated experiments is shown in Tab. 6.3. The results of the Tab. 6.1 shows that the 1st alg. calculates all the CPs much faster than 2nd alg. In the third experiment, the most apparent difference in the time calculation of the CPs was between the two algorithms because it was the largest measurement area $\mathcal{I}$ of all simulated rooms. The time results from the first three experiments also show that the larger the measurement area $\mathcal{I}$, the longer the calculation of both algorithms. Experiments focused on rooms with a column or more obstacles only confirmed previous conclusions on the time needed to calculate the CPs for both algorithms.

Table 6.3: The computation time for the 1st alg. is column A and the 2nd alg. is column B [25].

Room	Computation time [min] A	B
Simple geometric room (Fig. 6.8 and Fig. 6.10)	0.05	0.50
Real room (Fig. 6.11 and Fig. 6.12)	0.50	4.13
Large room (Fig. 6.13 and Fig. 6.14)	6.20	245.82
Larger room with column (Fig. 6.15 and Fig. 6.16)	0.33	8.37
Large room with obstacles (Fig. 6.17 and Fig. 6.18)	0.90	86.18

Comparison of the Results of the Seventh Experiment

The seventh experiment focused not on changing the floor plan of a room (static input parameter) but on changing the dynamic input parameters. As demonstrated in the previous sections, the algorithms correctly designed the measurement area and determined the CPs entire measurement area $\mathcal{I}$. The

assumption is that the algorithms also adjusted the time required to calculate the CPs.

The experiment results are shown in Tab. 6.4, where the 1st alg. is row A, and the 2nd alg. is row B. The results of the seventh experiment again show that the larger measurement area $\mathcal{I}$ has the longer CP calculation for both algorithms. Conversely, the longer the distance between the CPs, where no other CP may be placed, the shorter the calculation time. The 1st alg. also determines the maximum list of the CPs in the entire measurement area faster than the 2nd alg., which has the task of determining the minimum list of the CPs covering the entire measured area. The experiment proved the assumption with the proviso that both algorithms worked correctly.

Table 6.4: Computation time of the CPs depending on the distance between the CPs and the distance of the inner measurement area from the wall. The 1st alg. is row A and the 2nd alg. is row B.

			Distance [m]		
			0.5	**1.0**	**1.5**
Distance between the CPs [m]	**0.3**	**A**	5.94	1.47	0.50
		B	157.63	52.79	11.59
	0.5	**A**	1.09	0.28	0.10
		B	27.70	5.31	2.61
	0.7	**A**	0.48	0.11	0.04
		B	15.00	4.15	1.24
	0.9	**A**	0.33	0.06	0.02
		B	5.07	1.72	0.77
	1.1	**A**	0.20	0.04	0.02
		B	3.76	1.60	0.44
			Computation time [min]		

In real measurements, however, the difference in the time required to calculate the CPs is not decisive. Conversely, when measurement long-term stationary noise, a faster determination of the CPs is needed, because after recording the acoustic noise level at a given the CP, it is advisable to immediately go to the following CP. This procedure ensures that the acoustic noise values from all determined CPs in the measured area are recorded in a short period of time. For short-term recurring noise measurements, it is assumed that the algorithm has enough time to calculate. The time of the change of the CP is not known because the 2nd alg. waits until the specified acoustic noise level at the given CP is exceeded. However, while waiting for the acoustic noise level to be exceeded, the 2nd alg. can determine the following CPs based on the room's dimensions. Algorithms can also optionally calculate the CPs before measurement based on the floor plan of the room measured manually or automatically using laser rangefinder [91] of the second robotic unit (Sec. 5.3.2).

6.2.4 Robotic Experiments

As mentioned at the end of the previous section, both algorithms can calculate all the CPs before acoustic noise measurement. To calculate the CPs, it is enough for the algorithms to obtain a static input parameter (floor plan of the measured room) and set the required dynamic input parameters (more in Sec. 6.1). However, it is useful to verify that the algorithms can be integrated into the acoustic noise measurement process using a robotic platform.

The first such robotic experiments took place in [14], when a second robotic unit equipped with a sound level meter was used. Both algorithms were loaded into the control computer, and the algorithms were integrated into the software of the second robotic unit. Several robotic experiments were performed to test both algorithms. The first dynamic input parameter in these robotic experiments was set to 1.5 m, which determined the boundary of the measurement areas from the walls. The distance of 1.5 m was set only due to the part of the robot's software that is in charge of moving the second robot unit around the measured room.

Software modifications before the next robotic experiment

The development continued, and as mentioned in Sec 5.4.4 the second robotic unit has been upgraded with modified software. Based on the modification, the second robotic unit was able to approach the boundary of the measurement area 1 m from the wall when measuring the illuminance. This value of 1 m also meets the conditions for the distance of the CPs from the walls required by the standard [4] when measuring acoustic noise. Therefore, another robotic experiment could be performed, using the UT351 [95] sound level meter to measure acoustic noise.

According to the manufacturer, this sound level meter is stable, safe, and reliable. The sound level meter can be used for acoustic noise control, quality control and all different types of environmental acoustic noise testing. Tab. 6.5 contains the most important parameters of the UT351 sound level meter. The device is connected via an audio cable to the Arduino Uno development kit, which then communicates with the control computer of the second robotic unit.

The software of the second robotic unit is further modified so that the robotic experiment is completed in the shortest time possible. Software modifications will affect the measurement of both algorithms. The 1st alg. calculates the large number of the CPs covering the entire measured area. Due to the large number of CPs, it is stipulated that the measurement of the acoustic noise at each CP will be performed only once. This modification of additional software that obtains data from the sound level meter saves time. However, by simple software modification, multiple acoustic noise measurements can be performed at a single CP.

The 2nd alg. can calculate the CPs, but moving to the next CP depends on exceeding the set acoustic noise limit (event). The measurement is more time consuming because the algorithm is waiting for an event, it is decided

Table 6.5: Selected specifications of the UT351 instrument.

Specifications	Range	Accuracy
Measuring range	30-80 dB 50-100 dB 60-110 dB 80-130 dB	±1.5 dB ±1.5 dB ±1.5 dB ±1.5 dB
Frequency	31.5 Hz-8 kHz	
Sample rate	FAST: 8 Times/s SLOW: 1 Times/s	
Analogue outputs	AC: 0.707 Vrms full scale; Output impedance: around 600 Ω DC: 2 Vrms full scale; 10 mV/dB; Output impedance: around 100 Ω	
General characteristics		
Product Net Weight	330 g	
Product Size	273 × 70 × 36 mm	
Power	1.5 V Batteries	

that one acoustic noise measurement will be performed at each CP. The robot then moves to the next CP. However, again by simply modifying the software, it is possible to perform long-term measurements at each CP and wait for the set acoustic noise limit to be exceeded. These modifications will achieve faster verification of the goal of this robotic experiment.

Robotic experiment according to the standard

The robotic experiment aims to verify whether the proposed solution of acoustic noise measurement for two types of acoustic noise sources can calculate CPs in real conditions corresponding to the requirements of the standard [4]. The algorithms are loaded again into the control computer of the second robotic unit, which ensures the transmission of the measurement device to each calculated CP. At each CP, the robot then records the measured acoustic noise values.

The robotic experiment is divided into two parts. In the first part, the 1st alg. is verified and in the second part, the 2nd alg. is verified. The room has approximately 7×5 m and the room is completely empty for the purpose of the experiment. The robotic experiment has set dynamic input parameters:

- distance 1.0 m between the boundary of the measurement area $\partial\mathcal{I}$ and the wall $\partial\mathcal{P}$ and
- distance of 0.7 m from each CP.

In a real environment, the static input parameter (room floor plan) is either determined from the construction plans or measured. By measuring the floor plan, more accurate and realistic results are achieved. The floor plan measurement in this experiment is provided by the second robotic unit

by mapping the measured room. Fig. 6.23a shows the second robotic unit equipped with the UT351 sound level meter. Before each measurement of acoustic noise, the second robotic unit maps the room. Fig. 6.23b shows the reconstructed floor plan of the measured room, which uses the 1st alg. Fig. 6.23c shows the reconstructed floor plan of the same room, which uses the 2nd alg.

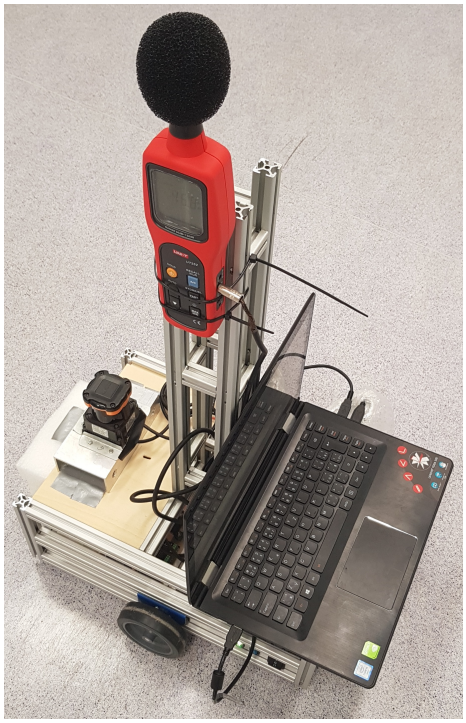

(a) : The entire second robotic unit equipped with the sound level meter UT351.

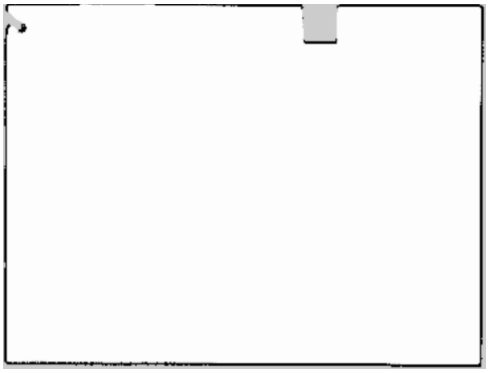

(b) : Constructed map for measurement long-term stationary noise.

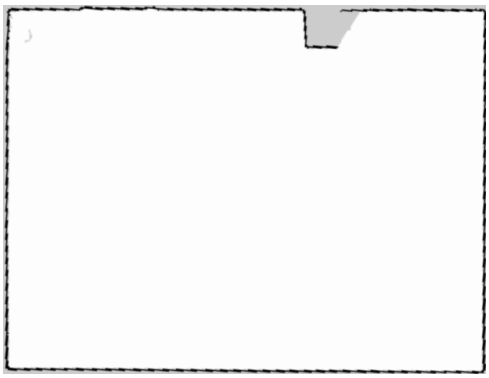

(c) : Constructed map for measurement short-term recurring noise.

Figure 6.23: The measured room and second robotic unit used for the robotic experiment.

The first part of the experiment is shown in Fig. 6.24. The 1st alg. first determined the measurement area based on the reconstructed floor plan of the measured room and then calculated the CPs. Fig. 6.24a shows the starting position of the variant at which the 1st alg. calculates the maximum list of the CPs in the measured area. In the fifteenth iteration, Fig 6.24b shows the gradual filling of the measured area with CPs. In the 28th iteration, most of the measured area is covered by CPs, which can be seen in Fig. 6.24c. Fig. 6.24d shows the last iteration when the 1st alg. determined 42 CPs as the maximum list of the CPs covering the measured area.

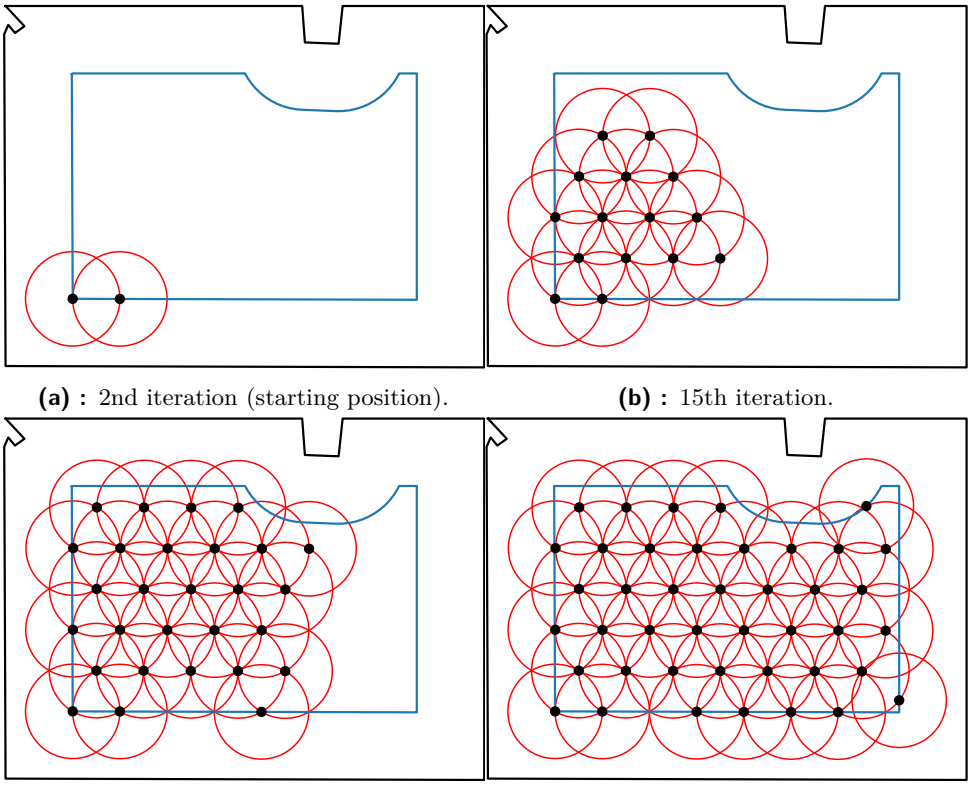

(a) : 2nd iteration (starting position). **(b) :** 15th iteration.

(c) : 28th iteration. **(d) :** 42nd iteration.

Figure 6.24: Results of the robotic experiment with the 1st alg. using the second robotic unit.

To verify that the 1st alg. works correctly, recall that the CPs should be at least 0.7 m apart. This boundary is shown by the red circle around each CP. The entire measurement area is to be covered by CPs and no CP is to be determined outside the measurement area. The boundary of the measurement area shall be 1 m from the wall. Thus, based on the calculation of all the CPs shown in Fig. 6.24d, it can be determined that the 1st alg. can correctly determine the measurement area and the CPs in the entire measurement area.

The list of CPs with their coordinates in the measured room is then passed by the 1st alg. to the next part of the robot's software. Based on the coordinates, the robot then drives to each CP and performs acoustic noise measurements. Fig. 6.25 shows the second robot unit during the measurement at the CP determined by the 1st alg. This verifies the 1st alg. in real conditions.

The second part of the experiment verified the functionality of the 2nd alg. in real conditions. Fig. 6.26 shows the deterministic calculation of the CPs in the measured area by the 2nd alg.. However, before the calculation itself, the 2nd alg. determined the measurement area of the reconstructed floor plan of the real room. Fig. 6.26a shows the first iteration in which the 2nd alg. found the minimum list of the CPs that cover the entire measured area.

Figure 6.25: Example of the procedure of measurement of acoustic noise using the second robotic unit.

This minimum list of the CPs is characterized by the fact that it is not possible to add another CP to the measurement area according to Sec. 6.1.2. Fig. 6.26b and Fig. 6.26c show the deterministic calculation of the CPs in the measurement area. Fig. 6.26d shows the last iteration in which the 2nd alg. determined 32 CPs.

The 2nd alg. determines the new CP at the farthest distance from the already determined CPs at each iteration. Based on the results, it is possible to determine that the 2nd alg. followed the mentioned procedure correctly. The calculated CPs are again passed to other parts of the robot's software. The robot then made measurements at the calculated CPs. The second part of the experiment also verified that the 2nd alg. works in real conditions.

The proposed solution meets the requirements of the standard [4], because the input parameters are the same as for the manual measurement. Therefore, it is not necessary to compare manual and robotic measurements. The only difference between manual measurement and the proposed solution for measurement of acoustic noise is in the movement of the measurement device around the room. The determination of the CPs is identical to the process established in practice, with the only difference that both algorithms calculate more CPs so that the algorithms cover the entire measured area. The larger number of the CPs achieves a more detailed acoustic noise map in the measured room.

The robotic experiment proved that the proposed solution is functional even in real conditions. The second robotic unit was used to move the measurement device around the room, thus automating the measurement process. This experiment concludes the work on the verification of the proposed solution for automatic measurement of acoustic noise.

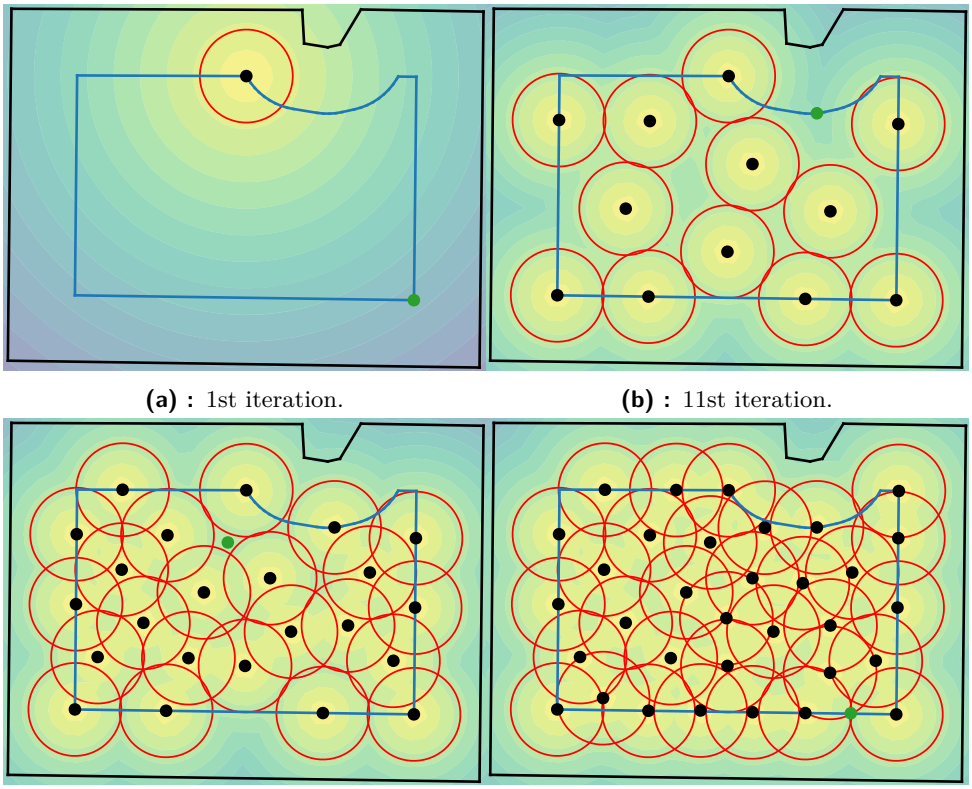

(a) : 1st iteration. **(b) :** 11st iteration.

(c) : 22nd iteration. **(d) :** 32nd iteration.

Figure 6.26: Results of the robotic experiment with the 2nd alg. using the second robotic unit.

6.3 Calculation of the Acoustic Noise Measurement Uncertainty

Each real measurement is accompanied by the determination of measurement uncertainty. Therefore, it is appropriate to determine the measurement uncertainty even during robotic experiments in which acoustic noise was measured. The last robotic experiment will be used to analyze the individual components of uncertainty, as it corresponds to the current method of measurement of acoustic noise in the real world. The experiment used a second robotic unit, which is equipped with a UT351 sound level meter and can measure acoustic noise at a distance of 1 m from the wall. This distance is determined from the requirements of the standard [7] for the location of the CPs in the measured room.

The last robotic experiment was divided into two parts, where in the first part the functionality of the calculation of the CPs of the 1st alg. was verified, and in the second part, the functionality of the calculation of the CPs of the 2nd alg. was verified. Recall that the 1st alg. determines the maximum number of CPs in the measured room. Due to the larger number of CPs, multiple measurements of acoustic noise at each CP during verification robotic

experiments would be inefficient. The 2nd alg. determines the minimum number of the CPs covering the entire measured room. The measured source of acoustic noise occurs recurring but randomly in the measured room. The 2nd alg. therefore waits at each CP to exceed the determined acoustic noise threshold. Only after measuring the acoustic noise value exceeding this threshold is it possible to move the measurement device to the next CP. Therefore, it is not appropriate to perform multiple acoustic noise measurements at each CP with respect to time. For these reasons, the determination of type A uncertainty is neglected.

This section focuses on the calculation of type B uncertainties, with the assumption that this uncertainty is the same for both algorithms. As a second robotic unit was used, two sources of error for type B uncertainty were identified. The first source is the location of the robotic unit using the UTM-30LX laser rangefinder and the second source is the accuracy of the UT351 measurement instrument used.

The analysis of other uncertainty components is determined according to the standard [4] and is not different from the manual measurement process established in practice. Eq. (6.3) is given in the standard, which states:

$$L = L^{'} + 10\mathrm{lg}\left(1 - 10^{-0.1\left(L^{'} - L_{resi}\right)}\right)\mathrm{dB} + \delta_{sou} + \delta_{met} + \delta_{loc}, \tag{6.3}$$

where is L is the estimated value during specific conditions for which a measured value is expected, expressed in decibels (dB), $L^{'}$ is the measured value, including residual noise, expressed in decibels (dB), L_{resi} is the residual sound, expressed in decibels (dB), δ_{sou} is an input quantity representing any uncertainty caused by deviations from the expected operating conditions of the source, expressed in decibels (dB), δ_{met} is an input quantity representing any uncertainty caused by meteorological conditions deviating from the assumed meteorological conditions, expressed in decibels (dB), δ_{loc} is an input quantity representing any uncertainty caused by choice of receiving site, expressed in decibels (dB) [4]. When using a second robotic unit, only δ_{loc} can be affected, which is caused by the selection of the receiving location in a manner similar to manual measurement. Therefore, during the measurement of acoustic noise, the second robotic unit switches off the motors and the laser rangefinder, which are devices that generate additional acoustic noise.

6.3.1 The Uncertainty of the Control Points Location in the interior - u_{Bl}

As mentioned in Sec. 5.5.1, the uncertainty is based only on data provided by the UTM-30LX laser rangefinder manufacturer. The partial standard uncertainty caused by the inaccuracy of the laser rangefinder used is determined according to general Eq. (5.19). In the last robotic experiment, the second robotic unit moved closest to 1 m from the wall, where it measured acoustic noise. This distance corresponds to the same data used to calculate the uncertainty according to Eq. (5.20) and is based on 1.73%. Similar to the

determination of the uncertainty of the illuminance measurement, this partial uncertainty is only applicable to the location of the second robotic unit in the room. Because we consider the measurement to determine the uncertainty for typically measured rooms, the gradient of spatial acoustic noise is small enough to allow this contribution to the overall uncertainty to be neglected.

6.3.2 The Uncertainty of the Measurement Device – u_{Be}

The robotic noise measurement unit uses the sound level meter UT351 [95]. The absolute partial uncertainty caused by the inaccuracy of the sound level meter used can generally be determined from:

$$u_{Be} = \frac{\triangle p}{\sqrt{3}}, \tag{6.4}$$

where $\triangle p$ is the accuracy of the sound level meter UT351. The documentation states that for a range of 50 dB to 100 dB, that usual range for measurement of acoustic noise in experiments, the accuracy is ±1.5 dB. From this accuracy data, u_{Be} can be calculated for:

$$u_{Be} = \frac{1.5}{\sqrt{3}} = 0.86 \text{ dB}. \tag{6.5}$$

6.3.3 Calculation of Combined and Expanded Uncertainty

This chapter focuses on the new method of calculating CPs in which the measurement of acoustic noise is performed in order to audit acoustic noise. From the measured acoustic noise values, it is possible to determine whether or not the measured room passed the acoustic noise audit on the basis of the regulation [98]. As the measured acoustic noise values do not affect the proposed measurement solution as for illuminance, It was decided that a more detailed analysis of the other components of the acoustic noise measurement uncertainty would not be performed. In this section, only an overview of the partial uncertainties that could have been determined in the robotic experiment is given. The summary of the calculated partial standard uncertainties of type B is limited only to the relative uncertainty u_{Bl} and the absolute uncertainty u_{Be}, where an overview of these uncertainties can be seen in Tab. 6.6. For this reason, the determination of combined and overall uncertainty is limited.

Table 6.6: Summary of calculated partial standard uncertainties of type B when measuring acoustic noise using the second robotic unit.

Error number	Source of error	Label	Calculated partial uncertainty
1	Location of the CPs in the interior	u_{Bl}	1.73%
2	The uncertainty of the measurement device	u_{Be}	0.86 dB

6.4 Conclusions

The goal of this Chapter was to develop, implement and validate the new method of acoustic noise measurement. Two algorithms have been developed to determine the CPs in which acoustic noise measurements are performed. Each algorithm has been developed due to the different sources of acoustic noise. Both algorithms use the floor plan of the measured room to determine the CPs. The CPs are determined to meet the conditions based on the standard [4].

At the beginning of this section, descriptions of both algorithms, their implementation, and illustrations of the measurements using the robotic unit are provided. The next part of this Chapter presents the experiments, which are divided into simulated and real experiments. The real experiments use the second robotic unit to move the UT351 sound level meter around the measured room. The proposed solution exploiting the second robotic unit automates the measurement process, and acoustic noise measurements can be performed without the presence of trained operators. The last part of this Chapter describes the determination of the measurement uncertainty based on the last robotic experiment.

The first algorithm is developed to determine the CPs for long-term stationary noise. The algorithm determines the maximum number of CPs that cover the entire measured room. The second algorithm is created to determine the CPs for short-term recurring noise. The algorithm does not know the number of possible measurements, and therefore the algorithm searches for the farthest location of the next CP in the measurement area from the already determined CPs in order to cover the largest possible measurement area. The algorithm, therefore, looks for the minimum number of CPs that cover the entire measured room.

Both algorithms were subjected to simulated experiments, which verified that both algorithms work correctly, i.e., in line with Sec. 6.1.1 and Sec. 6.1.2. The simulated experiments consisted of changes in static and dynamic input parameters. The static input parameter determined the different floor plans of the rooms, that is, from simple floor plans through large, diverse rooms to the room with obstacles. The dynamic input parameters varied the distance between the boundary of the measurement area and the wall and the distance

between the CPs. During most of the simulated experiments, the time required to determine all CPs and the number of the CPs in the measured area was determined. These data were then compared and it was found that the 1st alg. calculates the CPs significantly faster than the 2nd alg.. Simulated experiments have shown that both algorithms work correctly and can respond to changes in all input parameters.

In order to verify that the algorithms work in a real environment, real experiments were performed with the help of the second robotic unit. Both algorithms were able to calculate CPs from the measured and reconstructed floor plan of the real room. Furthermore, the algorithms provided the coordinates of the individual calculated CPs of another part of the software of the control computer of the second robotic unit. The control computer then initiated the movement of the second robotic unit to these coordinates and measured the acoustic noise in them.

From the last robotic experiment, the uncertainties were determined based on sources of error. The sources of error are the second robotic unit and the sound level meter. The calculation of the determined uncertainties is based on the corresponding equations.

The mentioned robotic experiment proved and verified that the proposed solution for measurement of acoustic noise is fully functional and meets the requirements of the standard [4]. Using the proposed solution and the second robotic unit, the process of measuring acoustic noise was automated. The measured values are stored with the coordinates of the CPs in the control computer and can be further processed in the future.

Chapter 7

Conclusions

People spend a lot of time indoors, in their homes, workplaces, malls, and other buildings and indoor places, e.g., schools, office buildings, hospitals, production halls. Therefore, it is necessary to provide at least sufficient or, preferably, comfortable living conditions indoors to everyone that stays there. Therefore, standards and hygienic limits that specify requirements on these conditions are defined. Thus, after completing buildings or finishing interior renovations, it is necessary to evaluate whether the conditions (parameters) are in line with the defined standards. These parameters are, in general, checked at control points (CPs) defined by the standards. This principle is exploited by national supervisory authorities, e.g., regional public health authority, or private companies, involved in the building design or certification of buildings.

In general, the entire measurement process is divided into several parts. The key parts of this process are calculation of the CPs and marking these CPs in the measured room. This is followed by, but is not limited to, the actual measurement of the required values at each CP.

The required parameters for verification include illuminance and acoustic noise levels, defined by the standards [1, 4]. Nowadays, these requirements are evaluated by measurements of illuminance and acoustic noise manually by trained operators. The operator first calculates and establishes a network of CPs based on the dimensions of the measured room. The operator then takes measurements at each CP via an appropriate measurement device. However, this process is both time and human resource intensive.

Therefore, this dissertation thesis focuses on development of a novel automated methods for checking whether the indoor spaces are in line with the requirements defined by the standards. The automated methods are proposed for audits of illuminance and acoustic noise in indoor environments. One of the key improvements of the proposed methods is minimizing the presence of a trained operator, who is replaced by an autonomous robotic unit. This is accomplished by completing the goals, as defined in Chapter 4:

- **Design, implement and test a new method for determining the CPs for measurement of illuminance.**

  A novel solution for determining the CPs for indoor illuminance measurement is proposed and described (Chapter 5). The proposed solution

is based on a virtual model of the measured luminaire that is placed in a created virtual model of a room with non-reflective black surfaces. The light propagation in the virtual model is determined via a simulated light propagation from the virtual luminaire and the actual measured illuminance values in the measured room. The validity of the proposed solution has been confirmed by the simulated experiments for various rooms with different floor plans. Although this solution uses room dimensions, its novelty lies in calculating of the spacing between the CPs from the virtual model of the measured luminaire, from which illuminance distribution is predicted.

- **Automate and test the process of determining the CPs for measurement of acoustic noise.**

  To automate the determination of the CPs and measurements of the acoustic noise (both long-term stationary noise and short-term recurring noise), we have proposed a novel solution (Chapter 6). This novel solution shares some similarities with the measurement of the illuminance, and enables us to automate the entire acoustic noise measurement process. Due to a difference between long-term stationary and short-term recurring acoustic noises, two tailored algorithms have been proposed. Both algorithms have been validated by the simulated experiments, and we have shown their applicability and adaptation to changes of input parameters (i.e., the floor plan of the measured room, the distance between the CPs and the distance between the boundary of the measurement area and the wall).

- **Verify the measurement process of both quantities using an autonomous robot.**

  To show that the proposed solutions for the measurement of both illuminance and acoustic noise work in the real environment, we have used two robotic units. We have implemented the proposed solutions in to both units and have performed the automated measurements in a real environment via these units. The proposed solutions implemented on the robotic units provide results close to the manual measurements, thus, showing that a trained human operator can be replaced during the measurement. Moreover, the results have shown that the proposed solution can replace not just one but two human operators, one for illuminance and one for acoustic noise measurement.

The results presented in this thesis demonstrate the functionality, versatility and adaptability of the proposed solutions. The proposed solutions revolutionize the current state of the art acoustic noise and illuminance measurements by automating the entire measurement process. Moreover, both proposed solutions can be combined within one robotic unit. Assuming the simultaneous use of several robotic units for parallel measurements within the entire buildings, the time and human resources required for the overall

audit are significantly reduced. From the simulated and robotic experiments in real conditions, it can be concluded that all stated goals have been met.

7.1 Future Research

This thesis proved that the proposed solutions for measurement of illuminance and acoustic noise indoors are functional and comparable with established methods of measurements by the human operators in real conditions. The proposed solutions can be adapted to different input parameters and are independent of the used robotic units. However, during the testing of the proposed solutions, ideas for the improvement of the proposed solutions and the developed second robotic unit have emerged.

7.1.1 Modification of the Second Robotic Unit

The proposed solution for the illuminance measurements has been evaluated in simulations for varying constraints, such as the distance of the measurement area boundary from the wall. This has been evaluated in the real world by a robotic unit, which led to a determination of some possible improvements. The first measurements were done with the minimal distance of the boundary of the measurement area from the wall set to 1.5 m. However, when carrying out measurements for a lower distance of the measurement area boundary from the walls (1 m) the limited computation capabilities of the robotic unit did not allow this.

Thus, we have updated the software that is responsible for moving the robotic unit to the calculated CPs, which is independent of the proposed solution. After the modifications, we have successfully completed the measurements with the boundary of the measurement area distance of 1 m from the wall. This distance is required by the standard [1]. However, in practice, the measurement procedure is commonly done with the distance of 0.5 m, which is defined by the standard [5].

One of the future goals is to modify the second robotic unit so that it can measure the CPs located at the distance of 0.5 m from the wall, and, thus, meet the requirements of the standard [5]. This would provide a full-fledged autonomous platform that can use the proposed solution to measure the illuminance in the measured room without the presence of the trained operator. Achieving such a goal could potentially lead to a change in legislation (standards) and allow measurements with the new method in practice.

7.1.2 Possible Modification of the Proposed Solution for Illuminance Measurement

The most important part of this thesis is the comparison of the illuminance measurements via the robotic unit exploiting the proposed solution and the illuminance measurement procedure by the human operator. From the results, we have observed a minor difference in the measured results. Even though

the difference between the results is not statistically significant, it is possible to improve the proposed solution to reduce the difference. The difference in the values measured by the robotic unit and the human operator is highest at the boundary of the measurement area and lower in the inner part of the measurement area. Therefore, to reduce the difference in the measured values, the future goal should be to modify the proposed solution so that a higher number of CPs is located at the boundary of the measurement area.

7.1.3 More Robotic Experiments

The simulated experiments proved the functionality of the proposed methods for the measurements of illuminance and acoustic noise. However, in real conditions, only a limited number of robotic experiments have been performed. Therefore, as a future goal, additional robotic experiments should be performed to verify that the robotic experiments correspond to the simulated experiments.

7.1.4 Completion of the Entire Measurement Process

In this thesis, we have described the proposed solutions for determining CPs in a measured room, the automated measurements via the robotic units and evaluation of the room for compliance with the existing standards. However, the entire measurement process is more complex and contains other parts. As a possible future extension of this thesis, is creating the automatic measurement process, which will contain all parts of the measurement process:

1. Preparing the measured room for measurement
2. Determining the dimensions of the measured room
3. Calculation of the CPs
4. Measurement at the CPs
5. Processing results

7.1.5 Automating Measurements of Other Quantities

As the future extension of this thesis, it is possible to measure other quantities in the interior of buildings. For this purpose, we can exploit one of the algorithms proposed in this thesis and adapt them to the needs of measuring various quantities, such as:

- Li-Fi, Wi-Fi, 4G and 5G signal propagation,
- magnetic field,
- light vector,
- humidity,

- radiation,
- dirt particles in the air,
- speed and direction of airflow, and
- temperature.

The values of these quantities are not homogeneous in the space (rooms), and as these quantities have an impact on the quality of living, the persons inhabiting the given space would benefit from the measurements of these quantities. The measurements of these quantities could be automated and done via a robotic unit equipped with appropriate measurement devices, while the measurements of multiple quantities can be done in parallel. This would further reduce the time required to measure these quantities.

7.2 The Scientific Contributions

The text presented in this thesis has been published in the following publications:

- T. Drábek, V. Petrík and J. Holub. "Statistical Based Control Points Selection for Indoor Illuminance Measurement." *IEEE Transactions on Instrumentation and Measurement*, 2020.

  The article describes the new approach to determining CPs for measurement of illuminance in buildings. The new method was verified in a real environment using the robotic unit that performed automatic measurements of indoor illuminance.

  - The text from the publication was used in Chapter 2, Chapter 3 and Chapter 5.

- T. Drábek, V. Petrík and J. Holub. "Automatic Control Points Computation for the Acoustic Noise Level Audits." In *17th IMEKO TC 10 and EUROLAB Virtual Conference: "Global Trends in Testing, Diagnostics & Inspection for 2030"*, pages 374-379. IMEKO TC10, 2020.

- T. Drábek and J. Holub. "The Improved Automatic Control Points Computation for the Acoustic Noise Level Audits." In *ACTA IMEKO*, pages 96-103. ACTA IMEKO Volume 10, ISSN: 2221-870X, 2021.

  Both papers describe an automated method for determining CPs for measurement of acoustic noise in buildings for two types of acoustic noise - long-term stationary noise and short-term recurring noise.

  - The text from the publications was used in Chapter 2, Chapter 3 and Chapter 6.

7.2.1 Contributions Related to the Thesis

I have been dealing with this topic since my master's degree, and during my research, I have published several papers in this area. I enclose a list of contributions below:

- M. Bálský and T. Drábek. "Automatizované měření osvětlenosti v interiéru." In *Kurz osvětlovací techniky XXX*. Ostrava: Česká společnost pro osvětlení, pages 115–118. ISBN 978-80-248-3173-2, 2013.
- M. Bálský, T. Drábek and R. Bayer. "Robotická jednotka pro měření osvětlenosti v interiérech." In *Sborník recenzovaných příspěvků Kurz osvětlovací techniky XXXI*. Ostrava: Česká společnost pro osvětlení, pages 40-44. ISBN 978-80-248-3553-2, 2014.
- T. Drábek and J. Holub. "The Innovation of the Autonomous System for Indoor Illuminance." In *Proceedings of the 21st International Conference LIGHT SVĚTLO 2015*. Brno: Brno University of Technology, FEEC, Department of Electrical Power Engineering, pages 273-276. ISBN 978-80-214-5244-2, 2015.

During my doctoral studies, I also led three bachelor's projects, which were closely related to and extended my research:

- P. Kůrka. "*A software for a robotic unit that measures indoor illumination in a control point network*." BS thesis. České vysoké učení technické v Praze. Vypočetní a informační centrum, 2020.
- A. Viktorová. "*Testing of a robotic unit for measuring indoor illuminance*." BS thesis. České vysoké učení technické v Praze. Vypočetní a informační centrum, 2021.
- J. J. Baroň. "*Testing of a robotic unit for measuring indoor noise*." BS thesis. České vysoké učení technické v Praze. Vypočetní a informační centrum, 2021.

Bibliography

[1] C. S. Institute, "Čsn 36 0011-1: Lighting measurement in areas. part 1: General regulations," *Czech Standards Institute*, 2014.

[2] ——, "Čsn 36 0011-3: Lighting measurement in areas. part 3: Measurement of artificial indoor lighting," *Czech Standards Institute*, 2014.

[3] ——, "Čsn iso 1996-1: Acoustics - description, measurement and assessment of environmental noise - part 1: Basic quantities and assessment procedures," *Czech Standards Institute*, 2018.

[4] ——, "Čsn iso 1996-2: Acoustics - description, measurement and assessment of environmental noise - part 2: Determination of sound pressure levels," *Czech Standards Institute*, 2018.

[5] E. C. for Standardization, "En 12464-1: Light and lighting-lighting of work places, part 1: Indoor work places," *European Committee for Standardization*, 2002.

[6] I. O. for Standardization, "1996-1:2016 acoustics - description, measurement and assessment of environmental noise - part 1: Basic quantities and assessment procedures," 2016.

[7] ——, "1996-2:2017 acoustics - description, measurement and assessment of environmental noise - part 2: Determination of sound pressure levels," International Organization for Standardization (ISO) Geneva, Switzerland, 2017.

[8] M. Bálský and T. Drábek, "Automatizované měření osvětlenosti v interiéru," in *Kurz osvětlovací techniky XXX*, 2013, pp. 115–118.

[9] T. Drábek, "Diploma thesis: Robotic unit for measuring illuminance in the optimal uniform control point mesh." 2014.

[10] M. Bálský, T. Drábek, and R. Bayer, "Robotická jednotka pro měření osvětlenosti v interiérech," in *Sborník recenzovaných příspěvků Kurz osvětlovací techniky XXXI*, 2014, pp. 40–44.

[11] T. Drábek and J. Holub, "The innovation of the autonomous system for indoor illuminance measurement," in *Proceedings of the 21st International Conference LIGHT SVĚTLO 2015*. Slovak Lighting Society, 2015, pp. 273–276.

[12] P. Kůrka, "A software for a robotic unit that measures indoor illumination in a control point network," B.S. thesis, České vysoké učení technické v Praze. Vypočetní a informační centrum, 2020.

[13] A. Viktorová, "Testing of a robotic unit for measuring indoor illuminance," B.S. thesis, České vysoké učení technické v Praze. Vypočetní a informační centrum, 2020.

[14] J. J. Baroň, "Testing of a robotic unit for measuring indoor noise," B.S. thesis, České vysoké učení technické v Praze. Vypočetní a informační centrum, 2020.

[15] T. Drábek, V. Petrík, and J. Holub, "Statistical based control points selection for indoor illuminance measurement," *IEEE Transactions on Instrumentation and Measurement*, 2020.

[16] T. Drábek, V. Petrík, and J. Holub, "Automatic control points computation for the acoustic noise level audits," pp. 374–379, 2020.

[17] M. Rea and I. E. S. of North America, *The IESNA Lighting Handbook: Reference & Application*, ser. IESNA LIGHTING HANDBOOK. Illuminating Engineering Society of North America, 2000. [Online]. Available: https://books.google.cz/books?id=0Ot4QgAACAAJ

[18] E. C. for Standardization, "En 13032-1: Light and lighting – measurement and presentation of photometric data of lamps and luminires – part 1: Measurement," *European Committee for Standardization*, 2012.

[19] I. O. for Standardization/International Commission on Illumination 19476: 2014, "Characterization of the performance of illuminance meters and luminance meters," 2014.

[20] T. Maixner, "Light measuring-since rumford to this day," pp. 1–4, 2018.

[21] P. Fiorentin and A. Scroccaro, "Detector-based calibration for illuminance and luminance meters—experimental results," *IEEE Transactions on Instrumentation and Measurement*, vol. 59, no. 5, pp. 1375–1381, 2010.

[22] I. E. Commission, "Čsn en 61672-1:2013 electroacoustics - sound level meters - part 1: Specifications," *EUROPEAN STANDARD*, 2014.

[23] ——, "Iec 61672-1: Electroacoustics – sound level meters – part 1: Specifications," *International Standard*, 2013.

[24] S. Carlisle, "The role of measurement in the development of industrial automation," *ACTA IMEKO*, vol. 3, no. 1, pp. 4–9, 2014.

[25] T. Drábek and J. Holub, "The improved automatic control points computation for the acoustic noise level audits," vol. 10, pp. 96–103, 2021.

[26] V. Haasz, J. Holub, M. Janošek, P. Kašpar, and V. Petrucha, *Elektrická měření: přístroje a metody.* Česká technika-nakladatelství ČVUT, 2018.

[27] M. BÁLSKÝ and J. HABEL, "Modernizace goniofotometru," *Světlo: časopis pro světlo a osvětlování*, pp. 1212–0812, 2009.

[28] K. REKTORYS *et al.*, "Applied mathematics (přehled užité matematiky)," *SNTL, Praha*, 1968.

[29] M. Miki, Y. Kasahara, T. Hiroyasu, and M. Yoshimi, "Construction of illuminance distribution measurement system and evaluation of illuminance convergence in intelligent lighting system," pp. 2431–2434, 2010.

[30] M. Przybyła, "Modern lighting audits-technology supporting designers and contractors to verify lighting installation quality," pp. 1–4, 2018.

[31] R. 111, "Radiolux 111 is a precision handheld instrument for photometric and radiometric measurements," 2021. [Online]. Available: https://luxmetry.cz/product/radiolux/

[32] D. GmbH, "Dialux, lighting, smart building. - dial," 2022. [Online]. Available: https://www.dial.de/en/home/

[33] N. Kubota, H. Sasaki, and K. Taniguchi, "Illuminance measurement of a mobile robot based on computational intelligence," in *IEEE International Conference Mechatronics and Automation, 2005*, vol. 2. IEEE, 2005, pp. 602–607.

[34] H. Sasaki, N. Kubota, K. Taniguchi, and Y. Nogawa, "Steady-state genetic algorithm for self-localization in illuminance measurement of a mobile robot," in *2006 IEEE International Conference on Systems, Man and Cybernetics*, vol. 3. IEEE, 2006, pp. 1897–1902.

[35] ——, "Illuminance measurement and slam of a mobile robot based on computational intelligence," in *2007 International Symposium on Computational Intelligence in Robotics and Automation.* IEEE, 2007, pp. 541–545.

[36] K. Kułakowski, P. Matyasik, and S. Ernst, "Modeling indoor lighting inspection robot behavior using concurrent communicating lists," *Expert Systems with Applications*, vol. 41, no. 4, pp. 984–989, 2014.

[37] C. Baier and J.-P. Katoen, *Principles of model checking.* MIT press, 2008.

[38] C. J. Bay, T. J. Terrill *et al.*, "Autonomous robotic building energy audits: Demonstrated capabilities and open challenges," *ASHRAE Transactions*, vol. 123, p. 3, 2017.

[39] M. Lindemann, R. Maass, and G. Sauter, "Robot goniophotometry at ptb," *Metrologia*, vol. 52, no. 2, p. 167, 2015.

[40] W. Brown, "Realization of the nml scale of total luminous flux," *Metrologia*, vol. 15, no. 4, p. 167, 1979.

[41] R. Inoue, T. Arai, Y. Toda, M. Tsujimoto, K. Taniguchi, and N. Kubota, "Intelligent control for illuminance measurement by an autonomous mobile robot," in *2019 IEEE International Conference on Advanced Robotics and its Social Impacts (ARSO)*. IEEE, pp. 270–274.

[42] M. Bonomolo, P. Ribino, C. Lodato, and G. Vitale, "Post occupancy evaluation and environmental parameters monitoring by a humanoid robot," in *2019 IEEE International Conference on Environment and Electrical Engineering and 2019 IEEE Industrial and Commercial Power Systems Europe (EEEIC/I&CPS Europe)*. IEEE, 2019, pp. 1–6.

[43] M. Genesca, J. Romeu, T. Pamies, and A. Sanchez, "Aircraft noise monitoring with linear microphone arrays," *IEEE Aerospace and Electronic Systems Magazine*, vol. 25, no. 1, pp. 14–18, 2010.

[44] J.-w. Pak and M.-k. Kim, "Convolutional neural network approach for aircraft noise detection," in *2019 International Conference on Artificial Intelligence in Information and Communication (ICAIIC)*. IEEE, 2019, pp. 430–434.

[45] C. Asensio, M. Ruiz, M. Recuero, G. Moschioni, and M. Tarabini, "A novel intelligent instrument for the detection and monitoring of thrust reverse noise at airports," *Acta Imeko*, vol. 4, no. 1, pp. 5–10, 2015.

[46] E. M. Ganic, F. Netjasov, and O. Babic, "Analysis of noise abatement measures on european airports," *Applied Acoustics*, vol. 92, pp. 115–123, 2015.

[47] A. Jamrah, A. Al-Omari, and R. Sharabi, "Evaluation of traffic noise pollution in amman, jordan," *Environmental Monitoring and Assessment*, vol. 120, no. 1, pp. 499–525, 2006.

[48] E. Murphy, E. A. King, and H. J. Rice, "Estimating human exposure to transport noise in central dublin, ireland," *Environment international*, vol. 35, no. 2, pp. 298–302, 2009.

[49] D. Schwela, "World health organization guidelines on community noise," *presentation at the TRB session*, vol. 391, 2001.

[50] K. M. Paiva, M. R. A. Cardoso, and P. H. T. Zannin, "Exposure to road traffic noise: Annoyance, perception and associated factors among brazil's adult population," *Science of the Total Environment*, vol. 650, pp. 978–986, 2019.

[51] M. Němec, A. Danihelová, T. Gergel', M. Gejdoš, V. Ondrejka, and Z. Danihelová, "Measurement and prediction of railway noise case study from slovakia," *International Journal of Environmental Research and Public Health*, vol. 17, no. 10, p. 3616, 2020.

[52] F. Bunn and P. H. T. Zannin, "Assessment of railway noise in an urban setting," *Applied acoustics*, vol. 104, pp. 16–23, 2016.

[53] X. Chen, D. Wang, X. Yu, and Z.-D. Ma, "Analysis and control of automotive interior noise from powertrain in high frequency," in *2009 IEEE Intelligent Vehicles Symposium*. IEEE, 2009, pp. 1334–1339.

[54] I. E. Commissio, "Iec 61400-11 wind turbines - part 11: Acoustic noise measurement techniques," *International Electrotechnical Commissio*, pp. 1–131, 2018.

[55] "Ieee standard for wind turbine aero acoustic noise measurement techniques," *IEEE Std 2400-2016*, pp. 1–24, 2016.

[56] S. Janhunen, A. Grönman, K. Hynynen, M. Hujala, M. Kuisma, and P. Härkönen, "Audibility of wind turbine noise indoors: Evidence from mixed-method data," in *2017 IEEE 6th International Conference on Renewable Energy Research and Applications (ICRERA)*, 2017, pp. 164–168.

[57] G. Graziuso, M. Grimaldi, S. Mancini, J. Quartieri, and C. Guarnaccia, "Crowdsourcing data for the elaboration of noise maps: a methodological proposal," in *Journal of Physics: Conference Series*, vol. 1603, no. 1. IOP Publishing, 2020, p. 012030.

[58] C. Buratti, "Indoor noise reduction index with open window," *Applied Acoustics*, vol. 63, no. 4, pp. 431 – 451, 2002. [Online]. Available: http://www.sciencedirect.com/science/article/pii/S0003682X01000408

[59] C. Guarnaccia, J. Quartieri, and A. Ruggiero, "Acoustical noise study of a factory: Indoor and outdoor simulations integration procedure," *International Journal of Mechanics*, vol. 8, 01 2014.

[60] S. Pujol, M. Berthillier, J. Defrance, J. Lardiès, R. Petit, H. Houot, J.-P. Levain, C. Masselot, and F. Mauny, "Urban ambient outdoor and indoor noise exposure at home: A population-based study on schoolchildren," *Applied Acoustics*, vol. 73, no. 8, pp. 741 – 750, 2012. [Online]. Available: http://www.sciencedirect.com/science/article/pii/S0003682X12000321

[61] P. Zannin and F. Ferraz, "Assessment of indoor and outdoor noise pollution at a university hospital based on acoustic measurements and noise mapping," *Open Journal of Acoustics*, vol. 06, pp. 71–85, 01 2016.

[62] B. Locher, A. Piquerez, M. Habermacher, M. Ragettli, M. Röösli, M. Brink, C. Cajochen, D. Vienneau, M. Foraster, U. Müller *et al.*, "Differences between outdoor and indoor sound levels for open, tilted, and closed windows," *International journal of environmental research and public health*, vol. 15, no. 1, p. 149, 2018.

[63] E. Martinson and R. C. Arkin, "Noise maps for acoustically sensitive navigation," in *Mobile Robots XVII*, vol. 5609. International Society for Optics and Photonics, 2004, pp. 50–60.

[64] P. I. Frazier, "A tutorial on bayesian optimization," *arXiv preprint arXiv:1807.02811*, 2018.

[65] S. Wilson, "Samuel wilson/parbayesianoptimization: Parallelizable bayesian optimization in r," https://github.com/AnotherSamWilson/ParBayesianOptimization.

[66] J. Yoo, K. H. Johansson, and H. J. Kim, "Indoor localization without a prior map by trajectory learning from crowdsourced measurements," *IEEE Transactions on Instrumentation and Measurement*, vol. 66, no. 11, pp. 2825–2835, 2017.

[67] N. Akai and K. Ozaki, "3d magnetic field mapping in large-scale indoor environment using measurement robot and gaussian processes," in *2017 International Conference on Indoor Positioning and Indoor Navigation (IPIN)*. IEEE, 2017, pp. 1–7.

[68] J. Hu, Y. Sun, G. Li, G. Jiang, and B. Tao, "Probability analysis for grasp planning facing the field of medical robotics," *Measurement*, vol. 141, pp. 227–234, 2019.

[69] K. Chatzilygeroudis, R. Rama, R. Kaushik, D. Goepp, V. Vassiliades, and J.-B. Mouret, "Black-Box Data-efficient Policy Search for Robotics," in *Proceedings of the IEEE/RSJ International Conference on Intelligent Robots and Systems*. IEEE, 2017.

[70] K. Chatzilygeroudis and J.-B. Mouret, "Using Parameterized Black-Box Priors to Scale Up Model-Based Policy Search for Robotics," in *Proceedings of the International Conference on Robotics and Automation*. IEEE, 2018.

[71] C. K. Williams and C. E. Rasmussen, *Gaussian processes for machine learning*. MIT press Cambridge, MA, 2006, vol. 2, no. 3.

[72] D. P. Kingma and J. Ba, "Adam: A method for stochastic optimization," *arXiv preprint arXiv:1412.6980*, 2014.

[73] M. Abadi, P. Barham, J. Chen, Z. Chen, A. Davis, J. Dean, M. Devin, S. Ghemawat, G. Irving, M. Isard *et al.*, "Tensorflow: A system for large-scale machine learning," in *12th Symposium on Operating Systems Design and Implementation (16)*, 2016, pp. 265–283.

[74] M. LLC, "Gpytorch regression tutorial," 2020. [Online]. Available: https://docs.gpytorch.ai/en/stable/examples/01_Exact_GPs/Simple_GP_Regression.html

[75] ——, "Likelihood in gpytorch," 2020. [Online]. Available: https://docs.gpytorch.ai/en/stable/likelihoods.html

[76] A. Paszke, S. Gross, F. Massa, A. Lerer, J. Bradbury, G. Chanan, T. Killeen, Z. Lin, N. Gimelshein, L. Antiga, A. Desmaison, A. Kopf, E. Yang, Z. DeVito, M. Raison, A. Tejani, S. Chilamkurthy, B. Steiner, L. Fang, J. Bai, and S. Chintala, "Pytorch: An imperative style, high-performance deep learning library," in *Advances in Neural Information Processing Systems 32*. Curran Associates, Inc., 2019, pp. 8024–8035. [Online]. Available: http://papers.neurips.cc/paper/9015-pytorch-an-imperative-style-high-performance-deep-learning-library.pdf

[77] s. s. r. MODUS, "Fixed general purpose luminaires, model: Llx," https://www.modus.cz/modus-llx/, 2021.

[78] G. Robots, "Jackal unmanned ground vehicle," https://www.generationrobots.com/en/402144-jackal-unmanned-ground-vehicle.html.

[79] L. Korba, S. Elgazzar, and T. Welch, "Active infrared sensors for mobile robots," *IEEE Transactions on Instrumentation and Measurement*, vol. 43, no. 2, pp. 283–287, 1994.

[80] T. Tsukiyama, "Measuring the distance and orientation of a planar surface using nonstructured lighting-3-d measurement system for indoor mobile robots," *IEEE transactions on instrumentation and measurement*, vol. 45, no. 5, pp. 885–893, 1996.

[81] G. Simon, G. Zachár, and G. Vakulya, "Lookup: Robust and accurate indoor localization using visible light communication," *IEEE Transactions on Instrumentation and Measurement*, vol. 66, no. 9, pp. 2337–2348, 2017.

[82] B. Gozick, K. P. Subbu, R. Dantu, and T. Maeshiro, "Magnetic maps for indoor navigation," *IEEE Transactions on Instrumentation and Measurement*, vol. 60, no. 12, pp. 3883–3891, 2011.

[83] R. Carotenuto, M. Merenda, D. Iero, and F. G. Della Corte, "An indoor ultrasonic system for autonomous 3-d positioning," *IEEE Transactions on Instrumentation and Measurement*, 2018.

[84] G. Grisetti, C. Stachniss, W. Burgard *et al.*, "Improved techniques for grid mapping with rao-blackwellized particle filters," *IEEE Transactions on Robotics*, vol. 23, no. 1, p. 34, 2007.

[85] G. Grisettiyz, C. Stachniss, and W. Burgard, "Improving grid-based slam with rao-blackwellized particle filters by adaptive proposals and selective resampling," in *Proceedings of the 2005 IEEE international conference on robotics and automation*. IEEE, 2005, pp. 2432–2437.

[86] S. Thrun, W. Burgard, and D. Fox, "Probabilistic robotics. 2005. isbn 0262201623."

[87] ——, "A probabilistic approach to concurrent mapping and localization for mobile robots," *Autonomous Robots*, vol. 5, no. 3-4, pp. 253–271, 1998.

[88] ——, *Probabilistic robotics*. MIT press, 2005.

[89] D. Fox, W. Burgard, F. Dellaert, and S. Thrun, "Monte carlo localization: Efficient position estimation for mobile robots," *AAAI/IAAI*, vol. 1999, no. 343-349, pp. 2–2, 1999.

[90] S. Thrun, D. Fox, W. Burgard, and F. Dellaert, "Robust monte carlo localization for mobile robots," *Artificial intelligence*, vol. 128, no. 1-2, pp. 99–141, 2001.

[91] HOKUYO, "Scanning rangefinder," https://www.hokuyo-aut.jp/search/single.php?serial=169, 2021.

[92] R. Electronics, "A complete robot drive system," https://www.robot-electronics.co.uk/rd02-12v-robot-drive.html, 2021.

[93] ——, "H bridge motor drive," https://www.robot-electronics.co.uk/htm/md25tech.htm, 2021.

[94] ——, "The emg30 - 12v motor," https://www.robot-electronics.co.uk/htm/emg30.htm, 2021.

[95] L. Uni-Trend Technology (China) Co., "Sound level meter ut351 unit," https://www.uni-trend.com/meters/html/product/Environmental/Environmental_Tester/UT350/UT351.html, 2021.

[96] M. Bálský, "Analýza procesu mnohonásobných odrazů," 2014.

[97] J. Vlach, "Diploma thesis: Nejistoty světelně technických měření." 2007.

[98] ČESKO, "Nařízení vlády č. 272/2011 sb., o ochraně zdraví před nepříznivými účinky hluku a vibrací," https://www.zakonyprolidi.cz/cs/2011-272, 2011.

[99] J. Svatos, J. Holub, and T. Pospisil, "A measurement system for the long-term diagnostics of the thermal and technical properties of wooden houses," *ACTA IMEKO*, vol. 9, no. 3, pp. 3–10, 2020.

[100] I. O. for Standardization, "Iso 9612:2009 acoustics — determination of occupational noise exposure — engineering method," International Organization for Standardization (ISO) Geneva, Switzerland, 2009.

[101] C. S. Institute, "Čsn en iso 9612 (011622): Acoustics – determination of occupational noise exposure – engineering method," *Czech Standards Institute*, 2009.

[102] S. Bolgert, "Tripy is a simple module with one purpose: triangulating polygons." https://github.com/linuxlewis/tripy.

[103] V. Agafonkin, "The fastest and smallest javascript polygon triangulation library." https://github.com/mapbox/earcut.

Appendix A

List of Publications

A.1 Publications Related to the Thesis

A.1.1 Publication in Journal with Impact Factor

- T. Drábek, V. Petrík and J. Holub. "Statistical Based Control Points Selection for Indoor Illuminance Measurement." *IEEE Transactions on Instrumentation and Measurement*, 2020.

  [**34%**-33%-33%]

A.1.2 Publication in ISI

- T. Drábek and J. Holub. "The Improved Automatic Control Points Computation for the Acoustic Noise Level Audits." In *ACTA IMEKO*, pages 96-103. ACTA IMEKO Volume 10, ISSN: 2221-870X, 2021.

  [**70%**-30%]

- T. Drábek, V. Petrík and J. Holub. "Automatic Control Points Computation for the Acoustic Noise Level Audits." In *17th IMEKO TC 10 and EUROLAB Virtual Conference: "Global Trends in Testing, Diagnostics & Inspection for 2030"*, pages 374-379. IMEKO TC10, ISBN 978-92-990084-6-1, 2020.

  [**34%**-33%-33%]

A.1.3 Other Publications

- T. Drábek and J. Holub. "The Innovation of the Autonomous System for Indoor Illuminance." In *Proceedings of the 21st International Conference LIGHT SVĚTLO 2015*. Brno: Brno University of Technology, FEEC, Department of Electrical Power Engineering, pages 273-276. ISBN 978-80-214-5244-2, 2015.

  [**50%**-50%]

- M. Bálský, T. Drábek and R. Bayer. "Robotická jednotka pro měření osvětlenosti v interiérech." In *Sborník recenzovaných příspěvků Kurz*

osvětlovací techniky XXXI. Ostrava: Česká společnost pro osvětlení, pages 40-44. ISBN 978-80-248-3553-2, 2014.

[33%-**33%**-33%]

- M. Bálský and T. Drábek. "Automatizované měření osvětlenosti v interiéru." In *Kurz osvětlovací techniky XXX*. Ostrava: Česká společnost pro osvětlení, pages 115–118. ISBN 978-80-248-3173-2, 2013.

  [50%-**50%**]

A.2 Publications Non-related to the Thesis

A.2.1 Publication in Journals with Impact Factor

- A. Hakob, T. Drábek, and J. Holub. "Low Bit-rate Coded Speech Intelligibility Tested with Parallel Task." In *Acta Acustica united with Acustica* 104.4, pages 678-684. ISSN 1610-1928, 2018.

  [35%-**20%**-45%]

A.2.2 Publication in ISI

- T. Drabek, J. Holub, and J. Fischer. "The new subject at the Czech Technical University in Prague: laboratories of industrial electronics and sensors." In *Photonics and Education in Measurement Science 2019*. Vol. 11144. International Society for Optics and Photonics, ISSN 1996-756X. ISBN 978-1-5106-2982-0, 2019.

  [**40%**-20%-40%]

A.2.3 Other Publications

- M. Schaefer, J. Holub, J. Reimes, and T. Drábek, "Subjective testing of car audio systems with and without parallel task." In *Proc. DAGA*, pages 1788-1791. ISBN 978-3-939296-13-3, 2018.

  [25%-25%-25%-**25%**]

- T. Drábek, and H. Avetisyan. "Prototype of Automated Device for Measurement of a Light Vector." In *Proceedings of the 20th International Scientific Student Conferenece POSTER 2016*. Praha: Czech Technical University in Prague, ISBN 978-80-01-05950-0, 2016.

  [**50%**-50%]

Appendix B

Calibration sheet the PRC Krochmann Radio-Lux 111 photometer

Český metrologický institut
Okružní 31, 638 00 Brno
tel. +420 545 555 111
www.cmi.cz

ilac-MRA K 2202

Kalibrační laboratoř č. 2202 akreditovaná Českým institutem pro akreditaci, o.p.s. podle ČSN EN ISO/IEC 17025:2005

Pracoviště: Laboratoře primární metrologie Praha, V Botanice 4, 150 72 Praha 5
Oddělení radiometrie a fotometrie, tel. +420 257 288 328, fax. +420 257 288 077

KALIBRAČNÍ LIST

8018-KL-R0261-18

Datum vystavení: 4. května 2018 List 1 ze 3 listů

Uživatel: České vysoké učení technické v Praze
Fakulta elektrotechnická
Technická 1902/2
166 27 Praha 6

Měřidlo: Digitální luxmetr
Výrobce: PRC Krochmann
Typ: Radiolux 111
Výrobní číslo: 121217

Výsledky kalibrace byly získány za podmínek a s použitím postupů uvedených v tomto kalibračním listě a vztahují se pouze k době a místu provedení kalibrace.

Datum kalibrace: 27. dubna 2018

Kalibraci provedl: Petr Linduška

Český metrologický institut -80-

Metrolog: Ing. Petr Kliment

Tento dokument nesmí být bez písemného souhlasu provádějící laboratoře rozmnožován jinak než v celkovém počtu listů.

KALIBRAČNÍ LIST **8018-KL-R0261-18** List 2 ze 3 listů

Použité etalony: Referenční fotometr v. č. 06A8342, kalibrační list 8018-KL-P0003-17
Fotometrická lavice ev. č. 80180073-B, kalibrační list 8015-KL-Z0169-14

Kalibrační postup: 818-MP-C811

Podmínky prostředí: Teplota v laboratoři (23,0 +/- 1,0)°C

Podmínky kalibrace: Měření fotometrické stupnice bylo provedeno porovnáním s referenčním fotometrem za použití světelného zdroje o teplotě chromatičnosti Tc=2856 K (zdroj A CIE) na několika úrovních osvětlenosti.

Výsledky kalibrace:

Tabulka: 1

Rozsah [lx]					
10		**100**		**1000**	
Měřený luxmetr [lx]	ČMI luxmetr [lx]	Měřený luxmetr [lx]	ČMI luxmetr [lx]	Měřený luxmetr [lx]	ČMI luxmetr [lx]
1,00	1,03	10,0	10,3	100	103
3,00	3,09	30,0	30,7	300	309
5,00	5,13	50,0	51,1	500	515
7,00	7,18	70,0	72,0	700	720
9,00	9,22	90,0	92,9	900	924
Průměrný korekční koeficient K_{2856i}					
1,028		1,026		1,029	

Tabulka: 2

Rozsah [lx]			
10000		**100000**	
Měřený luxmetr [lx]	ČMI luxmetr [lx]	Měřený luxmetr [lx]	ČMI luxmetr [lx]
1000	1027	10000	10208
3000	3065	15000	15262
5000	5124	20000	20290
7000	7159	25000	25301
9000	9192	30000	30273
Průměrný korekční koeficient K_{2856i}			
1,024		1,015	

Z naměřených hodnot vyplývá, že při měření světelného zdroje A, CIE, o teplotě chromatičnosti 2856 K je třeba hodnotu naměřenou luxmetrem zákazníka vynásobit pro daný měřicí rozsah osvětlenosti příslušným průměrným korekčním koeficientem K_{2856i}.

KALIBRAČNÍ LIST **8018-KL-R0261-18** List 3 ze 3 listů

Při měření jiného než světelného zdroje A o teplotě chromatičnosti 2856 K (žárovkové světlo) je nutno naměřené hodnoty osvětlenosti dále vynásobit korekčním koeficientem K_{dj} pro:

Světelný zdroj	K_{dj}
Světlo bílé zářivky	0,990
Světlo RVL výbojky s luminoforem	0,994
Světlo sodíkové výbojky	1,013
Světlo denní	0,996

Skutečná hodnota se tedy spočte dle vztahu:

$$E_i = K_{dj} \cdot K_{2856i} \cdot E_{mer}$$

Kde:

E_i	skutečná hodnota osvětlenosti
E_{mer}	hodnota osvětlenosti naměřená luxmetrem zákazníka
K_{2856i}	korekční koeficient pro daný rozsah osvětlenosti
K_{dj}	korekční koeficient jednotlivého typu zdroje

Nejistota měření: ± 2,2 %

Standardní nejistota měření byla určena v souladu s dokumentem EA–4/02. Uvedená rozšířená nejistota měření je součinem standardní nejistoty měření a koeficientu k, který odpovídá pravděpodobnosti pokrytí přibližně 95 %, což pro normální rozdělení odpovídá koeficientu rozšíření k = 2.

Konec kalibračního listu.

Cesky metrologicky institut
Laboratoře primární metrologie
V Botanice 4
150 72 Praha
5